2
2007

This is to certify that the
dissertation entitled

FORMATION, CHARACTERIZATION AND APPLICATIONS OF GOLD NANOPARTICLES AND SURFACE-MODIFIED GOLD

presented by

JANELLE DAWN SECL NEWMAN

has been accepted towards fulfillment
of the requirements for the

Ph.D degree in Chemistry

Major Professor's Signature

4/20/07

Date

MSU is an affirmative-action, equal-opportunity employer

FORMATION, CHARACTERIZATION AND APPLICATIONS OF GOLD NANOPARTICLES AND SURFACE-MODIFIED GOLD

By

Janelle Dawn Secl Newman

A Dissertation

Submitted to
Michigan State University
in partial fulfillment of the requirements
for the degree of

DOCTOR OF PHILOSOPHY

Department of Chemistry

2007

ABSTRACT
FORMATION, CHARACTERIZATION AND APPLICATIONS OF GOLD NANOPARTICLES AND SURFACE-MODIFIED GOLD

By
Janelle Dawn Secl Newman

Gold nanoparticles (AuNPs) have gained interest due to their unique properties. This dissertation will encompass three areas of current nanoparticle research. The first sections will discuss the formation of AuNPs using amines as both the reducing and stabilizing agent. Simple electrochemical measurements showed that the presence of the oxidation peak for an amine between the oxidation and reduction peaks of a solution of $HAuCl_4$ was a marker for thermodynamic feasibility of AuNP formation. In addition to thermodynamic considerations, kinetics of formation are also important and were explored using time-resolved ultraviolet-visible spectroscopy to measure PR evolution. It was seen that in amine reducing agents with a single amine per reducing agent molecule, that increasing oxidation potential resulted in a decrease in the rate of PR evolution. This is consistent with the AuNP formation occurring in the Marcus inverted region. Poly(allylamine hydrochloride) (PAH) was explored as a simple polymeric amine reducing agent. The thermodynamics and kinetics of the PAH system were explored as for the monomeric amines. The equilibrium behavior of the PAH-AuNP composite was also investigated and found to be readily controlled.

The characterization of quartz crystal microbalances with alkanethiol self-assembled monolayers (SAMs) adsorbed on the Au electrodes was explored using

impedance spectroscopy. The time-evolved impedance spectra for the SAMs were fitted to an equivalent circuit model and information was extracted about the assembly and viscoelastic behaviors of C_6-C_{18} SAMs. The initial deposition of the alkanethiols was found to occur within the first minute of QCM immersion. The organization rates for the C_6-C_{16} SAMs were found to be similar, indicating the aliphatic chain length had little impact on the rate of SAM assembly. The viscoelastic properties of the C_6 monolayer differed from those of the C_9-C_{16} SAMs and indicated that the shorter aliphatic chain resulted in a different solvent-monolayer interface than was seen for the longer aliphatic chain lengths. Additionally C_{18} was found to exhibit different behavior from the other SAMs. This was attributed to solubility limitations of the $C_{18}SH$ at the experimental deposition temperature.

Finally the application of AuNPs in sensors for organophosphate/phosphonate (OPP) compounds was explored. The sensors were created from the covalent attachment of AuNPs to silica gel or planar quartz. The AuNPs were then modified with zirconium-phosphorous (ZP) chemistry to create a sensor which was class-selective for OPP compounds. Both the silica gel and planar quartz substrates exhibited a spectral blue-shift when exposed to OPP compounds which could be attributed to changes in the local dielectric environment associated with OPP binding. The limit of detection was seen to be in the range of 5×10^{-7} to 5×10^{-5} M for the silica gel and planar quartz platforms, respectively. Additionally, the equilibrium of the binding was explored using the silica gel-AuNP-ZP sensor and estimated to have a $K \sim 2 \times 10^{6}$ M^{-1}.

To my parents, John M. and Gloria Secl

ACKNOWLEDGEMENTS

First, and foremost, I would like to acknowledge my advisor, Dr. Gary Blanchard. I came up with more than a few crazy ideas in my graduate research career and his willingness to let me explore taught me a lot about not only research but also about myself as a scientist. I would also like to thank my committee, Dr. Greg Swain, Dr. Merlin Bruening, and Dr. David Weliky for being supportive throughout my graduate career. They are all great educators and I have learned more about chemistry from them than I can begin to count. The Blanchard research group members, past and present, have made the past five years fly by. Thanks to them for insightful and revitalizing discussions. It has never been boring.

I would also like to take the opportunity to thank several individuals who were very helpful in this journey. First, I am grateful to Pavel Krysinski, for his helpful insight into the electrochemical studies. Also thanks to Ewa Danielewicz and Xudong Fan for their assistance in microscopic imaging studies. I would also like to thank Lisa Dillingham for all her assistance throughout my entire graduate career. She has gone above and beyond for me on many occasions and for that I am very grateful. I have had the opportunity to work with several undergraduate students during graduate school and I would especially like to thank one talented undergraduate, John Roberts. He is especially talented and his work was vital to the success of the sensor project. Best of luck to him in his future endeavors.

Special thanks is owed to Dr. William MacCrehan. He took a chance on the research ability of a first year masters student and without that opportunity I would most certainly have not have gotten this far. His suggestion to return to graduate school has most certainly changed the course of my life. I would also like to take this chance to thank Dr. William Wulff and his research group for all their delightful and insightful discussions. More than one scientific inspiration came over a bottle or two of wine on a Friday evening. Thanks for the honorary group membership.

I am most grateful for the support and encouragement I received from my family. Thanks to my mother-in-law and father-in-law, Diane and Tim Newman, for always keeping me grounded and providing an escape from the daily grind. Having someplace to go made being here much more enjoyable. It truly is great to have your in-laws be two of your greatest champions and true friends. Thanks to my brother, Matthew Secl, for always being there. I find your creativity inspirational and hope that when I grow up I can be as successful in my life as you are in yours. Thanks to my parents, Gloria and John Secl, for their endless encouragement and support. You have never set limits to me and have always provided me with every opportunity to explore whatever I wanted to. You helped me to understand the value of education and I really could not have done this without you.

Finally, thanks to my husband, Cory Newman. Perhaps only you can truly appreciate this journey. There is no one else I can imagine having been on it with. I never dreamed when I started graduate school that I would come out of it richer in life than I was in knowledge, but in you I found a friend and partner. I feel blessed. Thank you for everything you have done and have yet to do.

TABLE OF CONTENTS

LIST OF TABLES

LIST OF FIGURES

KEY TO SYMBOLS OR ABBREVIATIONS

APDMES	3-aminopropyldimethyethoxysilane
APTES	3-aminopropyltriethoxysilane
AuNPs	Gold nanoparticles
BVD	Butterworth-Van Kyke
CWC	Chemical Warfare Convention
MPTMS	3-mercaptopropyltrimethoxysilane
OPP	Organophosphate/phosphonate
PAH	Poly(allylamine hydrochloride)
PR	Plasmon resonance
QCM	Quartz crystal microbalance
SAM	Self-assembled monolayer
SEM.	Scanning electron microscopy
SERS	Surface enhanced Raman scattering
SHE	Standard hydrogen electrode
TEM	Transmission electron microscopy
ZP	Zirconium phosphate

Chapter 1

Introduction

Historical Perspective

Gold is one of the oldest metals known and has been used since the time of ancient civilizations.[1-4] It is known as a noble metal, due to its inertness, and occurs in nature in its native form.[1-3] Gold is present in the Earth's crust at a concentration of approximately 0.004 parts per million[3] and it is presumed that due to this relative rarity it was and has continued to be used both in coinage and as the basis for many monetary systems worldwide.[3, 5] Additionally, gold is a soft metal whose malleability makes it useful as a material in jewelry manufacturing, dentistry, and in electronics.[1, 2] In its bulk form, gold is a yellow metal and it is this color which is responsible for its chemical symbol, Au, which is derived from the Latin word for yellow, aurum.[2] In addition to gold being useful in its bulk form, it has also been used in its colloidal form for centuries. This thesis will address preparation, modification and characterization of colloidal gold, also known as gold nanoparticles (AuNPs), as well as the development of analytical techniques useful in applying AuNP chemistry to broader chemical problems.

AuNPs have been utilized by artisans for centuries. One of the earliest preparations of colloidal gold was in "purple of Cassius", which has was used as a colorant in art glasses and ceramic paints. [3-5] This colorant, as its name suggests, is

purple and is believed to have been formed by mixing tin(II) chloride with a solution containing the chloroaurate ion ($[AuCl_4]^-$).[3, 4] Solutions of gold ions have also been reduced to colloidal suspensions by reducing agents including tannin and phosphorous.[3-5] Throughout history, the preparations of these solutions were largely phenomenological. In the late 1850's, Michael Faraday determined that the color of ruby glass actually resulted from the incorporation of small particles of gold.[4-6] Faraday reduced yellow solutions of chloroaurate ions with phosphorous and created AuNP solutions. [4-6] Faraday suggested that "if a piece of this substance (phosphorous) be placed under the surface of a moderately strong solution of chloride of gold, the reduced metal adheres to the phosphorus as a granular crystalline crust".[6] He also discovered, in a broad sense, that by altering the concentration of the gold chloride he could get colloids ranging from ruby colored solutions to darker solutions which formed a gold precipitate.[6] Faraday was instrumental in introducing the study of these colloids using transmitted light. He noted the variety of colors that were present in the solutions prepared under various conditions.[6] It was his understanding of the colloidal color coming from the finely divided gold particles which paved the way for the harnessing of these gold clusters in the 20th century and beyond.

Theory and General Spectroscopic Behavior

The color of colloidal gold solutions is one piece of evidence for the behavior of these solutions of finely divided gold having properties which fall between that of atomic gold and bulk gold. These properties are both optical and electronic in nature, but it is the optical properties which have drawn the greatest amount of interest in the study of

AuNPs. In the early part of the 20th century, Gustav Mie solved Maxwell's equations with special conditions for small spherical metal particles.[7] This series of equations, now known as Mie Theory, elucidated the relationship between the size of the metal particles, the medium in which the particles were suspended, the absorption wavelength, and the absorbance intensity. In a general sense Mie determined that the optical response of AuNPs was the result of the summation of the electronic and magnetic oscillations and could be described as the extinction cross-section, σ_{ext}. This value could be further described as $\sigma_{ext} = \sigma_{abs} + \sigma_{sca}$, where σ_{abs} is the absorbance cross-section and σ_{sca} is the scattering cross-section.[7-10] Further, it was determined that for small particles the scattering cross-section was minimized so the majority of the optical response was due to the absorbance cross-section of the AuNPs (equation 1)[8, 11, 12]

$$\sigma_{abs}\lambda = 24\pi^2 R^3 \varepsilon_m^{3/2} \frac{\varepsilon''}{(\varepsilon' + 2\varepsilon_m)^2 + (\varepsilon'')^2} \quad (1)$$

The absorbance cross-section and the wavelength of absorbance (λ) can be shown to be related to the size of the particles which make up the analyte (R), the dielectric constant of the medium surrounding the particles (ε_m), and the real and imaginary components of the dielectric constant of the metal which makes up the particles (ε' and ε'', respectively). While surface modifications have the potential to affect ε' and ε'', this equation is most useful in its demonstration that the wavelength at which these colloidal solutions absorb energy can be predicted by the particle size and medium dielectric constant. The utility of this relationship will be discussed in greater detail later in this chapter.

While specific to spherical particles, Mie's equations allowed for the modification of Beer's Law in order to understand the absorbance behavior of AuNPs (equation 2).[13]

$$A_{abs,sca} = \frac{I}{I_0} = \frac{3cl\sigma_{abs,sca}}{4R\rho} \quad (2)$$

Here the value c represents the concentration of AuNPs in the analyzed solution, *l* is the pathlength, and $\sigma_{abs,sca}$ is the absorbance or scattering cross-section of the colloidal solution, R is the nanoparticle radius, and ρ is the density of Au. However, it is clear that Mie's elucidation of these relationships and their subsequent application to Beer's Law can be used to explain the variations in the colors and intensities of AuNP solutions used in both the arts and sciences. Most importantly variations in the particle sizes[14] and the medium surrounding the particles can be directly correlated to the wavelength of light which the particles absorb. With these AuNPs, the absorbance wavelength is in the visible region, leading to the red, blue and purple colors exhibited by these solutions.

The characteristic absorption exhibited by solutions of AuNPs is the result of the resonant excitation of the surface plasmons of nanoparticles which are much smaller than the wavelength of incident light and is most pronounced for AuNPs smaller than 25 nm[14, 15] This absorption, called the plamson resonance (PR), is the result of the collective and concerted oscillation of the conduction electrons on the surface of the AuNP.[14] This oscillation occurs, in the presence of an electric field, due to the immobile nature of the positively charged ions and the mobile nature of the free conduction band electrons on the particle surface. Equation 1 predicts that if ε" is small the resonance frequency can be predicted to fall at the wavelength where $\varepsilon' = -2\varepsilon_0$, the resonance condition.[16] The frequency of this oscillation can also be described by equation 3[17]

$$\omega_p = \sqrt{\frac{Ne^2}{\varepsilon_0 m_e}} \quad (3)$$

Where ω_p is the frequency of the plasmon oscillation, and N is density of the surface electrons. N is effectively related to the surface to volume ratio, or size and shape, of the nanoparticle. In practice, this predicted size dependence has been widely described and the position of the PR of AuNP colloids is widely variable with particle size.[5, 10, 11, 13-15, 17-21] As discussed previously, for small particles there is a dependence on both the particle size as well as the local dielectric environment surrounding the particles. However, for larger particles (> *ca.* 20 nm) the PR response is dependent only on the AuNP size[21], up to the limit where the particle aggregates to form bulk metal. Bogatyrev and co-workers have demonstrated that in the AuNP size range of approximately 18-30 nm a linear increase was seen in the PR repsponse[22]. Additionally, they found that increasing the particle size also resulted in an increase in the peak half-width and magnitude of absorbance, as would be predicted by equation 2.[22] Similar results have been reported by numerous others as well and are the basis for the utility of AuNPs in a variety of applications to be discussed later in this chapter.

Synthetic Advances

With the mathematical insight provided by Mie, AuNPs became a more interesting target of research due to the ability to theoretically predict and understand the spectroscopic behavior of the solutions. In the 1950's AuNPs became even more useful as chemical targets when a more clear understanding of the reduction of $[AuCl_4]^-$ into colloidal gold was elucidated through a series of experiments by John Turkevich, et al.[23] Turkevich studied the reduction of $[AuCl_4]^-$ by the citrate ion in detail, including efforts to determine the behavior of the reaction at both the nucleation and growth stages.[23-26]

AuNP synthesis using the $[AuCl_4]^-$ and citrate ions was simple and involved combining boiling dilute aqueous solutions of $[AuCl_4]^-$ and citrate, from either citric acid or sodium citrate, and stirring vigorously.[23] Turkevich examined the various stages of the AuNP preparation using transmission electron microscopy (TEM) to understand and attempt to delineate the nucleation and growth phases.[23] He understood nucleation to be the key step in the formation of AuNPs.[23] The actual nucleation event, however, was less well defined. Turkevich proposed the nucleation of reduced gold atoms resulted from the complexation of gold atoms inside of a matrix of the reducing agent. When enough of these gold atoms came into close spatial proximity, a spontaneous reorganization would occur which resulted in the formation of a nucleus. Following the nucleation event, the AuNPs would grow through aggregation of remaining gold ions and atoms into the final AuNP.[23] This growth was described by equation 4 and which predicts that the final particle size was dependent on the size of the nucleus created as well as the mass of the remaining Au in the solution[23, 26]

$$D_f = D_0 \sqrt[3]{\frac{M_i + M_m}{M_m}} \tag{4}$$

Subsequent investigations into this type of nucleation and growth, sometimes referred to as seed-mediated nucleation, have supported this mechanism.[27] The AuNP solutions resulting from this method are stabilized by the citrate ions which surround the reduced AuNP core. The negative charges of the citrate ions on the particle surface create an electronic hindrance to the further aggregation of Au atoms. Thus the final particle size is also dependent on the amount of reducing agent in this synthetic method as it also acts as the stabilizing agent as well. Frens exploited this reduction and stabilization mechanism and explored the effect of altering the ratio of the gold ion to the reducing

agent.[28] Like Turkevich, he found that the reaction reached completion quickly with no visual change in the colloid occurring after approximately five minutes of mixing.[28] Frens also found that simple alterations in the ratio of $AuCl_4^-$ to citrate ion resulted in the accessibility of a broad range of particle sizes and resulting spectral resonances and resulted in relatively monodisperse solution of the AuNPs in the range of 1.2-15 nm.[28] He suggested, as did Turkevich and co-workers, that the final particle size available from any AuNP synthesis was able to be determined primarily by the number of nuclei created and not by changes in the efficiency of the reduction event resulting from changes in the ratio.[28] Additionally, Jana reported that the rate at which the reducing agent is added also plays a role in the final AuNP size as well as the degree of dispersity in the final colloid.[27] The understanding of both the mechanism of the citrate reduction and the simple control over the final particles has resulted in this method being widely prevalent in the AuNP literature even as other methods have been discovered.

The citrate reduction method has a number of significant advantages as a synthetic method for creating AuNPs. First, it is a simple and time-efficient synthesis as it requires only boiling and mixing of the aqueous $AuCl_4^-$ and citrate solutions. In less than 15 minutes a stable colloidal solution results, requiring only stirring to complete the reaction. Additionally, as discussed previously, there is a great deal of control over the size of the AuNPs simply through alteration of the relative concentration of the Au^{3+} and citrate components. Finally, the particles are reduced and stabilized by the same compound, which minimizes the need for and additional stabilizing agent as well as ensuring that the particles are surrounded by only the citrate ions as opposed to another functional group which may be in the solution. Despite these advantages, there are

problems with the citrate reduction method. First, the AuNPs created in this synthesis are generally larger in size. This creates difficulties if the particles are to be removed from the aqueous solution and re-suspended in another aqueous or organic solution. This is a disadvantage if a stabilization shell is desired which is not soluble in aqueous solution. Much of the established gold surface chemistry is done in organic solvent, so this limits the surface chemistry being applied to these particles in the solution phase. Finally, while displacement of the citrate shell is desired with an aqueous-phase modifier is possible, it is still difficult to verify the complete exchange of one stabilizer for another. This can be a concern if a high concentration of the replacement stabilizer is required for further AuNP chemistries.

In the mid-1990's a new class of methods were developed which allowed for creation and stabilization of AuNPs in organic solvents.[29, 30] Brust and co-workers specifically introduced these methods as a technique for creating thiol stabilized AuNPs. In the two-phase method, first proposed in 1994, an aqueous solution of $HAuCl_4$ was combined with a solution of tetraoctylammonium bromide (TOAB) in toluene. The two solutions were agitated with the TOAB acting as a phase transfer agent, moving the Au^{3+} ions from the aqueous phase and into the toluene. Once the ion transfer is complete, a solution of the desired thiol stabilizer in toluene was added and the mixture reduced with aqueous sodium borohydride ($NaBH_4$).[30] A second method, reported in 1995, utilized a single organic phase.[29] Brust utilized *p*-mercaptophenol as the stabilizing thiol and did the entire synthesis in toluene, eliminating the need for the TOAB phase transfer agent. Again, the reduction was accomplished in this synthesis using $NaBH_4$. In these cases, the resulting AuNP colloids are sterically stabilized by the relatively bulky surface-bound

thiols. The AuNPs resulting from both these methods are in the 1-3 nm range and require reaction times in the range of 3 hours and equilibration times in the range of 4 hours.[29, 30] Due to the smaller particle size, it is possible to readily remove these AuNPs from solution for storage and to subsequently re-suspend them in a desired organic solvent.[30] Despite the obvious advantages that arise from the use of this method, including the much broader range of stabilizers that can be used, there are several disadvantages as well. First, while the use of organic solvents broadens the scope of possible reducing agents and allows the accessibility of much of the modification chemistry established for planar gold surfaces, it is also less environmentally and biologically friendly than using aqueous solvents. Secondly, the use of $NaBH_4$ as the reducing agent is required for AuNP formation. This not only adds an additional step to the synthetic procedure, but it can also be hazardous due to the violent nature of the reaction which occurs when the $NaBH_4$ is added to the organic phase containing the Au^{3+} and thiol stabilizer.

The first part of this thesis addresses the formation of AuNPs using amines as simultaneous reducing and stabilizing agents. These reactions are attractive as they have many of the advantages of both the Turkevich and Brust methods while minimizing the disadvantages associated with both these methods. Like the citrate reduction method, formation of AuNPs using amines allows for simultaneous reduction and stabilization, making the synthesis a single step. It also has the advantage of employing a wide variety of solvents, both aqueous and organic, depending on the desired amine. Finally, the ubiquitous nature of amines provides a wide variety of possible choices for reducing/stabilizing agents with multiple functionalities possible. This thesis addresses the study of monomeric and polymeric amines as reducing and stabilizing agents for the

formation of AuNPs via reduction of Au^{3+}. These studies will include investigations of the thermodynamic potential of amines of various structures to act as reducing agents for Au^{3+}. Following determination of the thermodynamic potential, kinetic investigations will be discussed where ultraviolet-visible spectroscopic investigations will be used to determine if amines with the appropriate electrochemistry actually demonstrate the presence of a PR, indicative of the formation of AuNPs. Reactions using both monomeric and polymeric amines will be discussed.

AuNP Characterization

Once synthesized, it is important to be able to characterize the AuNPs. While there are a number of parameters of interest in the measurement of AuNPs the size, polydispersity, degree of aggregation, and PR position are the characteristics of greatest interest to nanoparticle scientists. Despite challenges inherent to the relative size domains present challenges in AuNP colloids two primary methods have emerged as the analytical techniques most commonly employed in AuNP metrology: imaging techniques and UV-visible spectrometry.

Imaging. Imaging of AuNPs is, perhaps, the most powerful characterization tool available. Visualization of AuNPs can be accomplished by either scanning electron microscopy (SEM) or transmission electron microscopy (TEM), though the latter is more valuable as it does not require a conductive substrate. The importance of these imaging techniques comes from the ability to examine multiple characteristics simultaneously. Through examination of images obtained from microscopic techniques information can

be obtained about the structure of the nanoparticles[5] as well as the size and shape distribution of the AuNPs in a colloidal solution.

UV-visible spectroscopy. As discussed previously, the awareness of the existence of AuNPs came from the characteristic red to purple color. This leads to UV-visible spectroscopy being a very useful characterization tool for AuNP colloids. The presence of a strong absorption peak, the PR, in the UV-visible spectrum in the range of 500-600 nm is considered diagnostic of the presence of AuNPs in colloidal solutions. Also discussed previously is the ability to use the size and shape of this PR peak to determine the approximate size of the AuNPs in a given medium. [5, 10, 11, 13-15, 17-21] The speed and simplicity of this kind of measurement makes it the most widely used characterization method for AuNPs, both in solution and when attached to transparent surfaces.

Impedance spectroscopy. Impedance spectroscopy relies on measurement of the oscillation of quartz in the presence of an electric field. This oscillation can be monitored through a range of frequencies by an impedance analyzer. The impedance measurements are useful for a number of reasons. First, the Sauerbrey equation (equation 5) can be used to determine the mass of an adsorbed film by measurement of the shift of the resonance frequency.[31]

$$\Delta f = \frac{-2\Delta m \eta f_0^2}{A(\mu_q \rho_q)^{1/2}} \tag{5}$$

This relationship can be used in any case where the properties of the adsorbed monolayer are similar to the quartz used in the QCM. However, when the magnitude of the oscillation is measured across a range of frequencies near the resonance frequency, it is possible to also obtain information about the line-shape and line-width of the peak

associated with the oscillation. Through modeling the QCM system to an equivalent circuit such as a modified Butterworth-Van Dyke circuit[32-37], information can be obtained about the films attached to the QCM crystal. This information can be obtained for measurements obtained in both air and liquid and can be used for either equilibrium or kinetic measurements.

The second part of this thesis describes initial studies using impedance spectroscopy and corresponding equivalent circuit models to study the viscoelastic properties of thin films on gold. In the these initial studies, self-assembled monolayers (SAMs) of alkanethiols of various carbon chain lengths were chemisorbed, in situ, onto planar gold quartz crystal microbalance (QCM) substrates. A great deal is known about the behavior of alkanethiol SAMs[38], including information about the adsorption kinetics and basic information about monolayer formation. Impedance measurements offer another layer of information about the film-substrate interface. While these studies were conducted on planar substrates, the same techniques could be applied when investigating the properties of AuNPs bound to the QCM substrate or the properties of, for example, an AuNP composite material such as that described in Chapter 3.

Applications of AuNPs

Biological applications. One major advantage of understanding the formation of AuNPs by amines, as outlined in chapters 2 and 3 is the potential of these types of composite materials to be biologically compatible. Gold has been used for centuries as a remedy for a variety of health problems.[4, 5] Not surprisingly, as understanding about the

nature of gold nanoparticles has expanded so has the interest in using these nanoparticles for medicinal purposes.

AuNPs have been explored for use in a variety of different applications. One of the promising areas in which AuNPs have been investigated is in the area of drug and gene delivery.[39-41] In these applications, the nanoparticles are incorporated into a system which is responsive to temperature. Therefore, when the AuNP composite material is exposed to radiation at its resonant wavelength the matrix into which the AuNP has been incorporated undergoes a transition which releases the drug or gene. Thomas and co-workers have reported on the synthesis of spiropyran functionalized AuNPs which were used to bind and release amino acids based on thermal and photochemical reactions of the spiropyran.[40] In this case the zwitterionic form of the spiropyran-AuNP composite associates with amino acids and forms a relatively stable complex.[40] Upon irradiation of the AuNP-spiropyran-amino acid complex at the PR wavelength of 520 nm, the complex dissociates and releases the amino acid.[40] The authors suggest that this mechanism could be used, for example, to deliver L-DOPA, for treatment of Parkinson's disease or hypertension.[40]

One of the most promising areas for the medical use of AuNPs is in cancer research. There are currently two major areas where AuNPs have seen use. The first is imaging for cancer diagnostics and the second is cancer treatments. In the area of diagnostics, AuNPs have shown promise for use in enhancement of imaging of early stage tumors.[39, 42-44] Here, the ability of radiation in the near infra-red (NIR) region to harmlessly penetrate tissue, and the tunability of the PR wavelength of AuNPs are both exploited. The AuNPs, often synthesized with a dielectric core[39, 42, 43, 45], are created as to

have their PR in the desired wavelength regime. They are then subjected to a variety of imaging techniques which create a cross sectional image, illuminating the tumor with its enhanced uptake of AuNPs[39, 42, 43]. Tumor strains ranging from breast carcinoma cells (SK-BR-3) to oral epithelial live cancer cells (HOC 313 close 8, HSC 3) have been imaged using modifications of this kind of technique.[39, 42-44] The same types of AuNP composites which have been exploited for tumor imaging have also been explored for their potential in the destruction of tumor cells. Hirsch and Halas at Rice University have been instrumental in the field of NIR thermal therapies for tumor ablation. In these studies, gold nanoshells are prepared via coating of surface functionalized silica particles with 1-3 nm AuNPs.[41, 46, 47] The size of these particles makes it possible for the particles to pass into the tumors where they accumulate.[46, 47] Following uptake, the area of the tumor is irradiated with light in the NIR and localized heating occurs, thus destroying the tumor cells through a thermal mechanism.[46, 47] These studies have shown that mice with both SK-BR-3 human breast epithelial carcinoma and CT26.WT murine colon carcinoma tumor cells have been successfully treated in animal studies using this technique.[46, 47] After Additionally, animals with tumors but treated only with NIR irradiation in the absence of AuNPs showed experimental results similar to those of animals with tumors which remained untreated.[46, 47]

All of these applications point to the need for biologically-compatible AuNP composites. The enhanced understanding of amines as reducing and stabilizing agents in AuNP formation will be potentially useful in the creation of such AuNP materials.

Surface Enhanced Raman Spectroscopy (SERS) Substrates. Another area where AuNPs are quite useful is in the area of surface-enhanced Raman spectroscopy. As

discussed previously the PR exhibited by AuNPs is due to the collective oscillation of surface electrons on the particles. This excitation is also associated with an increase in the local electromagnetic field surrounding the particles.[16] The Van Duyne and Schatz groups have pioneered much of the work in the area of nanoparticles and SERS[10, 16, 48-52] and it has come to be focused primarily on the use of silver nanoparticles. However, the same basic enhancement principles which apply to the use of silver in SERS apply to gold as well and Raman intensity enhancements in the range of 10^5 (for AuNP solutions) to 10^{10} (for AuNP arrays) have been reported.[53, 54]

As early as 1982, Mabuchi and co-workers reported on the SERS spectrum of citrate ions adsorbed onto AuNPs after preparation using the Turkevich method.[54] After preparation, more sodium citrate was added to the colloidal solutions and they were aged for several days to ensure that all reactions had reached the maximum degree of aggregation.[54] They found that they were able to detect the sodium citrate in the Raman spectrum with and enhancement of about 10^5 times over samples with no AuNPs. Mabuchi proposed that the enhancement occurred as a result of the excitation of the surface plasmons of the AuNPs in the solution, in line with current understanding of the SERS mechanism.[54]

In more current evaluations of AuNPs as enhancing agents, AuNPs are typically bound to a substrate and the SERS activity of the substrate probed with Raman active molecules, such as *p*-aminophenol.[55] Zhu and co-workers found that surface-bound AuNPs showed the greatest enhancement of Raman intensity when there was a greater surface coverage and larger AuNP size, with the greatest enhancement coming from the latter.[55] They also found further confirmation of the need for a high surface density of

AuNPs in SERS substrates when the examined the effect of interparticle spacing on the degree of Raman signal enhancement and found that increasing the distance between AuNPs on the surface resulted in a significant decrease in the ability of the substrate to enhance the Raman signal.[55] However, they also verified, that while weak, Raman enhancement by single, uncoupled AuNPs was also possible to measure.[55]

AuNPs provide a useful tool in SERS thorough their ability to significantly enhance the observed Raman signal. This is particularly important in increasing the utility of Raman spectroscopy to evaluate very low concentration signals or to measure otherwise weakly-Raman active molecules.

AuNP-based Sensors. In addition to their use as diagnostic and therapeutic agents, AuNPs have also been used in sensory applications. These AuNP-based sensors can be used for the detection of molecules and interactions of biological interest or for more traditional chemical sensing applications.

When used in biosensing, there are two primary AuNP properties which are exploited. One sensing mechanism is based on AuNP aggregation of induced by interaction with the biomolecule of interest. This can be manifested in either the AuNP-biomolecule complex having properties unique from that of either component or a shift in the PR position.[39] The other mechanism is utilization of the AuNP light scattering to label biomolecules which are otherwise not optically active.[39]

As an example of the first mechanism, Cao and co-workers have functionalized AuNPs with antibodies and Raman dye to create an assay for small molecule (antibody)-protein interactions.[56] These AuNPs were exposed to proteins which were spotted onto a planar array.[56] When an interaction occurred between the proteins on the surface and the

Raman labeled AuNPs, a gray spot became visible on the array which could be further evaluated using a Raman spectrometer.[56] Additionally, the authors note that this method can be used in an analogous sense to test for protein-protein interactions as well.[56] A similar experiment was described by Frederix where thin films of AuNPs were immobilized onto quartz substrates and functionalized with anti-human serum albumin (anti-HSA).[57] The UV-visible spectrum was obtained for the sensor prior to exposure to human serum albumin (HSA). The presence of HSA was manifested as increases in both the PR wavelength and observed absorbance.[57] Similar mechanisms have also been utilized to detect specific strands of DNA, in immuno-sensing applications, in sugar sensing, and in the evaluation of biological interactions through conjugation with biomacromolecules.[4, 58, 59] Nath and Chilkoti utilized the changes observed in the spectrum of surface bound AuNPs in the detection of streptavidin.[60] They found that the peak position shift and change in absorbance could be correlated to the degree of binding and consequently the streptavidin concentration.[60] In addition to the sensor being simple to construct it was also useful because it required nothing more than a simple UV-visible spectrometer for analysis, thus making the sensor widely applicable.[60]

In addition to being useful as biosensors, the ability to utilize both the PR position in the visible region of the spectrum and the well established chemistry available on gold surfaces makes AuNPs useful as the basis of sensors for a variety of other compounds as well. There have been several recent examples of sensors created based upon the energy absorption properties of AuNPs. In 2004, a colorimetric sensor was reported on by Matsui and co-workers, which was useful in the detection of small molecules ranging from adrenaline to 2-phenylethylamine.[61] It was found that a molecularly imprinted

polymer with AuNPs imbedded within the matrix could be used in conjunction with UV-visible spectrometry to detect the target analytes in aqueous solutions.[61] The detection mechanism was based on a spectral blue-shift observed when the polymers bound to the analytes of interest.[61] This report is also interesting because the AuNPs themselves played no role in the binding of the polymer and the analytes of interest. Therefore, it demonstrated that the AuNP PR can be used as an indicator for other interactions taking place in the vicinity of the particles. In 2005, He and co-workers reported on a colorimetric and fluorometric Cu(II) sensor based on the quenching of a pyridyl-terminated perylene chromophore by AuNPs.[62] In the absence of a Cu(II) ion, the AuNPs will bind to the chromophore by interaction with the pyridyl N. However, because the Au-N interaction is weaker than the Cu-N interaction, when Cu(II) is present, the latter interaction is preferred and the quenching observed in the blank case is not seen.[62] They report a detection limit for Cu(II) of 1.0×10^{-6} M.[62] AuNPs have have also been reported as a sensor interface in a chemiresistor sensor device for detection of volatile organic compounds (VOCs).[63, 64] Pang and co-workers described the incorporation of AuNPs, either protected with monolayers or thiols, into a 3-D sensor matrix.[63, 64] The resistance and capacitance of the films were measured in the presence of VOCs with varying degrees of humidity. They showed that using AuNPs as the electrical interface in this sensor they were able to achieve fast reponse and low noise VOC detection at the hundreds of parts per million levels. These examples demonstrate the wide potential AuNPs have in the area of chemical sensing.

The final part of this thesis discusses the modification of citrate-stabilized AuNPs, through displacement of the citrate ion shell and subsequent functionalization with

zirconium phosphate (ZP) chemistry, in two optical sensors for detection of organophosphate/phosphonate (OPP) compounds. There have been examples where AuNPs were incorporated into OPP sensors[65, 66], however the previous examples rely on the measurement of acetylcholinesterase (AChE) inhibition. In the work discussed in Chapters 5 and 6, the detection scheme described is purely chemical in nature and does not rely on the use of the AChE, making it much more robust as it does not use enzymes. The AuNPs were bound to either silica gel or planar quartz using silanes. They were then modified using ZP chemistry[67-76] to create a Zr^{4+} terminated surface. This terminus takes advantage of the affinity of Zr^{4+} for phosphorous compounds and binds OPP compounds upon exposure. These sensors exhibited a blue-shift in the visible spectrum upon exposure to OPP compounds. This blue-shift, due to changes in the local dielectric environment experienced by the AuNPs upon OPP binding, is characteristic of the presence of OPPs. These sensors demonstrate the potential for using the characteristic PR of AuNPs to create sensors which are simple to construct, robust, and require minimal training to analyze.

Conclusion

The synthesis, characterization, and application of AuNPs have been the three areas of primary interest to researchers in the field of AuNPs. Since the initial understanding of the optical behavior of AuNP colloids by Michael Faraday and Gustav Mie, there has been tremendous growth in the area of understanding how to control, measure, and use AuNPs. This thesis will cover my contributions to this field. First I will discuss how the electrochemical behavior of the reducing agent and gold source can

be used in the prediction of when AuNPs will be formed. I will also discuss the role of the kinetics in the formation of the AuNPs in the optical behavior of the colloids. Then I will discuss the characterization of SAMs on a QCM crystal with Au electrodes using impedance spectroscopy. While used in this example on planar gold, the information obtained about the measurement of the viscoelastic properties of the SAMs could be applied to the measurement of the viscoelastic properties of composite materials which incorporate AuNPs. Finally, I will discuss my contribution to the field of chemical sensing using AuNPs. The design and development of optical sensors for OPP compounds will be discussed. These sensors, created on silica gel and planar quartz substrates, have shown promise for the simple optical detection of OPPs.

References

1. Greenwood, N. N. E., A., Copper, Silver and Gold. In *Chemistry of the Elements*, 2nd ed.; Butterworth-Heinemann: Oxford, 1997; pp 1173-1200.

2. Kirkemo, H. N., William L.; Ashley, Roger P. Gold. http://pubs.usgs.gov/gip/gold/ (12-13-2006).

3. Puddenphatt, R. J., *The Chemistry of Gold.* Elsevier: New York, 1978.

4. Daniel, M.-C.; Astruc, D., Gold Nanoparticles: Assembly, Supramolecular Chemistry, Quantum-Size-Related Properties, and Applications toward Biology, Catalysis, and Nanotechnology. *Chemical Reviews (Washington, DC, United States)* **2004,** 104, (1), 293-346.

5. Schmid, G.; Corain, B., Nanoparticulated gold: Syntheses, structures, electronics, and reactivities. *European Journal of Inorganic Chemistry* **2003**, (17), 3081-3098.

6. Faraday, M., The Bakerian Lecture:Experimental Relations of Gold (and Other Metals) to Light. *Philosophical Transactions of the Royal Society of London* **1857,** 147, 145-181.

7. Mie, G., Beitrage zur Optik truber Medien, speziell kolloidaler Metallosungen. *Ann. Phys.* **1908,** 25, 377-445.

8. Hutter, E.; Fendler, J. H., Exploitation of localized surface plasmon resonance. *Advanced Materials (Weinheim, Germany)* **2004,** 16, (19), 1685-1706.

9. Xia, Y.; Halas, N. J., Shape-controlled synthesis and surface plasmonic properties of metallic nanostructures. *MRS Bulletin* **2005,** 30, (5), 338-348.

10. Kelly, K. L.; Coronado, E.; Zhao, L. L.; Schatz, G. C., The Optical Properties of Metal Nanoparticles: The Influence of Size, Shape, and Dielectric Environment. *Journal of Physical Chemistry B* **2003,** 107, (3), 668-677.

11. Hoevel, H.; Fritz, S.; Hilger, A.; Kreibig, U.; Vollmer, M., Width of cluster plasmon resonances: bulk dielectric functions and chemical interface damping. *Physical Review B: Condensed Matter and Materials Physics* **1993,** 48, (24), 18178-88.

12. Charle, K. P.; Koenig, L.; Nepijko, S.; Rabin, I.; Schulze, W., The surface plasmon resonance of free and embedded Ag clusters in the size range 1.5 nm < D < 30 nm. *Crystal Research and Technology* **1998,** 33, (7-8), 1085-1096.

13. Khlebtsov, N. G.; Trachuk, L. A.; Mel'nikov, A. G., The Effect of the Size, Shape, and Structure of Metal Nanoparticles on the Dependence of Their Optical

Properties on the Refractive Index of a Disperse Medium. *Optics and Spectroscopy* **2005,** 98, (1), 77-83.

14. Bohren, C. F. H., D.R., *Absorption and Scattering of Light by Small Particles.* Wiley-Interscience: New York, 1983.

15. Kreibig, U.; Zacharias, P., Surface plasma resonances in small spherical silver and gold particles. *Zeitschrift fuer Physik* **1970,** 231, (2), 128-43.

16. Haes, A. J.; Haynes, C. L.; McFarland, A. D.; Schatz, G. C.; Van Duyne, R. R.; Zou, S. L., Plasmonic materials for surface-enhanced sensing and spectroscopy. *Mrs Bulletin* **2005,** 30, (5), 368-375.

17. Kreibig, U.; Genzel, L., Optical absorption of small metallic particles. *Surface Science* **1985,** 156, (2), 678-700.

18. Genzel, L.; Kreibig, U., Dielectric function and infrared absorption of small metal particles. *Zeitschrift fuer Physik [Sektion] B: Condensed Matter and Quanta* **1980,** 37, (2), 93-101.

19. Genzel, L.; Martin, T. P.; Kreibig, U., Dielectric function and plasma resonances of small metal particles. *Zeitschrift fuer Physik [Sektion] B: Condensed Matter and Quanta* **1975,** 21, (4), 339-46.

20. Quinten, M.; Kreibig, U.; Schoenauer, D.; Genzel, L., Optical absorption spectra of pairs of small metal particles. *Surface Science* **1985,** 156, (2), 741-50.

21. Link, S.; El-Sayed, M. A., Shape and size dependence of radiative, non-radiative and photothermal properties of gold nanocrystals. *International Reviews in Physical Chemistry* **2000,** 19, (3), 409-453.

22. Bogatyrev, V. A.; Dykman, L. A.; Khlebtsov, B. N.; Khlebtsov, N. G., Measurement of Mean Size and Evaluation of Polydispersity of Gold Nanoparticles from Spectra of Optical Absorption and Scattering. *Optics and Spectroscopy (Translation of Optika i Spektroskopiya)* **2004,** 96, (1), 128-135.

23. Turkevich, J.; Stevenson, P. C.; Hillier, J., The nucleation and growth processes in the synthesis of colloidal gold. *Discussions of the Faraday Society* **1951,** No. 11, 55-75.

24. Enustun, B. V.; Turkevich, J., Coagulation of colloidal gold. *Journal of the American Chemical Society* **1963,** 85, (21), 3317-28.

25. Fry, F. H.; Hamilton, G. A.; Turkevich, J., Kinetics and mechanism of hydrolysis of tetrachloroaurate(III). *Inorganic Chemistry* **1966,** 5, (11), 1943-6.

26. Turkevich, J.; Stevenson, P. C.; Hillier, J., The formation of colloidal gold. *Journal of Physical Chemistry* **1953,** 57, 670-3.

27. Jana, N. R.; Gearheart, L.; Murphy, C. J., Evidence for seed-mediated nucleation in the chemical reduction of gold salts to gold nanoparticles. *Chemistry of Materials* **2001,** 13, (7), 2313-2322.

28. Frens, G., Controlled nucleation for the regulation of the particle size in monodisperse gold suspensions. *Nature (London), Physical Science* **1973,** 241, (105), 20-2.

29. Brust, M.; Fink, J.; Bethell, D.; Schiffrin, D. J.; Kiely, C., Synthesis and reactions of functionalized gold nanoparticles. *Journal of the Chemical Society, Chemical Communications* **1995,** (16), 1655-6.

30. Brust, M.; Walker, M.; Bethell, D.; Schiffrin, D. J.; Whyman, R., Synthesis of thiol-derivatized gold nanoparticles in a two-phase liquid-liquid system. *Journal of the Chemical Society, Chemical Communications* **1994,** (7), 801-2.

31. Sauerbrey, G., Verwendung Von Schwingquarzen Zur Wagung Dunner Schichten Und Zur Mikrowagung. *Zeitschrift Fur Physik* **1959,** 155, (2), 206-222.

32. Bandey, H. L.; Martin, S. J.; Cernosek, R. W.; Hillman, A. R., Modeling the Responses of Thickness-Shear Mode Resonators under Various Loading Conditions. *Analytical Chemistry* **1999,** 71, (11), 2205-2214.

33. Granstaff, V. E.; Martin, S. J. Method for simultaneous measurement of mass loading and fluid property changes using a quartz crystal microbalance. 91-779727
5201215, 19911017., 1993.

34. Granstaff, V. E.; Martin, S. J., Characterization of a thickness-shear mode quartz resonator with multiple nonpiezoelectric layers. *Journal of Applied Physics* **1994,** 75, (3), 1319-29.

35. Martin, S. J.; Bandey, H. L.; Cernosek, R. W.; Hillman, A. R.; Brown, M. J., Equivalent-Circuit Model for the Thickness-Shear Mode Resonator with a Viscoelastic Film Near Film Resonance. *Analytical Chemistry* **2000,** 72, (1), 141-149.

36. Martin, S. J.; Granstaff, V. E.; Frye, G. C., Characterization of a quartz crystal microbalance with simultaneous mass and liquid loading. *Analytical Chemistry* **1991,** 63, (20), 2272-81.

37. Noel, M. A. M.; Topart, P. A., High-Frequency Impedance Analysis of Quartz-Crystal Microbalances .1. General-Considerations. *Analytical Chemistry* **1994,** 66, (4), 484-491.

38. Ulman, A., Formation and Structure of Self-Assembled Monolayers. *Chemical Reviews (Washington, D. C.)* **1996,** 96, (4), 1533-1554.

39. Sonvico, F.; Dubernet, C.; Colombo, P.; Couvreur, P., Metallic colloid nanotechnology, applications in diagnosis and therapeutics. *Current Pharmaceutical Design* **2005,** 11, (16), 2091-2105.

40. Thomas, K. G.; Kamat, P. V., Chromophore-Functionalized Gold Nanoparticles. *Accounts of Chemical Research* **2003,** 36, (12), 888-898.

41. Halas, N., Playing with plasmons. Tuning the optical resonant properties of metallic nanoshells. *Mrs Bulletin* **2005,** 30, (5), 362-367.

42. Loo, C.; Lin, A.; Hirsch, L.; Lee, M.-H.; Barton, J.; Halas, N.; West, J.; Drezek, R., Nanoshell-enabled photonics-based imaging and therapy of cancer. *Technology in Cancer Research & Treatment* **2004,** 3, (1), 33-40.

43. Loo, C.; Lowery, A.; Halas, N.; West, J.; Drezek, R., Immunotargeted nanoshells for integrated cancer imaging and therapy. *Nano Lett.* **2005,** 5, (4), 709-11.

44. Santra, S.; Dutta, D.; Walter, G. A.; Moudgil, B. M., Fluorescent nanoparticle probes for cancer imaging. *Technology in Cancer Research & Treatment* **2005,** 4, (6), 593-602.

45. Westcott, S. L.; Jackson, J. B.; Radloff, C.; Halas, N. J., Relative contributions to the plasmon line shape of metal nanoshells. *Physical Review B: Condensed Matter and Materials Physics* **2002,** 66, (15), 155431/1-155431/5.

46. Hirsch, L. R.; Stafford, R. J.; Bankson, J. A.; Sershen, S. R.; Rivera, B.; Price, R. E.; Hazle, J. D.; Halas, N. J.; West, J. L., Nanoshell-mediated near-infrared thermal therapy of tumors under magnetic resonance guidance. *Proceedings of the National Academy of Sciences of the United States of America* **2003,** 100, (23), 13549-13554.

47. O'Neal, D. P.; Hirsch Leon, R.; Halas Naomi, J.; Payne, J. D.; West Jennifer, L., Photo-thermal tumor ablation in mice using near infrared-absorbing nanoparticles. *Cancer Letters.* **2004,** 209, (2), 171-6.

48. Haes, A. J.; Zou, S.; Schatz, G. C.; Van Duyne, R. P., Nanoscale Optical Biosensor: Short Range Distance Dependence of the Localized Surface Plasmon Resonance of Noble Metal Nanoparticles. *Journal of Physical Chemistry B* **2004,** 108, (22), 6961-6968.

49. Haes, A. J.; Zou, S.; Zhao, J.; Schatz, G. C.; Van Duyne, R. P., Localized Surface Plasmon Resonance Spectroscopy near Molecular Resonances. *Journal of the American Chemical Society* **2006,** 128, (33), 10905-10914.

50. Haes, A. J.; Zou, S.; Schatz, G. C.; Van Duyne, R. P., A Nanoscale Optical Biosensor: The Long Range Distance Dependence of the Localized Surface Plasmon Resonance of Noble Metal Nanoparticles. *Journal of Physical Chemistry B* **2004,** 108, (1), 109-116.

51. Yang, W.-H.; Schatz, G. C., Discrete dipole methods for calculating surface enhanced raman intensities. *Book of Abstracts, 210th ACS National Meeting, Chicago, IL, August 20-24* **1995,** (Pt. 2), PHYS-177.

52. Haynes, C. L.; Van Duyne, R. P., Plasmon-sampled surface-enhanced Raman excitation spectroscopy. *Journal of Physical Chemistry B* **2003,** 107, (30), 7426-7433.

53. Genov, D. A.; Sarychev, A. K.; Shalaev, V. M.; Wei, A., Resonant Field Enhancements from Metal Nanoparticle Arrays. *Nano Letters* **2004,** 4, (1), 153-158.

54. Mabuchi, M.; Takenaka, T.; Fujiyoshi, Y.; Uyeda, N., Surface-enhanced Raman scattering of citrate ions adsorbed on gold sol particles. *Surface Science* **1982,** 119, (2-3), 150-8.

55. Zhu, Z.; Zhu, T.; Liu, Z., Raman scattering enhancement contributed from individual gold nanoparticles and interparticle coupling. *Nanotechnology* **2004,** 15, (3), 357-364.

56. Cao, Y. C.; Jin, R.; Nam, J.-M.; Thaxton, C. S.; Mirkin, C. A., Raman dye-labeled nanoparticle probes for proteins. *Journal of the American Chemical Society* **2003,** 125, (48), 14676-14677.

57. Frederix, F.; Friedt, J.-M.; Choi, K.-H.; Laureyn, W.; Campitelli, A.; Mondelaers, D.; Maes, G.; Borghs, G., Biosensing based on light absorption of nanoscaled gold and silver particles. *Analytical Chemistry* **2003,** 75, (24), 6894-6900.

58. Khlebtsov, N. G.; Bogatyrev, V. A.; Dykman, L. A.; Melnikov, A. G., Spectral extinction of colloidal gold and its biospecific conjugates. *Journal of Colloid and Interface Science* **1996,** 180, (2), 436-445.

59. Xie, H.; Tkachenko, A. G.; Glomm, W. R.; Ryan, J. A.; Brennaman, M. K.; Papanikolas, J. M.; Franzen, S.; Feldheim, D. L., Critical Flocculation Concentrations, Binding Isotherms, and Ligand Exchange Properties of Peptide-Modified Gold Nanoparticles Studied by UV-Visible, Fluorescence, and Time-

Correlated Single Photon Counting Spectroscopies. *Analytical Chemistry* **2003,** 75, (21), 5797-5805.

60. Nath, N.; Chilkoti, A., A colorimetric gold nanoparticle sensor to interrogate biomolecular interactions in real time on a surface. *Analytical Chemistry* **2002,** 74, (3), 504-509.

61. Matsui, J.; Akamatsu, K.; Nishiguchi, S.; Miyoshi, D.; Nawafune, H.; Tamaki, K.; Sugimoto, N., Composite of Au nanoparticles and molecularly imprinted polymer as a sensing material. *Analytical chemistry.* **2004,** 76, (5), 1310-5.

62. He, X. R.; Liu, H. B.; Li, Y. L.; Wang, S.; Li, Y. J.; Wang, N.; Xiao, J. C.; Xu, X. H.; Zhu, D. B., Gold nanoparticle-based fluorometric and colorimetric sensing of copper(II) ions. *Advanced Materials* **2005,** 17, (23), 2811-2815.

63. Pang, P. F.; Guo, J. L.; Wu, S. H.; Cai, Q. Y., Humidity effect on the dithiol-linked gold nanoparticles interfaced chemiresistor sensor for VOCs analysis. *Sensors and Actuators B-Chemical* **2006,** 114, (2), 799-803.

64. Pang, P. F.; Guo, Z. D.; Cai, Q. Y., Humidity effect on the monolayer-protected gold nanoparticles coated chemiresistor sensor for VOCs analysis. *Talanta* **2005,** 65, (5), 1343-1348.

65. Lin, T. J.; Huang, K. T.; Liu, C. Y., Determination of organophosphorous pesticides by a novel biosensor based on localized surface plasmon resonance. *Biosensors & Bioelectronics* **2006,** 22, (4), 513-518.

66. Pavlov, V.; Xiao, Y.; Willner, I., Inhibition of the Acetylcholine Esterase-Stimulated Growth of Au Nanoparticles: Nanotechnology-Based Sensing of Nerve Gases. *Nano Letters* **2005,** 5, (4), 649-653.

67. Major, J. S.; Blanchard, G. J., Covalently Bound Polymer Multilayers for Efficient Metal Ion Sorption. *Langmuir* **2001,** 17, (4), 1163-1168.

68. Kohli, P.; Rini, M. C.; Major, J. S.; Blanchard, G. J., Elucidating the balance between metal ion complexation and polymer conformation in maleimide vinyl ether polymer multilayer structures. *Journal of Materials Chemistry* **2001,** 11, (12), 2996-3001.

69. Kohli, P.; Blanchard, G. J., Design and Demonstration of Hybrid Multilayer Structures: Layer-by-Layer Mixed Covalent and Ionic Interlayer Linking Chemistry. *Langmuir* **2000,** 16, (22), 8518-8524.

70. Afanasiev, P., Zr(IV) basic carbonate complexes as precursors for new materials: synthesis of the zirconium-surfactant mesophase. *Materials Research Bulletin* **2002,** 37, (12), 1933-1940.

71. Bakiamoh, S. B.; Blanchard, G. J., Demonstration of Oriented Multilayers through Asymmetric Metal Coordination Chemistry. *Langmuir* **1999,** 15, (19), 6379-6385.

72. Katz, H. E., Multilayer Deposition of Novel Organophosphonates with Zirconium(IV). *Chemistry of Materials* **1994,** 6, (12), 2227-32.

73. Kohli, P.; Blanchard, G. J., Probing Interfaces and Surface Reactions of Zirconium Phosphate/Phosphonate Multilayers Using 31P NMR Spectrometry. *Langmuir* **2000,** 16, (2), 695-701.

74. Lee, H.; Kepley, L. J.; Hong, H. G.; Akhter, S.; Mallouk, T. E., Adsorption of Ordered Zirconium Phosphonate Multilayer Films on Silicon and Gold Surfaces. *Journal of Physical Chemistry* **1988,** 92, (9), 2597-2601.

75. Ruvarac, A.; Milonjic, S.; Clearfield, A.; Garces, J. M., On the mechanism of ion exchange in zirconium phosphates. XVIII. Effect of crystallinity upon the K+-H+ exchange of a-zirconium phosphate. *Journal of Inorganic and Nuclear Chemistry* **1978,** 40, (1), 79-85.

76. Schilling, M. L.; Katz, H. E.; Stein, S. M.; Shane, S. F.; Wilson, W. L.; Buratto, S.; Ungashe, S. B.; Taylor, G. N.; Putvinski, T. M.; Chidsey, C. E. D., Structural Studies of Zirconium Alkylphosphonate Monolayers and Multilayer Assemblies. *Langmuir* **1993,** 9, (8), 2156-2160.

Chapter 2

Formation of Gold Nanoparticles Using Amine Reducing Agents

Introduction

Amines have been reported to be useful as both reducing agents and stabilizers in the formation of AuNPs[1-6]. A wide variety of amines have been used to reduce gold salts to AuNPs including primary amines[4, 6], multifunctional amines[3], and amino acids[1, 2, 7]. They are attractive choices for reducing agents for several reasons. First, they are ubiquitous in nature and a wide variety of amine compounds are readily available commercially. Additionally, their prevalence in biological systems indicates that composite materials formed from the reduction of $HAuCl_4$ by amines may have the potential to be biologically compatible. This could be useful in potential applications of the resulting colloidal materials.

One of the earliest reports of the use of amines in the spontaneous formation of AuNPs was by Turkevich in 1951. In this instance, hydroxylamine hydrochloride was used to facilitate the reduction of $HAuCl_4$ into colloidal gold[8]. Turkevich examined much more closely the reduction of $HAuCl_4$ by citrate ions[8-11] and much of the research on AuNPs which followed used this reduction method. In the mid-1990's thiols began to emerge as stabilizing agents after a series of reports by Brust and co-workers which established organic solvent based methods, which were amenable to use with thiols[12, 13]

Amines were less examined than thiols as reducing and stabilizing agents because the amine-gold bond (bond strength ~ 6 kcal/mol[14]) is weaker than the sulfur-gold bond seen in thiol adsorption (44 kcal/mol[15]). However, in 1996, Leff reported that amine stabilized AuNPs were similar to AuNP colloids stabilized with thiols[4]. In this instance, the $HAuCl_4$ was added in aqueous solution while an alkylamine was added in toluene. The reduction was facilitated by sodium borohydride and the resulting AuNPs were found in the organic phase at reaction completion[4]. This body of work demonstrates that amines can be used to successfully stabilize AuNPs, but it was not until the early 2000's that amines began to be used as reducing agents as well as stabilizers.

In 2004, Selvakannan and co-workers reported on AuNPs formed by the spontaneous reduction of $HAuCl_4$ by tryptophan in aqueous solution at elevated temperatures, resulting in AuNPs dispersible in water[5]. UV-visible spectroscopy showed the appearance of spectral features in the region characteristic of AuNP PR. The demonstrated peak grew in intensity with reaction time and also blue shifted as the reaction neared completion[5]. This is characteristic of the growth and aggregation of AuNPs in solution. The authors in this case report that it was the indole group of the tryptophan, a secondary amine, which was singly responsible for the reduction of $HAuCl_4$, to the exclusion of the primary amine segment, glycine[5].

Aromatic amines were discussed in 2005 as reducing agents capable of forming AuNPs from $HAuCl_4$. Subramaniam and co-workers reported on the use of 2-methyl aniline, a primary amine, as a reducing and stabilizing agent in AuNP synthesis. This synthesis, like Selvakannan's, was carried out in aqueous solution at elevated temperature. In addition to the UV-visible spectrum demonstrating a PR in the

characteristic range, Subramaniam also demonstrated that the position of the PR could be blue-shifted by increasing the volume of reducing agent added to the synthetic solution[5].

In 2006, Kuo and co-workers reported on the formation of gold threads from the reduction of $HAuCl_4$ by triethylamine[16]. In this case the reduction was carried out by combining triethylamine, a tertiary amine, and $HAuCl_4$ (20-fold excess of triethylamine) in aqueous solution at room temperature. Kuo reported that a characteristic PR was also seen in the visible region of the spectrum. As expected, the PR band increased in intensity with increasing reaction time. The PR band also blue-shifted with reaction time, due to a spontaneous change in the form of the reduced gold from small spherical particles to organized gold thread structures[16].

Despite these and other reports about use of amines in the reduction and stabilization of AuNPs, most of the information about which amines are appropriate for use as reducing agents is phenomenological. Little is known about the properties which make some amines function well as reducing agents and others do not successfully reduce $HAuCl_4$. A brief overview of the types of amines which have been used reveals that primary, secondary, and tertiary amines as well as alkyl, aromatic, and aliphatic amines have all been successful. Additionally, reduction has been accomplished in organic and aqueous media. Understanding what the most important properties of a potential reducing agent are is important in gaining control and predictability over nanoparticle formation, growth, and stabilization. This study investigates the thermodynamic and kinetic factors which can be used to gain predictability over whether a given amine will function as a reducing agent for $HAuCl_4$.

Materials and Methods

Chemicals. $HAuCl_4 \cdot 3H_2O$ (99.9+%), 3-aminophenol, 4-aminophenol, triethylamine, acetone, indole, 1,4-phenlyenediamine, aniline, 4-bromoaniline, 3-indolepropionic acid, 3-amino-1-propanol, 1-methylindole, pyridine, citric acid, hydroxylamine hydrochloride, sodium citrate, D,L-tryptophan, and lithium perchlorate were purchased from Aldrich Chemical Co. and used as received. Glycine was purchased from Tyron (Okemos, MI) and used as received.

Electrochemistry. $HAuCl_4$ solutions were prepared at a concentration of 0.1 M in 0.5 M $LiClO_4$. Solutions of amines to be evaluated as reducing agents were prepared to a concentration of 0.1 - 0.5M$LiClO_4$ in either acetonitrile (MeCN) or H_2O, depending on solubility. Due to solubility limitations, D,L-tryptophan was prepared as a 0.005 M solution in 0.5 M $LiClO_4$ (aq). Cyclic voltammetry was conducted using an electrochemical bench (CH Instruments model 604B, Austin, TX) in cyclic voltammetry (CV) mode with a scan rate of 50 mV/s and a sensitivity of 10^{-5} A full scale. A standard three electrode configuration was used with a glassy carbon working electrode, a platinum wire counter electrode, and a reference electrode. The reference electrodes used were Ag/AgCl with 3 M KCl (aq) for aqueous measurements and 1 mM $AgNO_3$ (MeCN) for nonaqueous measurements. The potentials measured using the Ag/AgCl reference electrodes are reported against a standard hydrogen electrode (SHE) to facilitate comparison to reported tabular values for Au reduction potentials. Three forward and three reverse scans were recorded for each sample.

Kinetics and Stability Studies. AuNPs were synthesized by combining a 0.005 M reducing agent solution (5 mL) with a 0.005 M $HAuCl_4$ (50 *l*L) solution in the same solvent and shaking to agitate. The reducing agents used for the kinetics studies were 4-aminophenol, triethylamine, glycine, indole, 1,4-phenylenediamine, tryptophan, and sodium citrate. The solutions were combined and analyzed at room temperature, and UV-visible spectra were obtained at intervals for the resulting undiluted solution. The spectra were obtained at either 10 or 15 min intervals for up to 100 scans or until a depletion of the absorbance was noted. The duration of a given measurement was determined by the rate of the process being monitored. The spectra were acquired from 350 to 800 nm using a Cary model 300 UV-visible spectrometer (Varian) and acquisition time was ca. 1 min per spectrum. Initial rate information was extracted from the temporal dependence of the plasmon resonance absorbance band following the initial mixing of the reactants.

Results and Discussion

The purpose of these studies is threefold. The first goal is determining which amine compounds are thermodynamically capable of reducing $HAuCl_4$ to AuNPs. The second goal is to verify the ability of the amines to successfully reduce $HAuCl_4$ to form gold nanoparticles and to subsequently investigate the formation rate. The third goal is to understand any side reactions which may either compete with or facilitate the formation of AuNPs by amine reducing agents.

Electrochemistry. The formation of AuNPs occurs through an electron transfer reaction wherein electrons are transferred from the reducing agent to the Au^{3+} source. In the case

of amine reducing agents, the reduction of $HAuCl_4$ to Au_0 can be described generally by Scheme I.

$HAuCl_4 + 3\ NR_3 \rightarrow Au^0 + 3\ NR_3^{+\cdot} + H^+ + 4\ Cl^-$ (Scheme I)

The Au^0 may then undergo association with other Au^0 atoms to begin the nucleation and growth of AuNPs in the solution. The radical amine species is transient and will be either quickly quenched or act as the initiation step to a resulting polymeric species. NMR experiments suggest the presence of oligomeric species of the amine reducing agent in some cases and will be discussed in greater detail later in this chapter.

The most important information to be acquired from electrochemical measurements is the determination of whether the reaction shown in Scheme I is thermodynamically allowed. This can be derived through comparison of the oxidation potential of a given amine with the reduction and oxidation potentials of the $HAuCl_4$ and Au^0 in solution. Evaluation of $HAuCl_4$ in both aqueous and MeCN solution shows oxidation and reduction potentials present. In aqueous solution the reduction potential of $HAuCl_4$ to Au^0 was found to be 0.853V (vs SHE) and the oxidation potential of Au^0 to Au^{1+} was found to be 1.425 V (vs SHE), in 0.5 M $LiClO_4$ solution. In MeCN the reduction potential of $HAuCl_4$ to Au^0 was found to be 0.888 V (vs SHE) and the oxidation potential of Au^0 to Au^{1+} was found to be 1.555 V (vs SHE), in 0.5 M $LiClO_4$ solution (Figure 2.1, panels a and b, respectively).

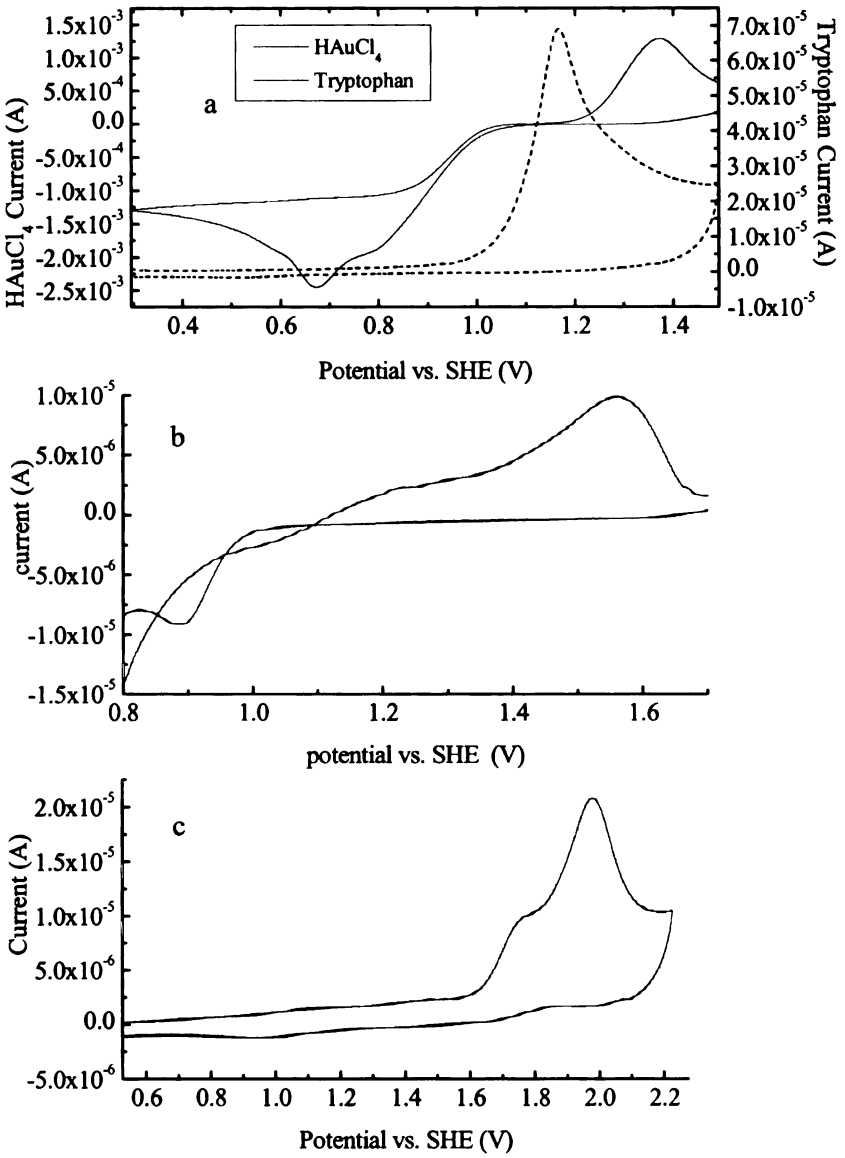

Figure 2.1. a) Comparison between the CV of $HAuCl_4$ (solid line) and tryptophan (dashed line) in aqueous 0.5 M $LiClO_4$ electrolyte b) CV of $HAuCl_4$ 0.5 M $LiClO_4$ electrolyte (MeCN) and c) CV of pyridine in 0.5 M $LiClO_4$ (MeCN).

These oxidation and reduction potentials represent the upper and lower boundaries for the oxidation potential of the amines examined in this work (Figure 2.2).

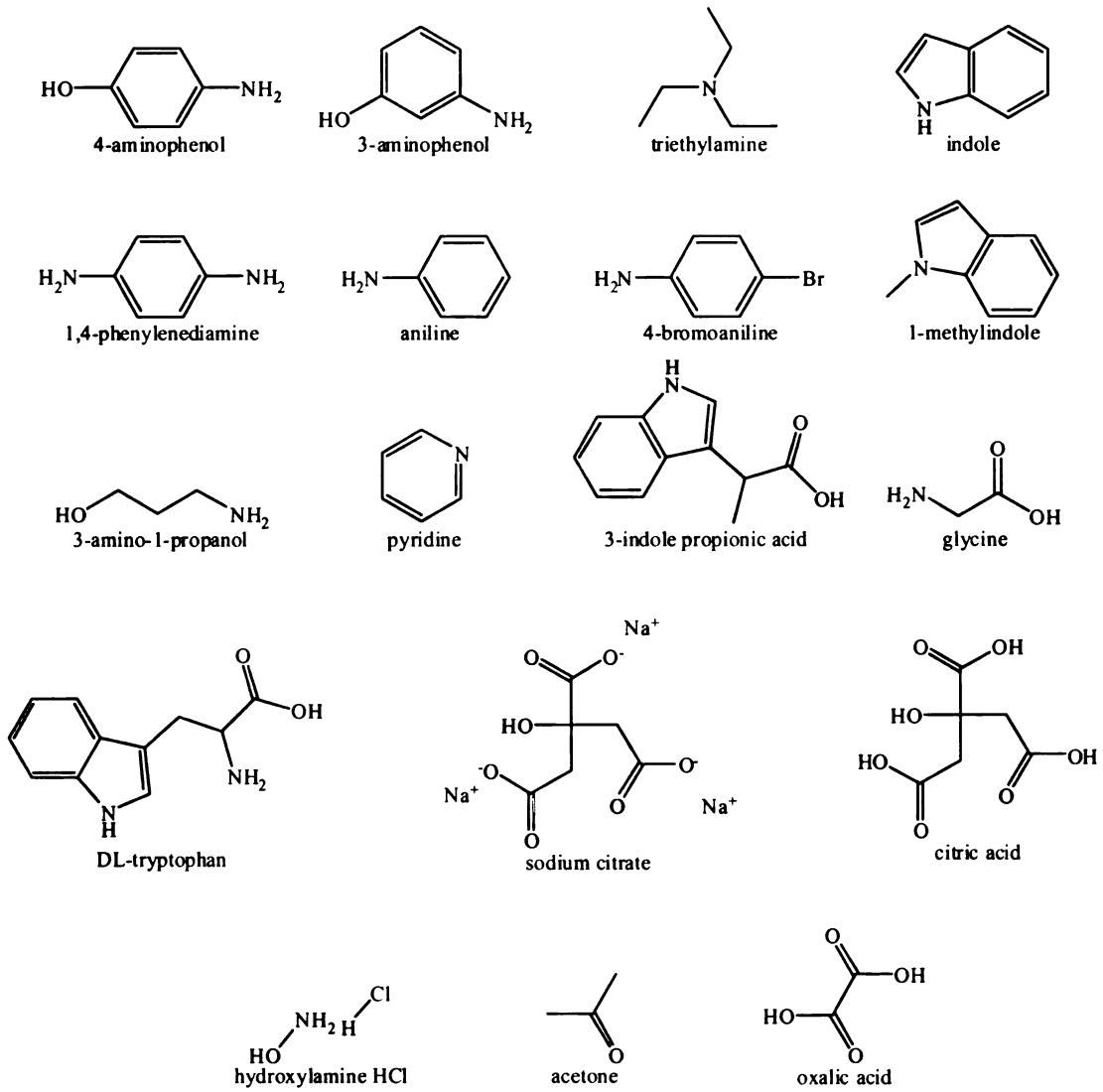

Figure 2.2. Structures of reducing agents examined in this work

In these systems the reduction of $HAuCl_4$ to Au^0 in the form of AuNPs is irreversible, as is the conversion of the amine to its corresponding oxidized product. For this reason, a comparison will be made between the reduction and oxidation potentials of the gold solution and the oxidation potentials of the amine species. The first requirement for the reduction reaction to proceed is for the oxidation potential of the amine to be greater than

the reduction potential of the $HAuCl_4$ and less than the oxidation potential of Au^0 in the same solvent system (Figure 2.1a). When the oxidation potential of the amine is lower than that observed for the $HAuCl_4$, AuNPs are not expected because the reaction will not proceed spontaneously. Conversely, if the oxidation potential of the amine is greater than that observed for the oxidation of Au^0 to Au^{1+}, AuNPs would not be expected to form as the Au^0 would be oxidized before the amine. This is the case for pyridine (Figure 2.1, panels b and c). For the non-amine reducing agents previously reported to spontaneously form AuNPs without additional reducing agents (eg. acetone, citric acid, and sodium citrate)[8], the oxidation potential was shown to fall between the $HAuCl_4$ reduction potential and the Au^0 oxidation potential and were therefore allowed under thermodynamic arguments. Follow-up experiments on those amines not thermodynamically anticipated to form AuNPs verifies that AuNPs do not form spontaneously. Of the amines studied here, only 3-amino-1-propanol, 1-methylindole, and pyridine are thermodynamically disallowed (Table 2.1).

Amine	Solvent	Concentration (M)	Oxidation Potential (V)
3-aminophenol	MeCN	0.1	1.021
4-aminophenol	MeCN	0.1	1.062
Triethylamine	MeCN	0.1	1.079
Glycine	H_2O	0.1	1.112
4-bromoaniline	MeCN	0.1	1.122
Indole	MeCN	0.1	1.129
1,4-phenylenediamine	MeCN	0.1	1.160
Aniline	MeCN	0.1	1.183
DL-tryptophan	H_2O	.005	1.283
3-indolepropionic acid	MeCN	0.1	1.308
3-amino-1-propanol	MeCN	0.1	1.589
1-methylindole	MeCN	0.1	1.641
Pyridine	MeCN	0.1	1.980

Table 2.1. Oxidation potentials of amines in a 0.5 M $LiClO_4$ electrolyte solution

There are, however, several amines which are thermodynamically predicted to reduce $HAuCl_4$ to AuNPs which do not, experimentally, function as reducing agents. Specifically, these are 3-aminophenol (oxidation potential 1.012 V vs SHE), aniline (oxidation potential 1.183 vs SHE), and 4-bromoaniline (1.112 V vs SHE). The reason for the failure of these amines to function as reducing agents is due to competitive polymerization effects and will be discussed in more detail later in this chapter.

It is clear from this data that the oxidation potential of an amine, or any potential reducing agent, can be used to quickly screen out compounds which will not, on thermodynamic grounds, function as agents to reduce $HAuCl_4$ to AuNPs. However, control of the redox reaction needs to also be understood from a kinetics standpoint to be able to gain control over the formation of AuNP colloids.

AuNP Growth Kinetics. The presence of a characteristic PR band in the visible spectrum is indicative of the presence of AuNPs in a solution. As such, the growth rate of the PR band can be used to examine the growth of the AuNPs in a given system. In these studies, the amine and $HAuCl_4$ were added as 0.005 M solutions in either MeCN or water with the amine in 100-fold excess. As noted previously, the position and shape of the PR band are dependent on the particle size, degree of particle aggregation, and solvent system[17]. In these experiments, AuNP-forming systems which demonstrated a PR showed an increase in the absorbance but did not show significant variation in either position or shape with time. Depending on the system the PR centered at either 530 nm or 560 nm but did not vary significantly in time. While the reduction process involves both the reduction of Au^{3+} and the formation of AuNPs, the spectral data used for growth determination is strictly probing the presence of AuNPs in the system.

The initial rates were determined from the linear portion of a maximum PR absorbance versus time plot. The initial rates calculated ranged across several orders of magnitude (Table 2.2).

Reducing Agent	Oxidation Potential (V)	Rate (AU/min)
4-aminophenol	1.062	$3.4x10^{-3}$
Triethyl amine (TEA)	1.079	$6.6x10^{-4}$
Glycine	1.112	$2.5x10^{-5}$
Indole	1.129	$5.9x10^{-6}$
1,4-phenylenediamine	1.160	$2.8x10^{-3}$
Tryptophan	1.283	$8.2x10^{-4}$
Sodium citrate	1.271	$6.1x10^{-5}$

Table 2.2. Summary of kinetic data from UV-visible spectroscopy.

Within groups of amines with the same number of nitrogens, there is a general trend toward an increasing oxidation potential corresponding to a decrease in the AuNP PR growth rate. However, due to limited data for most multiple nitrogen systems, the single amine data will be the only data set more closely examined. In the instance of amines with a single nitrogen per reducing agent molecule, the rate of AuNP formation was found to decrease exponentially with increasing oxidation potential (Table 2.2 and Figure 2.3).

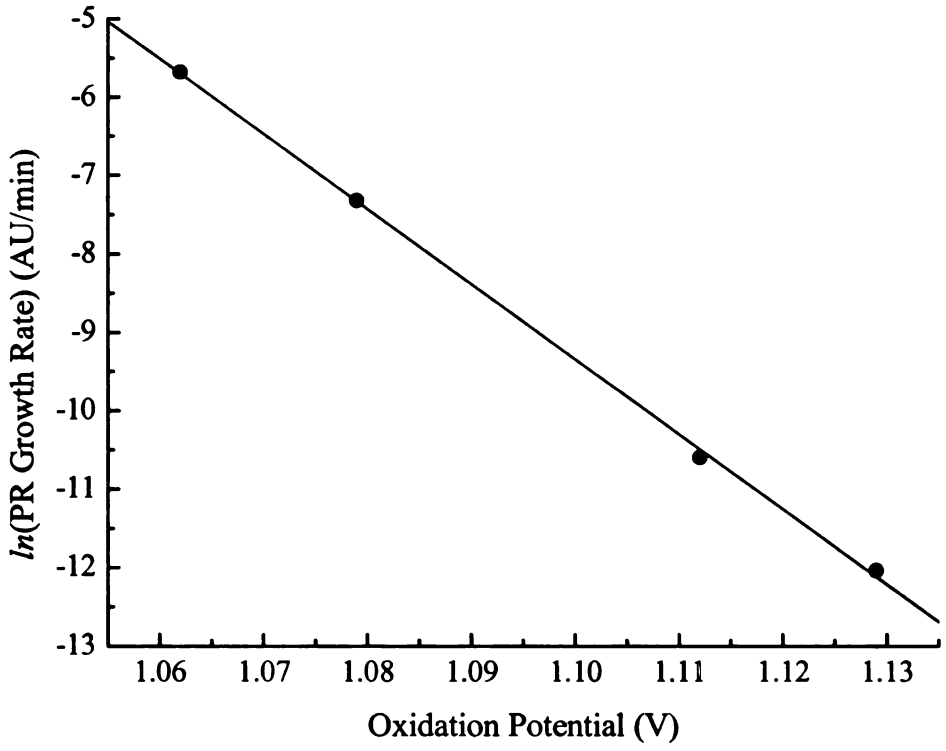

Figure 2.3. Relationship between oxidation potential and initial growth rate when one nitrogen is present per mole reducing agent.

This rate decrease with increasing difference between the reduction potential of $HAuCl_4$ and the oxidation potential of the amine is indicative of the system operating in the Marcus inverted region as understood in Marcus electron transfer theory[18-21].

Marcus electron transfer theory operates under the assumption that an electron transfer event is occurring on a much faster time scale than any structural rearrangement which results from the reaction. To understand this, it is useful to think of the process in terms of the Franck-Condon principle, wherein an increase in the difference between the potential energy minima of the reactant and product results in an increase of the electron transfer rate. This relationship is expected to hold true until the product energy curve passes through the energy minima of the reactant curve. This is the point where the

optimum electron transfer rate is achieved, and the reaction proceeds essentially without barrier. After this point is passed, increasing the energy difference between the two results in a decrease in the electron transfer rate. Within the context of a solvent environment this decrease is caused by the necessity of a sufficiently large structural difference necessitating a change in either the solvation environment or molecular structure. These changes serve to slow down the electron transfer kinetics under these electronic conditions. Here, we can consider the reactant and the product energy curves to correspond to the oxidation potential of the amine and the reduction potential of the $HAuCl_4$, respectively. Using the aforementioned logic, the onset of reduction of $HAuCl_4$ by an amine reducing agent occurs at the point when the amine oxidation and $HAuCl_4$ reduction potential are equal. The rate at this point is slow but increases with increasing difference between the oxidation and reduction potentials. At some oxidation-reduction potential combination, the optimum electron transfer rate is achieved. Beyond this point, the kinetics of the reduction reaction decrease. This region is known as the Marcus inverted region. The decrease continues until the amine oxidation potential exceeds the Au^0 oxidation potential. At this point, the reduction of $HAuCl_4$ by the amine is no longer thermodynamically viable. From the data obtained for the series of reducing agents examined in this study, the decrease in PR growth rate with increasing oxidation potential indicate that the $HAuCl_4$-amine redox system, and consequently the AuNP growth, is operating in the Marcus inverted region.

Competitive Polymerization of the Reducing Agent. As previously noted, there are several amines which are predicted on thermodynamic grounds to form AuNPs which do not show significant, if any, spectral evidence of a PR. Specifically, the solutions of

anline, 3-aminophenol, and 4-bromoaniline do not react to form AuNPs, despite oxidation potentials in the thermodynamically allowed region. In the instance of aniline and 3-aminophenol, this is likely due to polymerization of the reducing agent[22, 23] which competes with $HAuCl_4$ reduction. This does not mean that no Au^0 is formed, but rather that no significant nucleation to AuNPs occurs, and therefore no PR is observed. In these systems, AuNPs may be formed during amine monomer oxidation and then oxidized during the polymerization process, if the reaction rates of $HAuCl_4$ reduction and polymerization are significantly different, or Au^0 may be formed but never undergo nucleation due to similarity in rates of the the Au^{3+} reduction and reducing agent polymerization.

Aniline and 3-aminophenol show similar time-resolved spectral profiles. The CV obtained for aniline shows an oxidation peak at 1.183 V (vs SHE) with a second broad peak after the initial oxidation (Figure 2.4).

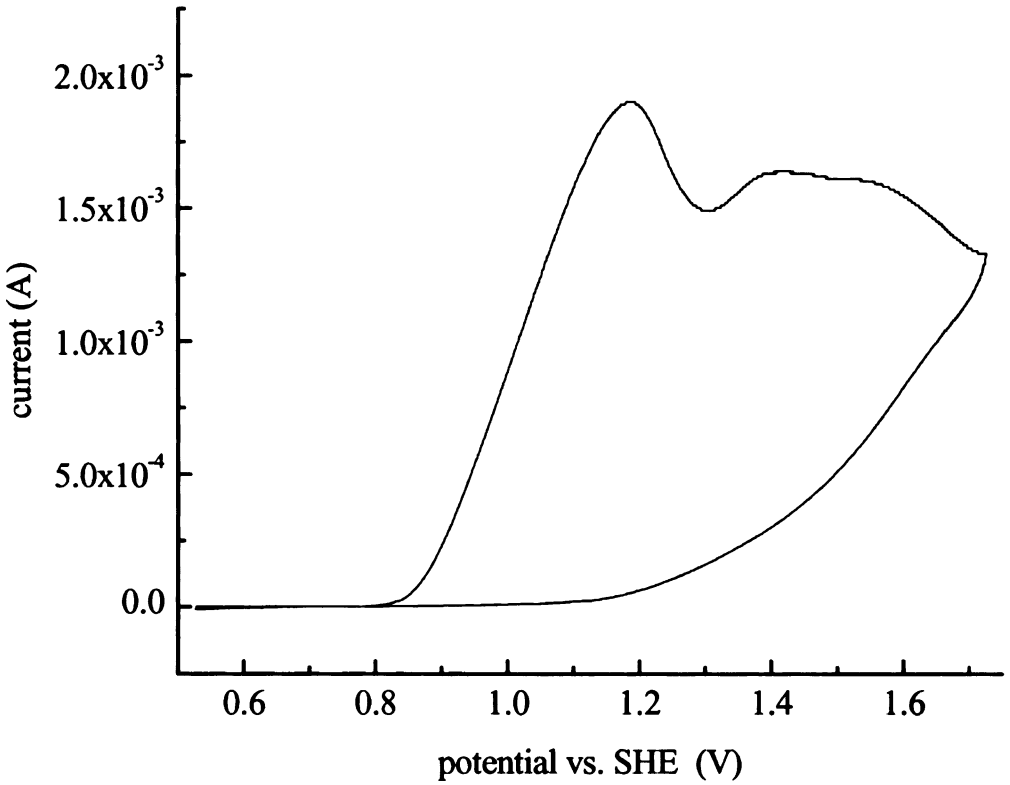

Figure 2.4. CV of aniline in 0.5 M $LiClO_4$ (MeCN).

The second broad peak is indicative of a radical initiated polymerization resultant from aniline oxidation. This oxidative polymerization has been reported in the literature[22] when aniline is present in solution with an oxidizing agent. The ^1H NMR of the aniline sample after CV was conducted, shows evidence of a downfield shift and slight peak broadening (Figure 2.5), which is typical of oligomerization or polymerization events.

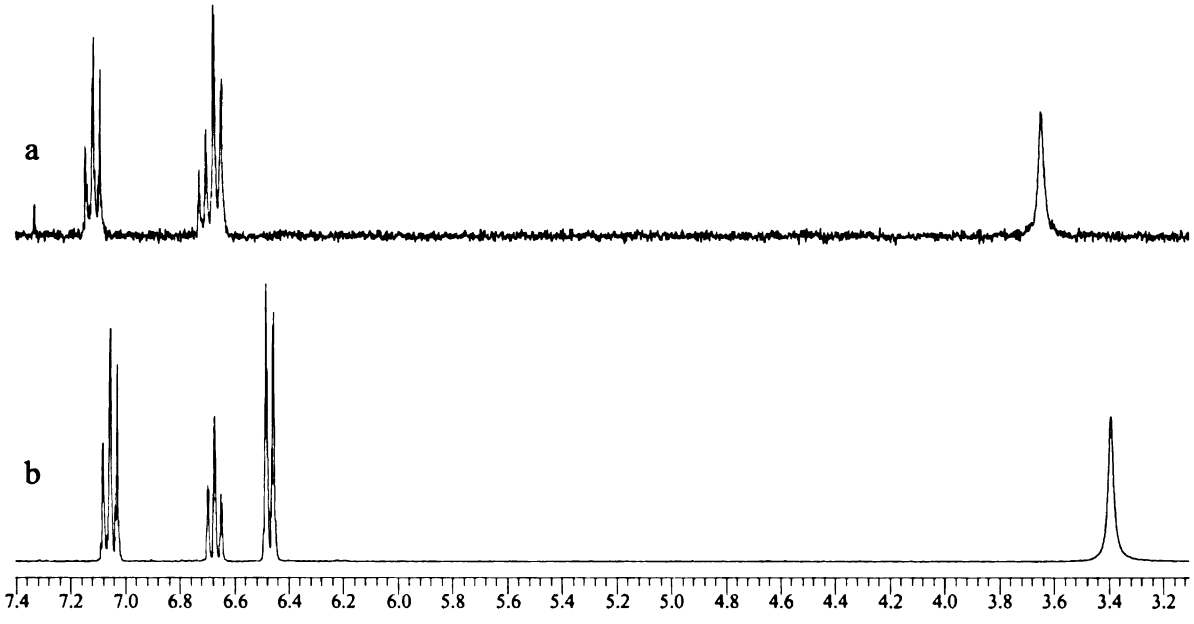

Figure 2.5. . ^{1}H NMR in $CDCl_3$ for a) aniline after completion of electrochemistry and b) prior to electrochemical oxidation.

Additionally, the time-resolved UV-visible spectrum indicates the development of a peak in the 410 nm range (Figure 2.6) which is consistent with literature reports for the spectrum of polymerized aniline.[24]

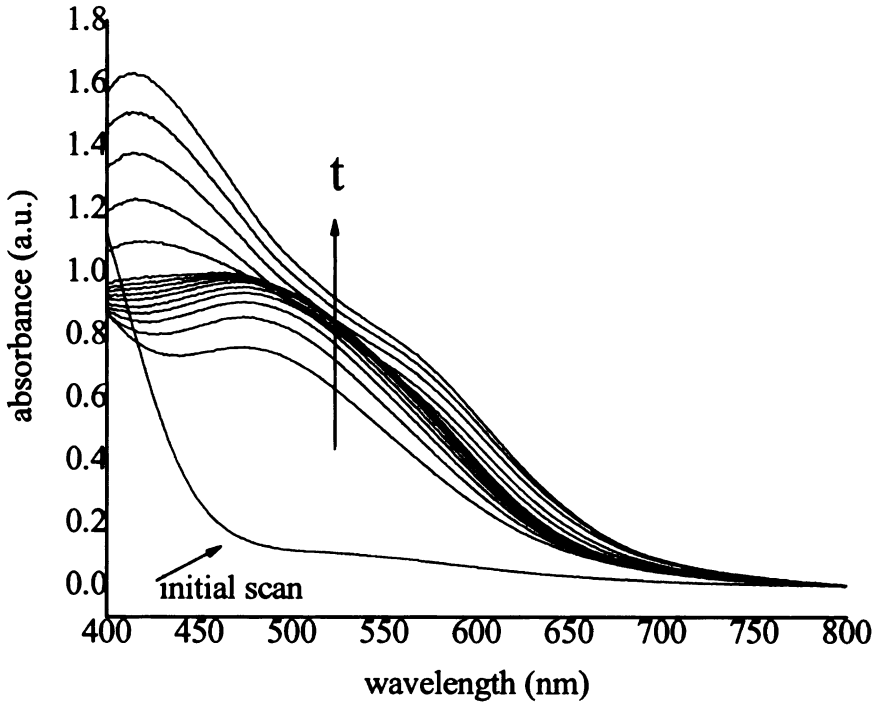

Figure 2.6. Time resolved US-visible spectrum of 100:1 0.005 M aniline-0.005 M $HAuCl_4$ conversion to poly(aniline).

Similar features are observed in the CV and time-resolved UV-visible spectrum of 3-aminophenol (Figure 2.7 a and b, respectively), indicating a similar competitive polymerization mechanism for this reducing agent as well.

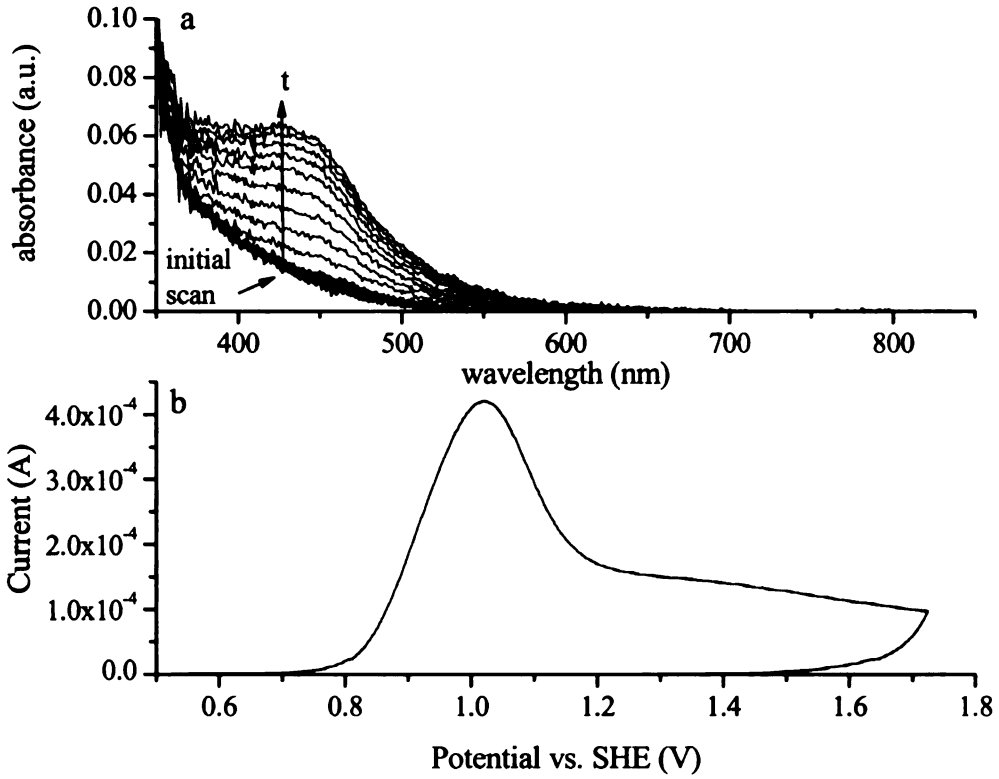

Figure 2.7. a) CV and b) UV-vis of 3-aminophenol

4-aminophenol is a case where both AuNP formation and polymerization are observed. This is due to the kinetics of $HAuCl_4$ being different from the polymerization kinetics. The PR growth rate determined for AuNPs reduced and stabilized with 4-aminophenol was the fastest for any reducing agent studied. However, the AuNPs resulting were the least stable of any successful system. As enzymatic and electrochemical polymerization of 4-aminophenol has literature precedent[23, 25, 26] with the resulting poly(4-aminophenol) being electroactive, the polymerization and resulting polymer are likely both the source of the AuNP formation and the instability of the resulting colloid. The initial reduction of $HAuCl_4$ and subsequent nucleation and growth

of AuNPs occurs on a faster time scale than the radical initiated polymerization of 4-aminophenol. However, the polymeric reducing agent exists in both oxidized and reduced form. Thus, the reduction of the polymer in solution results in the oxidation of the AuNPs. As Au^{1+} is the most stable Au ion, the AuNPs are in equilibrium in this system with Au^{1+}, not Au^{3+}. To examine this system in greater detail Au was added to 4-aminophenol in the form of both $HAuCl_4$ (Au^{3+}) and Au^0. 4-aminophenol demonstrates spectral growth characteristic of polymerization (Figure 2.8, panels a and b), with the band around 500nm (Figure 2.8, panel a) indicative of AuNP formation and the band at approximately 375 being associated with polymer growth.

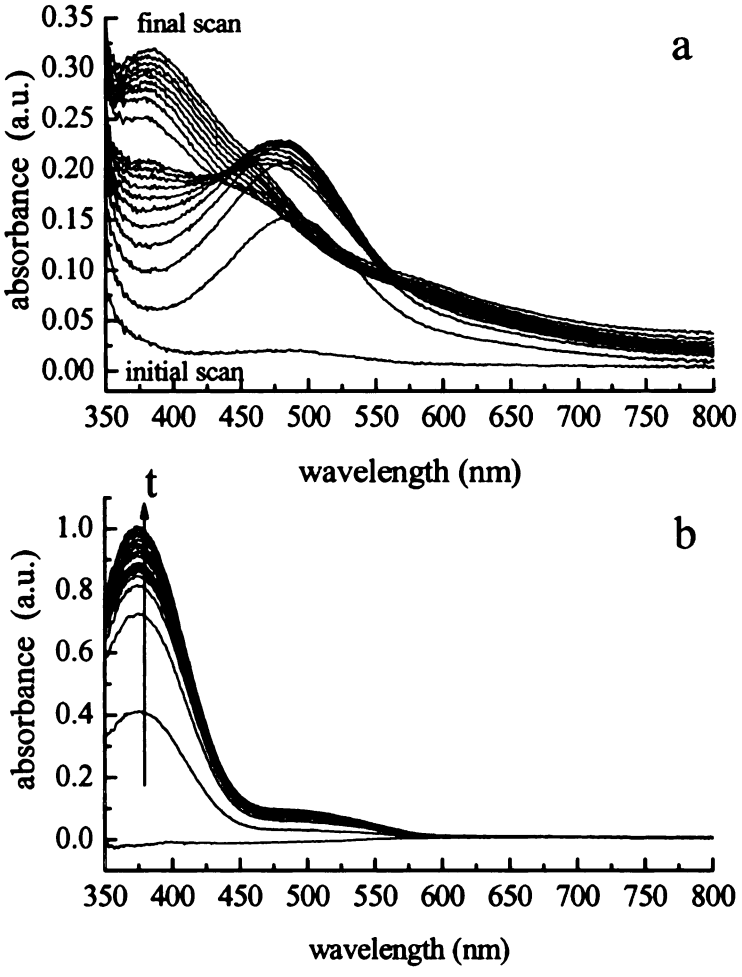

Figure 2.8. UV-visible spectrum of a) 100:1 0.005 M 4-aminophenol-0.005 M $HAuCl_4$ and b) excess Au^0 and 0.005 M 4-aminophenol conversion to poly(4-aminophenol).

The disappearance of the AuNP peak in the case of the $HAuCl_4$-4-aminophenol system is due to the oxidized and reduced forms of poly(4-aminophenol) reaching an equilibrium with Au^0 and Au^{1+} in the solution.

Conclusion

The oxidation potential of a potential amine reducing agent can be compared to the reduction and oxidation potentials of $HAuCl_4$ and Au^0, respectively, to determine the

thermodynamic feasibility of the amine functioning as a reducing agent for the formation of AuNPs from $HAuCl_4$. This provides a first line of predictability to determine the ability of a given compound to reduce $HAuCl_4$ to Au^0 with subsequent formation of AuNPs. Amines that have oxidation potential that lies between the reduction potential of $HAuCl_4$ to Au^0 and the oxidation potential of Au^0 to Au^{1+}, are candidate reducing agents. This method can be used for initial screening of potential reducing agents. Amines with oxidation potentials outside this range will not react with the $HAuCl_4$ to form AuNPs. In some cases, however, the amines may undergo polymerization which competes with AuNP formation, so the electrochemical measurement can only be used to determine thermodynamic feasibility.

The kinetics of the oxidation and reduction reactions also play a large role in AuNP formation in amine-$HAuCl_4$ systems. At room temperature, thermodynamically predicted amines with the same number of nitrogens per reducing agent unit, where AuNPs are observed in the UV-visible spectrum, show an exponential decrease in the PR growth rate with increasing oxidation potential. This can be understood in the context of Marcus electron transfer theory where the kinetics indicate the redox reactions are taking place in the Marcus inverted region. In the instance of amines which undergo polymerization under the reaction conditions the relative kinetics of the reducing agent and $HAuCl_4$ determine whether AuNPs will be observed. In the case of aniline and 3-aminophenol, the polymerization of the reducing agents takes place faster than the formation of AuNPs and therefore no AuNPs are observed spectroscopically. In the case of 4-aminophenol, the kinetics of the reduction of $HAuCl_4$ to AuNPs and the

polymerization of the amine are similar and both AuNPs and poly(4-aminophenol) are observed in the time-resolved spectrum.

Taken together the thermodynamic information gained from electrochemical measurements and the kinetic information from the time-resolved UV-visible spectroscopy can be useful to make some predictions about reasonable reducing agents for $HAuCl_4$ and to begin to understand how control can be gained over the reduction process.

References

1. Aslam M, Fu L, Su M, Vijayamohanan K, Dravid VP. Novel one-step synthesis of amine-stabilized aqueous colloidal gold nanoparticles. *Journal of Materials Chemistry.* 2004;14(12):1795-1797.

2. Bhargava SK, Booth JM, Agrawal S, Coloe P, Kar G. Gold Nanoparticle Formation during Bromoaurate Reduction by Amino Acids. *Langmuir.* 2005;21(13):5949-5956.

3. Iwamoto M, Kuroda K, Zaporojtchenko V, Hayashi S, Faupel F. Production of gold nanoparticles-polymer composite by quite simple method. *European Physical Journal D: Atomic, Molecular and Optical Physics.* 2003;24(1-3):365-367.

4. Leff DV, Brandt L, Heath JR. Synthesis and Characterization of Hydrophobic, Organically Soluble Gold Nanocrystals Functionalized with Primary Amines. *Langmuir.* 1996;12(20):4723-4730.

5. Selvakannan PR, Mandal S, Phadtare S, et al. Water-dispersible tryptophan-protected gold nanoparticles prepared by the spontaneous reduction of aqueous chloroaurate ions by the amino acid. *Journal of Colloid and Interface Science.* 2004;269(1):97-102.

6. Subramaniam C, Tom RT, Pradeep T. On the formation of protected gold nanoparticles from AuCl-4 by the reduction using aromatic amines. *Journal of Nanoparticle Research.* 2005;7(2-3):209-217.

7. Selvakannan PR, Mandal S, Phadtare S, Pasricha R, Sastry M. Capping of Gold Nanoparticles by the Amino Acid Lysine Renders Them Water-Dispersible. *Langmuir.* 2003;19(8):3545-3549.

8. Turkevich J, Stevenson PC, Hillier J. The nucleation and growth processes in the synthesis of colloidal gold. *Discussions of the Faraday Society.* 1951;No. 11:55-75.

9. Turkevich J, Stevenson PC, Hillier J. The formation of colloidal gold. *Journal of Physical Chemistry.* 1953;57:670-673.

10. Enustun BV, Turkevich J. Coagulation of colloidal gold. *Journal of the American Chemical Society.* 1963;85(21):3317-3328.

11. Fry FH, Hamilton GA, Turkevich J. Kinetics and mechanism of hydrolysis of tetrachloroaurate(III). *Inorganic Chemistry.* 1966;5(11):1943-1946.

12. Brust M, Fink J, Bethell D, Schiffrin DJ, Kiely C. Synthesis and reactions of functionalized gold nanoparticles. *Journal of the Chemical Society, Chemical Communications.* 1995(16):1655-1656.

13. Brust M, Walker M, Bethell D, Schiffrin DJ, Whyman R. Synthesis of thiol-derivatized gold nanoparticles in a two-phase liquid-liquid system. *Journal of the Chemical Society, Chemical Communications.* 1994(7):801-802.

14. Pong BK, Lee JY, Trout BL. First principles computational study for understanding the interactions between ssDNA and gold nanoparticles: Adsorption of methylamine on gold nanoparticulate surfaces. *Langmuir.* Dec 2005;21(25):11599-11603.

15. Dubois LH, Nuzzo RG. Synthesis, Structure, and Properties of Model Organic-Surfaces. *Annual Review of Physical Chemistry.* 1992;43:437-463.

16. Kuo P-L, Chen C-C. Generation of gold thread from Au(III) and triethylamine. *Langmuir.* 2006;22(18):7902-7906.

17. Leff DV, Ohara PC, Heath JR, Gelbart WM. Thermodynamic Control of Gold Nanocrystal Size: Experiment and Theory. *Journal of Physical Chemistry.* 1995;99(18):7036-7041.

18. Marcus RA. The theory of oxidation-reduction reactions involving electron transfer. I. *Journal of Chemical Physics.* 1956;24:966-978.

19. Marcus RA. Electrostatic free energy and other properties of states having nonequilibrium polarization. I. *Journal of Chemical Physics.* 1956;24:979-989.

20. Marcus RA. The theory of oxidation-reduction reactions involving electron transfer. III. Applications to data on the rates of organic redox reactions. *Journal of Chemical Physics.* 1957;26:872-877.

21. Marcus RA. The theory of oxidation-reduction reactions involving electron transfer. II. Applications to data on the rates of isotopic exchange reactions. *Journal of Chemical Physics.* 1957;26:867-871.

22. Mallick K, Witcomb MJ, Dinsmore A, Scurrell MS. Polymerization of aniline by auric acid: formation of gold decorated polyaniline nanoballs. *Macromolecular Rapid Communications.* 2005;26(4):232-235.

23. Shan J, Han L, Bai F, Cao S. Enzymatic polymerization of aniline and phenol derivatives catalyzed by horseradish peroxidase in dioxane(II). *Polymers for Advanced Technologies.* 2003;14(3-5):330-336.

24. Kogan YL, Davidova GI, Knerelman EI, et al. Kinetic peculiarities of chemical aniline polymerization. *Synthetic Metals.* 1991;41(3):887-890.

25. Salavagione HJ, Arias-Pardilla J, Perez JM, et al. Study of redox mechanism of poly(o-aminophenol) using in situ techniques: evidence of two redox processes. *Journal of Electroanalytical Chemistry.* 2005;576(1):139-145.

26. Taj S, Ahmed MF, Sankarapapavinasam S. Poly(para-aminophenol): a new soluble, electroactive conducting polymer. *Journal of Electroanalytical Chemistry.* 1992;338(1-2):347-352.

Chapter 3

Polymeric Amine Reducing Agent

Introduction

The unique properties of AuNPs make them of interest to materials chemistry. However, in order to harness their optical and electronic properties, it is necessary to incorporate AuNPs into a stable and usable matrix. AuNPs have previously been incorporated into a variety of materials used for chemical sensing and separations[1-11] and medical applications[12-15] including as potential tools in the diagnosis and treatment of some types of tumors[16-19]. Use of AuNPs in the medical field requires not only that AuNPs be stable and easy to incorporate into a matrix, it also requires that matrix be bio-compatible. As such it would be useful to have AuNPs which are reduced, stabilized and incorporated into a matrix in a single step.

To date, AuNPs have been incorporated into matrices in several ways. AuNPs have been suspended in solutions and then physically deposited onto substrates of interest[4, 9]. There are several problems with this type of substrate fabrication. First, the AuNPs are not actually dissolved in solution but are instead suspended. This requires the AuNPs meet two requirements. First, the particles must be able to be stably suspended in the necessary solvent. Secondly, the suspension in the solvent must not result in any undesired particle aggregation. Additionally, simply physisorbing the particles to the substrate is not ideal due to the weak interactions holding the particles to the surface. A

more promising way to create AuNP materials is to directly incorporate the AuNPs into a polymer matrix. This has been previously carried out in limited ways where the AuNPs are imbedded into polymer films subsequent to formation[7, 8, 10]. The post reduction addition of AuNPs to polymer films has some problems, especially the polymer matrix itself providing a stable but accessible environment for the AuNPs. A better method of incorporation of AuNPs in a polymer matrix is to utilize the matrix to reduce $HAuCl_4$ to AuNPs in situ. This study addresses the reduction of $HAuCl_4$ by the amine moiety in poly(allylamine hydrochloride) (PAH) as well as the ability to gain control over the PR resonance of the AuNPs in the resulting composite materials.

As discussed in the previous chapter, since the year 2000 amines, and especially amino acids, have been reported as functioning as reducing and stabilizing agents in AuNP forming systems[20, 21] leading to stable water soluble AuNP suspensions. This methodology has been extended to use larger macromolecules, dendrimers, and polymeric systems for reduction of $HAuCl_4$ and stabilization of the resulting AuNPs[22-31]. AuNPs have also begun to be formed directly in polymer matrices[30, 32-34]. Work by Iwamoto[33] showed that the amine functionality in an amine-terminated poly(ethylene oxide) system was the moiety responsible for reduction of $HAuCl_4$. However, this study did not address the potential control over the PR position of the resulting matrices and required extensive heating as the polymer itself was also the solvent matrix.

This study addresses the benefits of growth of AuNPs in a PAH matrix. These benefits may include enhanced nanoparticle stability, control over growth rate, and control over resulting PR. The structurally simple PAH is a useful analog for more

complex systems and can also be used to begin to understand, in greater detail, the mechanism of the reduction of $HAuCl_4$ by amines.

Materials and Methods

Chemicals. Hydrogen tetrachloroaurate trihydrate ($HAuCl_4 \cdot 3H_2O$) and poly(allylamine hydrochloride (PAH) were obtained from Sigma-Aldrich (Milwaukee, WI) and used as received.

PAH-AuNP Synthesis. PAH-AuNP composites were made by combining an aqueous solution of the polymer with an aqueous solution of $HAuCl_4$ under temperature conditions dictated by either the kinetics experiments or the equilibrium plamson resonance experiments. Room temperature kinetics studies were carried out in aqueous solution in molar ratios ranging between 50:1 and 1000:1 PAH-$HAuCl_4$. Concentration dependence studies were carried out on aqueous solutions in the concentration range of 0.001M to 0.1M PAH and $HAuCl_4$. For elevated temperature studies PAH and $HAuCl_4$ were combined in mass ratios ranging from ~50:1 PAH:$HAuCl_4$ to ~775:1 PAH:$HAuCl_4$, corresponding to mole ratios between ~1.3:1 and ~20.4:1. Solutions were diluted with distilled water to make them ~10^{-3} M in the polymer. The polymer concentration was made the same for all solutions in order to maintain approximately constant viscosity. These solutions were stirred in air at 95°C for 45 minutes. Following the reduction of $HAuCl_4$, the solutions were cooled and stored at room temperature in clear glass vials. The solutions were stable at room temperature for more than one month, with no visible evidence of AuNP precipitation.

Spectroscopy of PAH-AuNP composite. UV-visible spectra of the solutions for kinetics studies were obtained undiluted. UV-visible spectra of the aqueous polymer-AuNP composites were obtained on samples that had been diluted to 1/3 of their original concentration. Absorbance spectra were acquired from 700 nm to 300 nm a Cary 300 UV-visible spectrometer (Varian). ^{1}H NMR spectra were obtained in D_2O using a Varian Inova-300 MHz NMR spectrometer.

TEM Imaging. TEM samples were prepared by drying a drop of the aqueous composite solution on TEM grids in air. Images of the resulting samples were collected using a JEM-100CX transmission electron microscope operated at 100kV accelerating potential. The images were collected digitally using Soft-Image-System MegaViewIII.

Results and Discussion

Room temperature kinetics and growth. As discussed previously, amine moieties can be used as agents for the reduction of $HAuCl_4$ into AuNPs. Here, PAH is used as the reducing agent and while the kinetics of this formation process are expected to differ from monomeric amine reducing agents, this approach to AuNP formation is important because it allows direct incorporation of AuNPs into a water-soluble polymer matrix. This can be taken advantage of from a materials chemistry standpoint because the polymer can then be utilized within the framework of well-developed layer deposition methodologies.

If the reduction of $HAuCl_4$ to Au^0 occurs by the proposed mechanism (Scheme I), the reduction requires the presence of three nitrogen atoms to reduce a single Au^{3+} ion.

$HAuCl_4 + 3\ NR_3 \rightarrow Au^0 + 3\ NR_3^{+\cdot} + H^+ + 4\ Cl^-$ (Scheme I)

The resulting AuNP imbedded in PAH may appear as seen in Figure 3.1, although the exact nature of the composite is unknown.

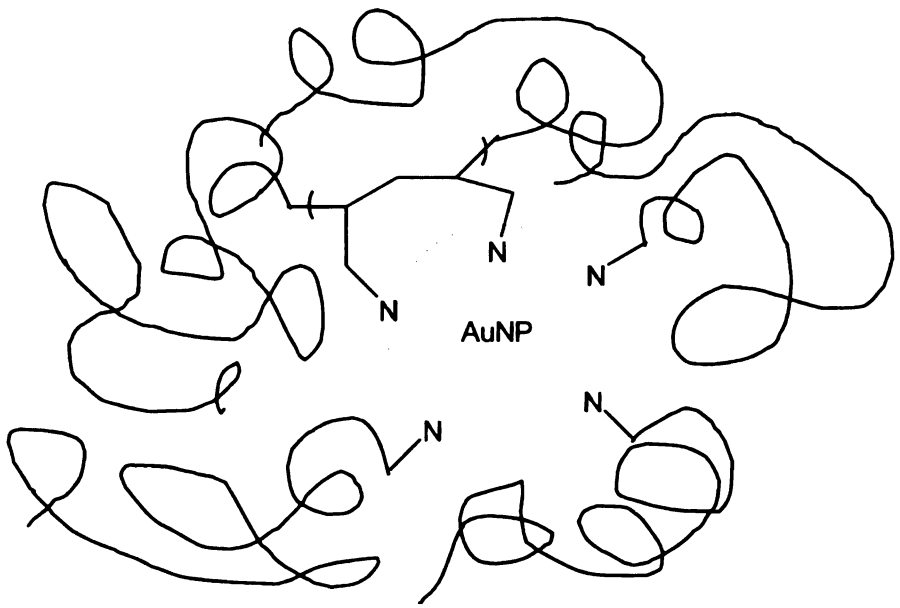

Figure 3.1 AuNP imbedded in PAH matrix

When the ratio of polymer to $HAuCl_4$ is small, while there is still an excess of amine groups present, there is a comparatively low concentration of reducing agent as compared to higher polymer:$HAuCl_4$ ratio systems. This would be expected to manifest itself in formation of many smaller AuNPs as the nucleation and growth processes occur competitively. When the polymer:$HAuCl_4$ ratio increases, the growth processes become more efficient, leading to larger particles at the completion of the reaction. This is consistent with other groups which have found the initial ratio of stabilizer-to-Au^{3+} can be manipulated to effect changes in the final AuNP size[33, 35, 36].

To probe the behavior of this system, the concentration of the PAH was held relatively constant to control the systems viscosity, while the $HAuCl_4$ concentration was varied. Molar ratios of 50:1 to 1000:1 PAH:$HAuCl_4$ were used. The solutions were

mixed immediately before beginning UV-visible absorbance scans. At these ratios, increasing the concentration of $HAuCl_4$ in the reaction mixture led to an increase in the PR growth rate. The kinetics of this system was shown to be first order in [$HAuCl_4$] (Figure 3.2).

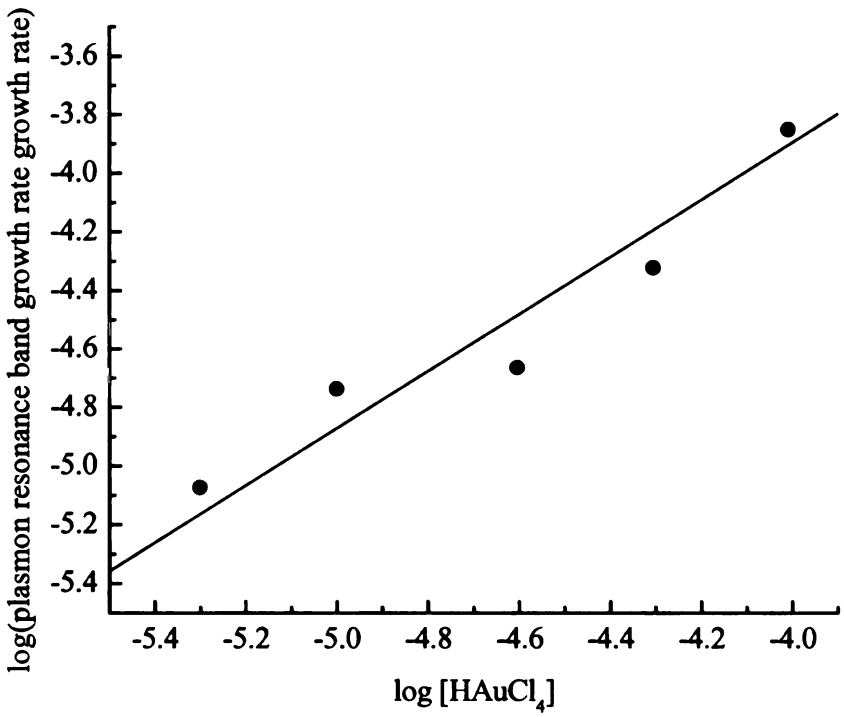

Figure 3.2. First order plot of the dependence of the plasmon resonance band growth rate on the concentration of $HAuCl_4$ for nominally constant PAH concentration. The line is a calculated best-fit, with the slope being 0.86 log(a.u.)/log(M $HAuCl_4$) (1.39 a.u./M $HAuCl_4$).

The growth kinetics of this system was also explored with respect to changing the concentration of PAH. In this case PAH was prepared in solutions ranging from 0.001-0.05 M. The 0.05 M solution was the upper limit of PAH solubility in water at room temperature. The molar ratio of PAH:$HAuCl_4$ was maintained throughout at 100:1. The PR growth rate scaled to the third power in the range of 0.001-0.03 M PAH (Figure 3.3).

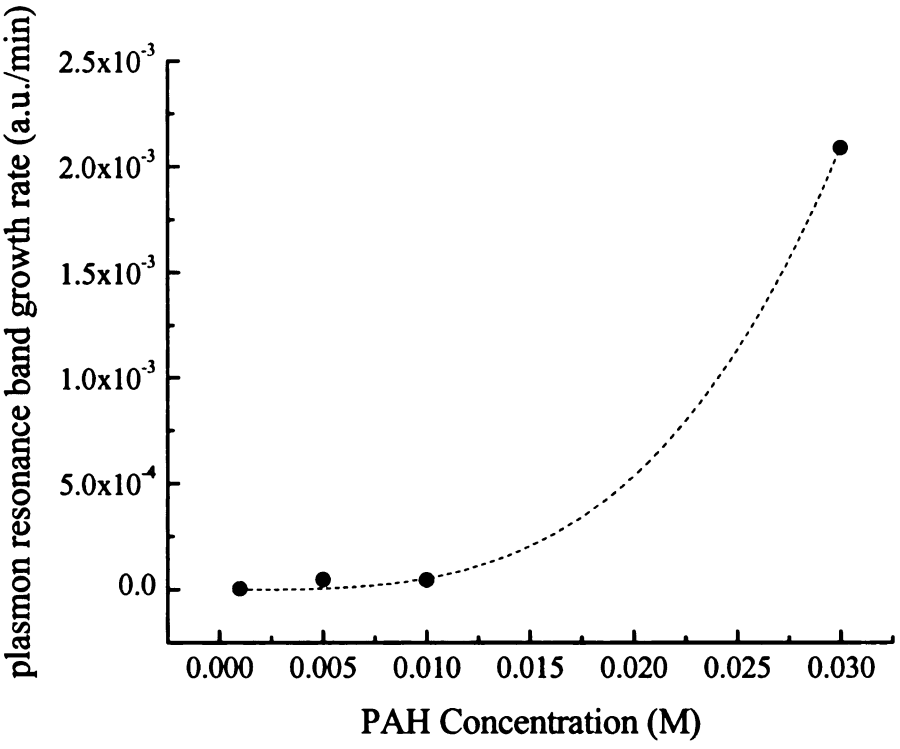

Figure 3.3. Concentration effect on plasmon resonance band growth rate at 100:1 PAH:$HAuCl_4$. The dashed line is a fit of the data to a third order growth curve.

At concentrations exceeding 0.03 M, the reduction proceeds rapidly enough that instead of the formation of colloidal gold particles, bulk gold is observed on both the top of the solution and the sides of the cuvette. These data indicate that within the solubility limits the room-temperature reaction rate can be controlled by simply controlling the reagent concentrations. It is also interesting to note that over the concentration ranges of PAH and $HAuCl_4$ used in these studies, there was no significant variation in the PR wavelength. This suggests that the size of the AuNPs formed remained approximately constant throughout. Overall these kinetic studies have findings that are consistent with

the proposed reduction mechanism where three nitrogens were required to reduce one Au^{3+}.

Equilibrium PR Control. The kinetics of the PAH-$HAuCl_4$ system are predictable at high reducing agent-$HAuCl_4$ ratios, the kinetics are also quite slow. At room temperature, a molar ratio of 100:1 PAH-$HAuCl_4$ has a PR growth rate of 4.75 absorbance units/min (Figure 3.4).

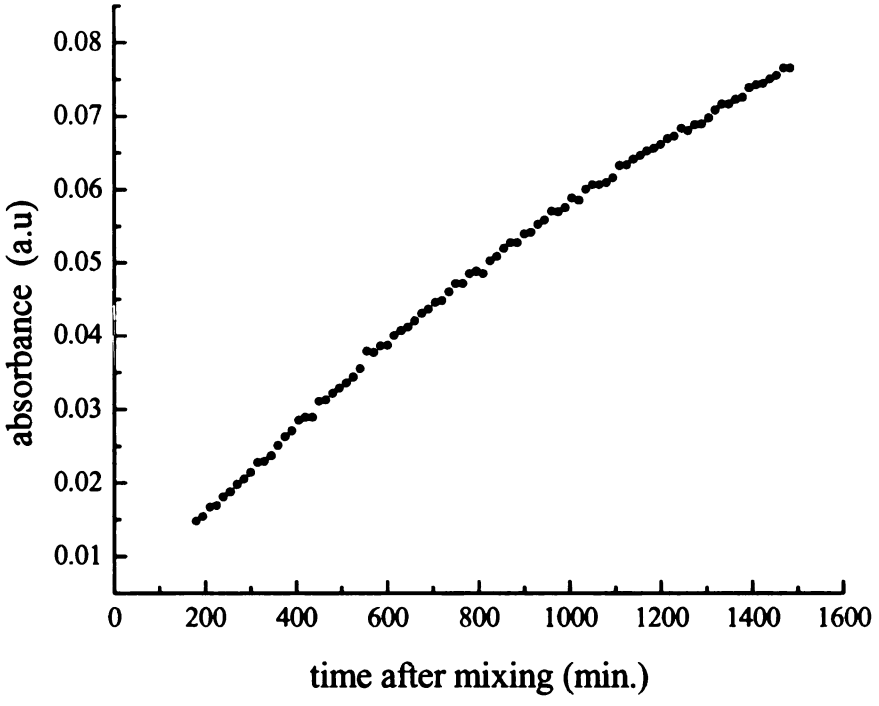

Figure 3.4. Plasmon resonance band spectral growth for a 100:1 PAH:$HAuCl_4$ mixture at room temperature. Solution concentrations were 0.005 M for both PAH and $HAuCl_4$.

The onset of the PR is not seen until approximately 3 hours after the initial mixing. In order to increase the reaction rate in order to facilitate a more practical investigation of the equilibrium behavior of the system, the composites used for equilibrium measurements were synthesized at 95°C. Under these conditions the color of the solution changed from light yellow, characteristic of aqueous $HAuCl_4$, to pink-purple,

characteristic of AuNP presence, in less than 15 minutes. The reaction was allowed to continue to a total reaction time of 45 minutes, but no further color change was observed after the first 15 minutes. The reactant molar ratios were maintained in ratios where the PR remained concentration dependent. In total, five composites were synthesized with ratios ranging from 1.3:1 to 20.4:1 PAH-$HAuCl_4$. The solutions of each of the composites were different in color, ranging from light pink to purple-blue (Figure 3.5).

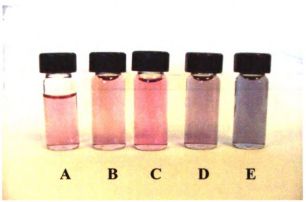

Figure 3.5. Polymer-AuNP composites with mass ratio increasing from left to right. A) Sample 1.3:1; B) Sample 4.5:1; C) Sample 9.2:1; D) Sample 13.1:1; E) Sample 20.4:1 (This image is presented in color.)

Spectroscopically, these composites were characterized by different plamson resonances. The absorbance spectrum of the polymer itself has no absorbance in the region of interest (Figure 3.6).

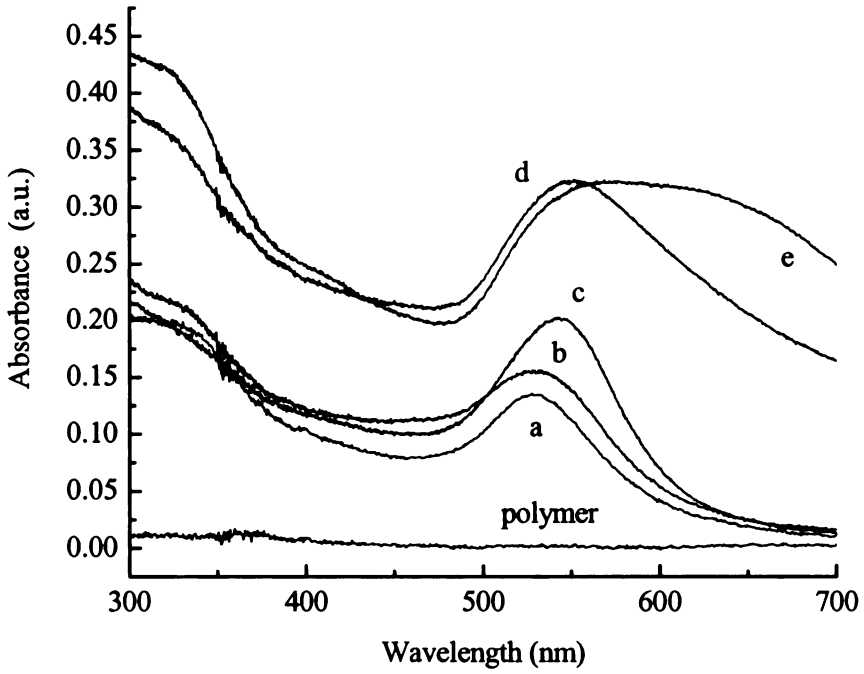

Figure 3.6. UV-visible spectra of the five polymer-AuNP composites and the aqueous PAH. Mass ratios for the spectra are (a) 1.3:1 PAH:$HAuCl_4$, (b) 4.5:1, (c) 9.2:1, (d) 13.1:1, and (e) 20.4:1. Baseline offset for highest polymer concentrations is due to light scattering.

When $HAuCl_4$ is added to the polymer solution, the absorption band in the region of 530 nm is prominent (Figure 3.6, traces a-e). The presence of this band is consistent literature reports of the characteristic absorbance for AuNPs and is hereafter assigned as the PR band[35, 37, 38]. It can be seen that as the ratio increases, the observed PR band red-shifts and the band broadens. This is consistent with the macroscopically observed color changes. Because the wavelength observed for the PAH-AuNP composites is expected to be dependent on both the size of the AuNPs and the dielectric environment of the surrounding medium, the solution phase polymer concentration was maintained

thoughout and the ratio was controlled by changing the amount of $HAuCl_4$ solution added. The PR maximum varies linearly with the polymer-gold ratio (Figure 3.7).

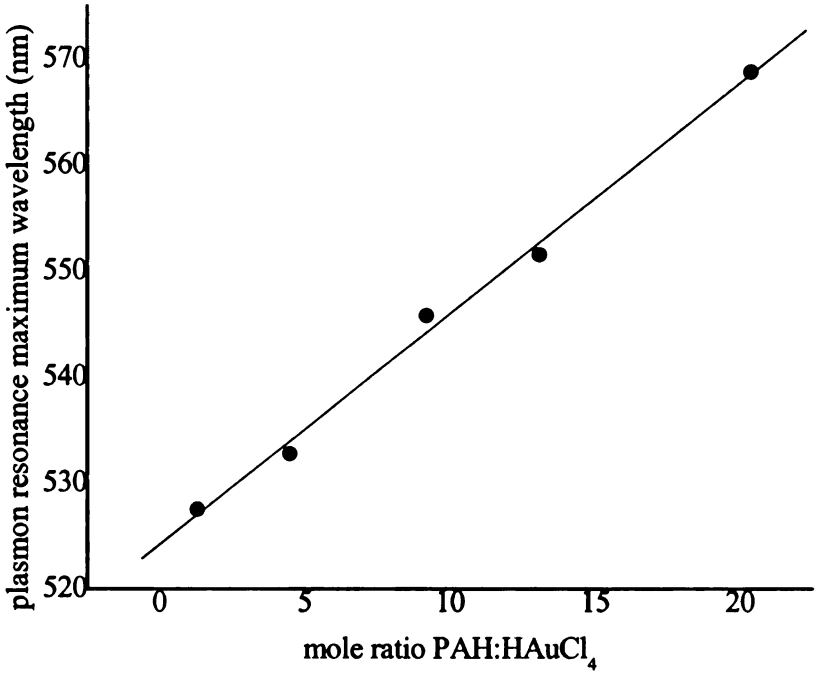

Figure 3.7. Linear relationship between polymer-to-gold mass ratio and plasmon resonance maximum. The line through the data is a best-fit line.

Because the dielectric constant of the AuNP environment is essentially constant at these ratios, the variations in the PR resonance are due to variances in the AuNP size. This will be discussed in more detail later in this chapter.

It is important to understand what impact, if any, the oxidation of the PAH has on the polymer structure in order to appreciate the nature of the final composite material. The ^{1}H-NMR spectra obtained for the polymer before and after the reduction of $HAuCl_4$ are, as expected, identical (Figure 3.8).

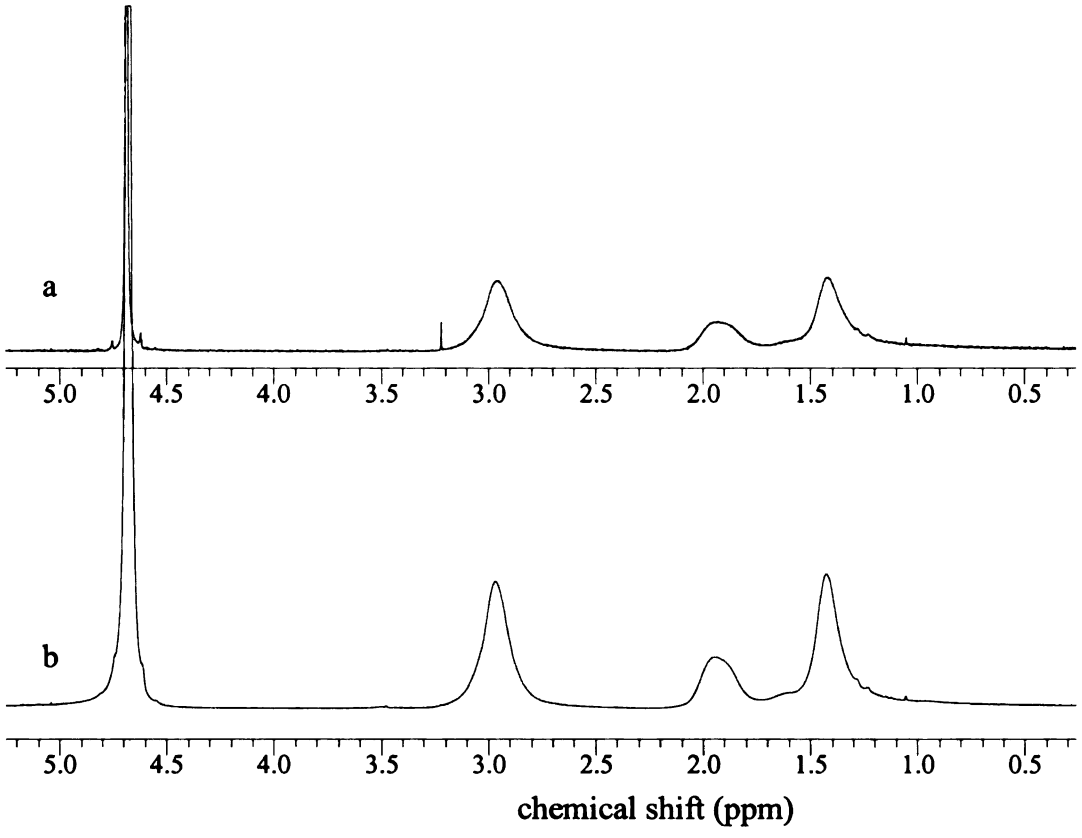

Figure 3.8. ^{1}H NMR spectra of a) poly(allylamine hydrochloride) in D_2O and b) AuNPs in a poly(allylamine hydrochloride) (from a 1:1 molar ratio) matrix in D_2O.

The peak areas integrate as calculated and the linewidths are characteristic of a polymer. Three peaks are observed which correspond to PAH. The broad singlets located at 1.419, 1.931, and 2.964 result from the secondary, tertiary, and amine protons, respectively. There is no evidence of any stable oxidized nitrogen species present in the post-oxidation NMR spectrum. This is not surprising as even at a molar ratio of 1:1, there is still an approximately 160:1 excess of $N:Au^{3+}$.

The PR maxium has been reported to be related to the AuNP size [35, 37, 38] so the linear relationship between the PR band position and molar PAH-$HAuCl_4$ is significant because it indicates that there is a relationship between reactant ratio and the size of the resultant AuNPs. Particularly significant in this case is that simple variations in the

amount of aqueous reagents can allow for tenability of the optical properties of the composite material. This can be important in applications which require control of the optical response of AuNPs.[23]

Imaging. Transmission electron microscopy (TEM) images of the composite materials can be used to a) verify the presence of AuNPs in the composite and b) examine the relationship between particle size and the reaction conditions. In all composite materials, AuNP were observed as approximately spherical particles. Non-aggregated particles were then used to determine the size and approximate distribution of the particles (Figure 3.9).

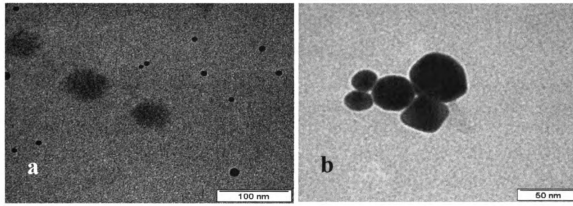

Figure 3.9. TEM images of a) a sample made from 4.5:1 polymer-to-gold ratio solution, with particle sizes ranging from 5-15nm in diameter (measurement bar indicates 100 nm) and b) a sample made from 20.4:1 polymer-to-gold ratio solution, with particle sizes ranging from 35-50nm in diameter (measurement bar indicates 50 nm).

As the mole ratio of the reagents increases from 1.3:1 to 13.1:1, there was an increase in the diameter of the non-aggregated particles from 13 nm to 22 nm (Figure 3.10).

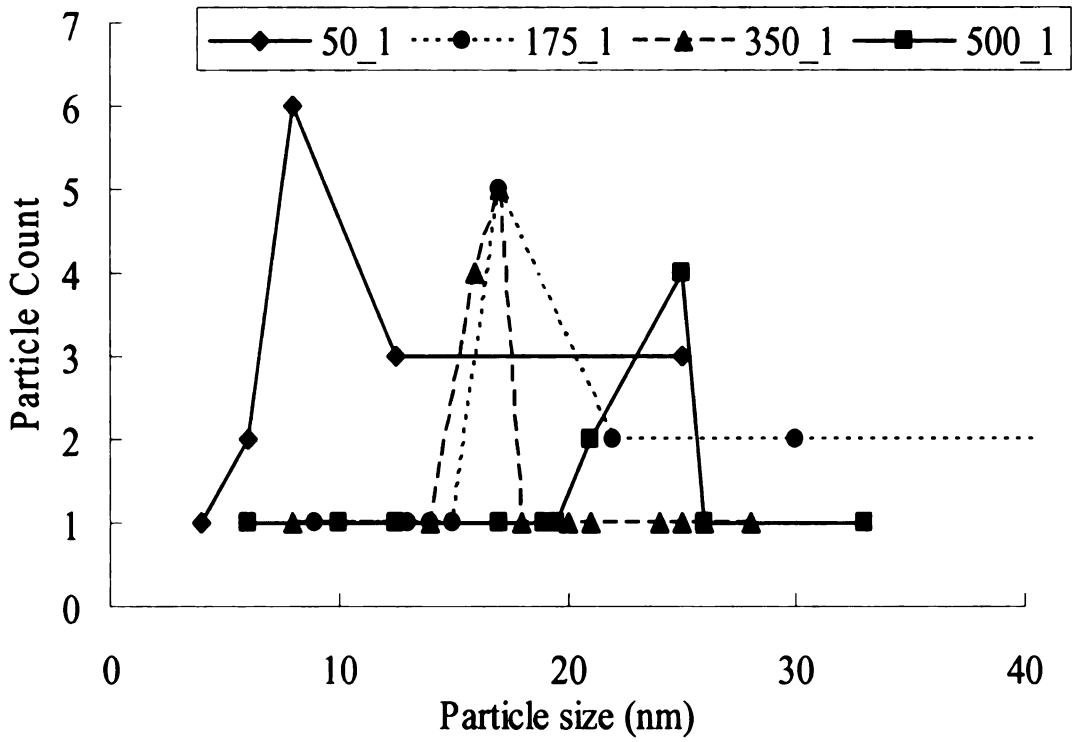

Figure 3.10. Particle size distributions recovered from TEM micrographs for AuNPs synthesized and imbedded in PAH. For each distribution, the PAH:$HAuCl_4$ ratio is indicated in the legend.

The observed trend of red-shifting particle size with increasing PAH:$HAuCl_4$ ratio can correlated in this range to increasing particle size. At 20.4:1, the degree of particle aggregation was too great to determine the size of a non-aggregated particle. The mean particle size for the 9.2:1 and 13.1:1 ratios was the same. However, there were more particles observed in the 13.1: ratio that were larger than the mean. This accounts for the overall red-shift for this composite, making the PR of this composite longer in wavelength than the 9.2:1 composite. While it should be noted that a limited number of measured particles were used to draw these conclusions, taken collectively, these imaging data support the absorption data.

Conclusion

The kinetics of PR growth, and by association AuNP growth, can be readily and predictably controlled through variation in the ratio or overall concentrations of PAH:$HAuCl_4$ in aqueous solution. The kinetics of the system are first order in $HAuCl_4$ at constant PAH concentration. When the PAH concentration is varied, the system kinetics vary to the third power. This validates the postulated reduction mechanism where one Au^{3+} ion is reduced by three amine groups. These data can be used to optimize the efficiency of room temperature reactions resulting in AuNP-polymer composites.

While the kinetics of the system at room temperature can be readily predicted, the reaction rate is also quite slow. In order to speed up the reaction it is possible to add heat to the system and still have a measure of control over the optical behavior of the resulting system. At small molar ratios of PAH:$HAuCl_4$, the position of the PR band can be both controlled and correlated to AuNP size. A linear relationship exists between the position of the PR band and the ratio of the reactants in solution. Additionally, a general increase is seen in the size of non-aggregated particles in the composite material with an increase in the reactant ratio. This data can be considered together to conclude that the increase in particle size is responsible for the red-shift in the PR band maximum.

Formation of AuNPs using this method provides a simple means of formation polymer-AuNP composite materials with control over the optical properties of the composite. This could be significant when designing polymer films for sensing applications and biomedical applications. It could also be important for understanding potential *in situ* AuNP formation for use as therapeutic agents.

References

1. Dos Santos, D. S., Jr.; Goulet, P. J. G.; Pieczonka, N. P. W.; Oliveira, O. N., Jr.; Aroca, R. F., Gold nanoparticle embedded, self-sustained chitosan films as substrates for surface-enhanced raman scattering. *Langmuir* **2004,** 20, (23), 10273-10277.

2. Faulds, K.; Littleford, R. E.; Graham, D.; Dent, G.; Smith, W. E., Comparison of Surface-Enhanced Resonance Raman Scattering from Unaggregated and Aggregated Nanoparticles. *Analytical Chemistry* **2004,** 76, (3), 592-598.

3. Frederix, F.; Friedt, J.-M.; Choi, K.-H.; Laureyn, W.; Campitelli, A.; Mondelaers, D.; Maes, G.; Borghs, G., Biosensing based on light absorption of nanoscaled gold and silver particles. *Analytical Chemistry* **2003,** 75, (24), 6894-6900.

4. Grate, J. W.; Nelson David, A.; Skaggs, R., Sorptive behavior of monolayer-protected gold nanoparticle films: implications for chemical vapor sensing. *Analytical chemistry* **2003,** 75, (8), 1868-79.

5. Gross, G. M.; Nelson, D. A.; Grate, J. W.; Synovec, R. E., Monolayer-Protected Gold Nanoparticles as a Stationary Phase for Open Tubular Gas Chromatography. *Analytical Chemistry* **2003,** 75, (17), 4558-4564.

6. Grubisha, D. S.; Lipert, R. J.; Park, H.-Y.; Driskell, J.; Porter, M. D., Femtomolar Detection of Prostate-Specific Antigen: An Immunoassay Based on Surface-Enhanced Raman Scattering and Immunogold Labels. *Analytical Chemistry* **2003,** 75, (21), 5936-5943.

7. Krasteva, N.; Besnard, I.; Guse, B.; Bauer, R. E.; Muellen, K.; Yasuda, A.; Vossmeyer, T., Self-Assembled Gold Nanoparticle/Dendrimer Composite Films for Vapor Sensing Applications. *Nano Letters* **2002,** 2, (5), 551-555.

8. Matsui, J.; Akamatsu, K.; Nishiguchi, S.; Miyoshi, D.; Nawafune, H.; Tamaki, K.; Sugimoto, N., Composite of Au nanoparticles and molecularly imprinted polymer as a sensing material. *Analytical chemistry* **2004,** 76, (5), 1310-5.

9. Nath, N.; Chilkoti, A., Label-Free Biosensing by Surface Plasmon Resonance of Nanoparticles on Glass: Optimization of Nanoparticle Size. *Analytical Chemistry* **2004,** 76, (18), 5370-5378.

10. Tokareva, I.; Minko, S.; Fendler, J. H.; Hutter, E., Nanosensors Based on Responsive Polymer Brushes and Gold Nanoparticle Enhanced Transmission Surface Plasmon Resonance Spectroscopy. *Journal of the American Chemical Society* **2004,** 126, (49), 15950-15951.

11. Zhang, Z.-F.; Cui, H.; Lai, C.-Z.; Liu, L.-J., Gold nanoparticle-catalyzed luminol chemiluminescence and its analytical applications. *Analytical Chemistry* **2005,** 77, (10), 3324-3329.

12. Andersson, M.; Fromell, K.; Gullberg, E.; Artursson, P.; Caldwell, K. D., Characterization of Surface-Modified Nanoparticles for in Vivo Biointeraction. A Sedimentation Field Flow Fractionation Study. *Analytical Chemistry* **2005,** 77, (17), 5488-5493.

13. Aslan, K.; Lakowicz, J. R.; Geddes, C. D., Nanogold Plasmon Resonance-Based Glucose Sensing. 2. Wavelength-Ratiometric Resonance Light Scattering. *Analytical Chemistry* **2005,** 77, (7), 2007-2014.

14. Niidome, T.; Nakashima, K.; Takahashi, H.; Niidome, Y., Preparation of primary amine-modified gold nanoparticles and their transfection ability into cultivated cells. *Chemical Communications (Cambridge, United Kingdom)* **2004,** (17), 1978-1979.

15. Rojo, J.; Diaz, V.; De la Fuente, J. M.; Segura, I.; Barrientos, A. G.; Riese, H. H.; Bernad, A.; Penades, S., Gold glyconanoparticles as new tools in antiadhesive therapy. *ChemBioChem* **2004,** 5, (3), 291-297.

16. Hirsch, L. R.; Stafford, R. J.; Bankson, J. A.; Sershen, S. R.; Rivera, B.; Price, R. E.; Hazle, J. D.; Halas, N. J.; West, J. L., Nanoshell-mediated near-infrared thermal therapy of tumors under magnetic resonance guidance. *Proceedings of the National Academy of Sciences of the United States of America* **2003,** 100, (23), 13549-13554.

17. Loo, C.; Lin, A.; Hirsch, L.; Lee, M.-H.; Barton, J.; Halas, N.; West, J.; Drezek, R., Nanoshell-enabled photonics-based imaging and therapy of cancer. *Technology in Cancer Research & Treatment* **2004,** 3, (1), 33-40.

18. Loo, C.; Lowery, A.; Halas, N.; West, J.; Drezek, R., Immunotargeted nanoshells for integrated cancer imaging and therapy. *Nano Lett* **2005,** 5, (4), 709-11.

19. O'Neal, D. P.; Hirsch Leon, R.; Halas Naomi, J.; Payne, J. D.; West Jennifer, L., Photo-thermal tumor ablation in mice using near infrared-absorbing nanoparticles. *Cancer letters* **2004,** 209, (2), 171-6.

20. Bhargava, S. K.; Booth, J. M.; Agrawal, S.; Coloe, P.; Kar, G., Gold Nanoparticle Formation during Bromoaurate Reduction by Amino Acids. *Langmuir* **2005,** 21, (13), 5949-5956.

21. Selvakannan, P. R.; Mandal, S.; Phadtare, S.; Gole, A.; Pasricha, R.; Adyanthaya, S. D.; Sastry, M., Water-dispersible tryptophan-protected gold nanoparticles

prepared by the spontaneous reduction of aqueous chloroaurate ions by the amino acid. *Journal of Colloid and Interface Science* **2004,** 269, (1), 97-102.

22. Bao, C.; Jin, M.; Lu, R.; Zhang, T.; Zhao, Y., Hyperbranched poly(amine-ester) templates for the synthesis of Au nanoparticles. *Materials Chemistry and Physics* **2003,** 82, (3), 812-817.

23. Chen, S.-J.; Chang, H.-T., Nile red-adsorbed gold nanoparticles for selective determination of thiols based on energy transfer and aggregation. *Analytical chemistry* **2004,** 76, (13), 3727-34.

24. Cho, J.; Caruso, F., Investigation of the Interactions between Ligand-Stabilized Gold Nanoparticles and Polyelectrolyte Multilayer Films. *Chemistry of Materials* **2005,** 17, (17), 4547-4553.

25. Esumi, K.; Suzuki, A.; Yamahira, A.; Torigoe, K., Role of poly(amidoamine) dendrimers for preparing nanoparticles of gold, platinum, and silver. *Langmuir* **2000,** 16, (6), 2604-2608.

26. Grohn, F.; Bauer, B. J.; Kim, G.; Amis, E. J., Nanoparticle formation within dendrimer-containing polymer networks: route to new organic-inorganic hybrid materials. *Polymeric Materials Science and Engineering* **2001,** 84, 78-79.

27. Kim, Y.-G.; Garcia-Martinez, J. C.; Crooks, R. M., Electrochemical Properties of Monolayer-Protected Au and Pd Nanoparticles Extracted from within Dendrimer Templates. *Langmuir* **2005,** 21, (12), 5485-5491.

28. Mayer, A. B. R.; Mark, J. E., Colloidal gold nanoparticles protected by water-soluble homopolymers and random copolymers. *European Polymer Journal* **1998,** 34, (1), 103-108.

29. Srivastava, S.; Frankamp, B. L.; Rotello, V. M., Controlled Plasmon Resonance of Gold Nanoparticles Self-Assembled with PAMAM Dendrimers. *Chemistry of Materials* **2005,** 17, (3), 487-490.

30. Sun, X.; Dong, S.; Wang, E., One-step synthesis and characterization of polyelectrolyte-protected gold nanoparticles through a thermal process. *Polymer* **2004,** 45, (7), 2181-2184.

31. Zhang, P.; Sham, T. K., Tuning the electronic behavior of Au nanoparticles with capping molecules. *Applied Physics Letters* **2002,** 81, (4), 736-738.

32. Hussain, I.; Brust, M.; Papworth, A. J.; Cooper, A. I., Preparation of acrylate-stabilized gold and silver hydrosols and gold-polymer composite films. *Langmuir* **2003,** 19, (11), 4831-4835.

33. Iwamoto, M.; Kuroda, K.; Zaporojtchenko, V.; Hayashi, S.; Faupel, F., Production of gold nanoparticles-polymer composite by quite simple method. *European Physical Journal D: Atomic, Molecular and Optical Physics* **2003,** 24, (1-3), 365-367.

34. Sun, X.; Dong, S.; Wang, E., One-step polyelectrolyte-based route to well-dispersed gold nanoparticles: Synthesis and insight. *Materials Chemistry and Physics* **2006,** 96, (1), 29-33.

35. Hostetler, M. J.; Wingate, J. E.; Zhong, C.-J.; Harris, J. E.; Vachet, R. W.; Clark, M. R.; Londono, J. D.; Green, S. J.; Stokes, J. J.; Wignall, G. D.; Glish, G. L.; Porter, M. D.; Evans, N. D.; Murray, R. W., Alkanethiolate Gold Cluster Molecules with Core Diameters from 1.4 to 5.2 Nanometers: Core and Monolayer Properties as a Function of Core Size. *Langmuir* **1998,** 14, (1), 17-30.

36. Leff, D. V.; Ohara, P. C.; Heath, J. R.; Gelbart, W. M., Thermodynamic Control of Gold Nanocrystal Size: Experiment and Theory. *Journal of Physical Chemistry* **1995,** 99, (18), 7036-41.

37. Murillo, L. E. V., O.; Vicuna, E.; Briano, J.G.; Castro, M.; Ishikawa, Y.; Irizarry, R.; Sola, L., *Computational Nanoscience and Nanotechnology* **2002**, 435-438.

38. Sonnichsen, C.; Geier, S.; Hecker, N. E.; von Plessen, G.; Feldmann, J.; Ditlbacher, H.; Lamprecht, B.; Krenn, J. R.; Aussenegg, F. R.; Chan, V. Z. H.; Spatz, J. P.; Moller, M., Spectroscopy of single metallic nanoparticles using total internal reflection microscopy. *Applied Physics Letters* **2000,** 77, (19), 2949-2951.

Chapter 4

Investigations of Alkanethiol Self-Assembled Monolayer Organization and Viscoelastic Properties using Impedance Spectroscopy

Introduction

Alkanethiol monolayers on gold have been studied extensively because of their facile growth properties and the resulting well organized molecular assemblies. Following initial work in this area in the 1980's,[1-8] the field has grown enormously and thiol/gold monolayers find use in a variety of technological applications today. Much is understood about the fundamental structural and growth properties of alkanethiol monolayers, but a persistent issue in the field remains the separation of the various events that occur during monolayer growth. The initial step in monolayer growth is the gold-sulfur interaction,[9-12] in which the thiol hydrogen is lost, being sequestered as either H_2 or H_2O_2 on the Au surface, depending on the amount of water present.[13-16] The gold-sulfur bond is on the order of 5-6 kcal/mol, a value that represents a balance between a modest gold-sulfur bond enthalpy (ca. 20 kcal/mol) and a large entropic penalty (ca. 50 cal/mol-K) that results from the formation of a two-dimensional quasi-crystalline assembly from solution.[10, 13, 17] The modest net driving force for monolayer formation implies that the monolayer will likely be labile, and AFM data on alkanethiol islands on Au has shown this to be the case.[18] Subsequent to the initial mass deposition of the monolayer, which

occurs on the timescale of seconds to minutes[2], there is a more subtle structural rearrangement of the monolayer, sometimes termed "annealing", which serves to organize the aliphatic chains of the monolayer, producing a well organized, hydrophobic surface.[2, 19] The details of this annealing process remain to be understood in detail, despite extensive examination. Infrared spectroscopic data have shown that the CH stretching resonances of the aliphatic chains go from being liquid-like initially to quasi-crystalline over a timescale of hours to days, depending on the monolayer chain length, temperature and environment.[19, 20] This information addresses average structure, but there remain open issues regarding interchain interactions and the evolution of organization within the film. We are interested in examining this issue from the standpoint of how the viscoelastic properties of the monolayers change following initial deposition. Viscosity, in the traditional sense, is a measure of the strength of intermolecular interactions, a phenomenon that will depend sensitively on monolayer chain organization. In order to evaluate the monolayer viscoelastic properties, quartz crystal microbalances (QCMs) with Au electrodes have been used as the growth substrates for alkanethiol monolayers. By measuring the complex impedance response of the QCM in solution as a function of time after thiol introduction, and modeling changes in this response in the context of an equivalent circuit model, information can be extracted on what factors change most during monolayer structural evolution. This study demonstrates that the structural evolution of the monolayer depends on both the thiol aliphatic chain length and on the annealing time. For alkanethiols in the range of C_6-C_{16}, initial deposition and organization occurs on roughly the same time scale. However, the C_6 monolayer, which is expected to be relatively less organized at equilibrium, has

different viscoelastic properties than C_9-C_{16} SAMs, which are essentially indistinguishable from one another in terms of their viscoelastic properties. Solubility of the alkanethiols will also be shown to play a large role in determining the functional form of impedance spectral data, as C_{18} monolayers demonstrated bulk adsorption under the deposition conditions used. This bulk deposition could be observed visually, and it was also evident in the evolution of the C_{18} SAM impedance spectra. We consider first the QCM response and the information content of our measurements.

Background. Quartz crystal microbalance (QCM) gravimetry is a highly sensitive technique capable of quantitating nanogram mass changes. The measurements are based on the piezoelectric behavior of crystalline quartz under the influence of an AC electric field. In the case of the QCM, the oscillations induced by the electric field are parallel to the surface of the crystal and occur at a frequency determined by the properties of the quartz, including thickness and shear modulus. In the simplest application, changes in the thickness of the quartz crystal determine changes in its resonance frequency. In the limit that the mass added to the QCM surface is rigid, as in many vapor phase deposition applications, the QCM resonance frequency changes in direct proportion to the mass added to the device, and this frequency change is described by the Sauerbrey equation,[21]

$$\Delta f = \frac{-2\Delta m n f_0^2}{A\left(\mu_q \rho_q\right)^{1/2}} \tag{1}$$

where n is the harmonic of f_0, the resonance frequency of the unperturbed QCM crystal, A is the area of the QCM crystal, μ_q is the quartz shear modulus, ρ_q is the quartz density, Δf is the frequency change upon deposition, and Δm is the mass change upon deposition. This relationship has been used extensively to interpret QCM resonance frequency shift

data, and in applications such as measuring the formation kinetics of self-assembled monolayers.[22]

The most common measurement method for QCMs is to monitor the frequency change of the device as a function of some deposition parameter. This measurement scheme records only the center frequency of the crystal resonance, but does not provide direct information on changes in the shape of the resonance associated with the addition of non-rigid materials to the face(s) of the device. Measurement of the complex device impedance as a function of frequency provides information on changes in resonance line shape as a function of experimental variables, and this information can be related to the viscoelastic properties of the adsorbed film(s). To measure the complex impedance response of the QCM as a function of frequency, we use an impedance analyzer which senses phase shift and standing wave ratio of the reflected signal that is applied to the crystal. The quantities |Y|, the magnitude of the admittance, and θ, the phase angle, are measured experimentally and are related to the real and imaginary parts of the device response. An equivalent circuit[23-28] is used to model the frequency-dependence of these data, and relate the quantities in the model to the properties of the QCM.

The equivalent circuit approach to the analysis of QCM data has proven to be remarkably useful. The Butterworth-Van Dyke (BVD) circuit model (Figure 4.1a) is an effective model for QCM impedance data on mass loaded QCM crystals.[27, 29, 30] This model is useful for understanding a gas phase moiety adsorbing onto a QCM. However, in more complex cases the BVD circuit can be modified (Figure 4.1b) to account for both the effect of liquid viscous drag and mass loading on the QCM surface. The modification lies not in the functional form, but in making the correspondence between the model

circuit components and the properties of the QCM adsorbate. Using the model circuit shown in Figure 4.1b, the frequency-dependent complex response of the QCM is given by Eq. 2,

$$Y = j\omega(C_0 + C_p) + \frac{R - j\left(\omega L - \frac{1}{\omega C_1}\right)}{R^2 + \left(\omega L - \frac{1}{\omega C_1}\right)^2}$$

$$|Y| = \sqrt{\left(Y_R^2 + Y_I^2\right)} \qquad (2)$$

$$\theta = \tan^{-1}\left(\frac{Y_I}{Y_R}\right)$$

Where Y_R is the real part of the admittance and Y_I is the imaginary part.

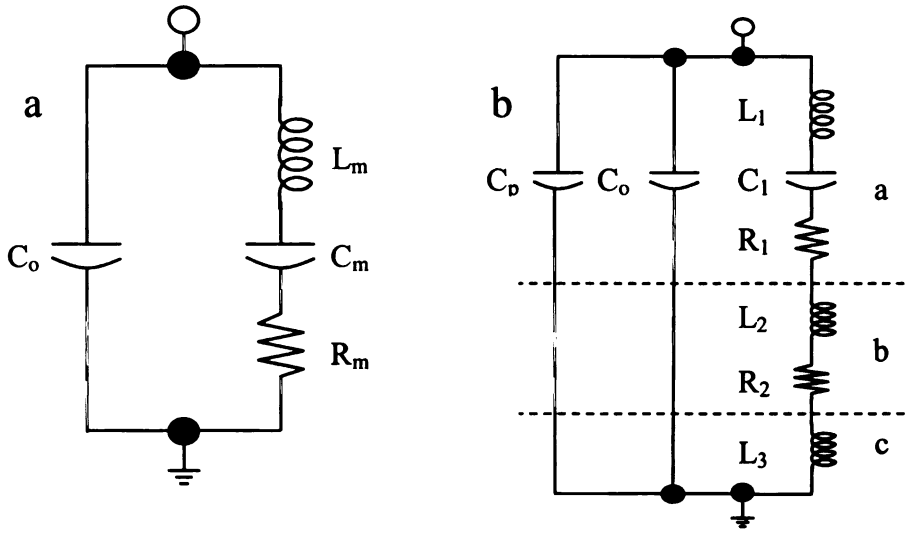

Figure 4.1. (a) BVD equivalent circuit where the left arm of the circuit is the static capacitance (C_o) and the right arm is the motional arm where L_m is the motional inductance, C_m is the motional capacitance, and R_m is the motional resistance. (b) Equivalent circuit describing the unperturbed (L_1, C_1, R_1), liquid loaded (R_2, L_2) and mass loaded (L_3) portions of the QCM crystal

In this model, the inductance L is comprised of three inductors in series, $L = L_1 + L_2 + L_3$, and R likewise represents two resistors in series, $R = R_1 + R_2$, as shown in Figure

4.1b. The key to this model is the correspondence between the equivalent circuit components and the physical quantities of interest. Martin has made this connection, describing the relationship between the quantities C, L and R, the properties of the QCM, and the characteristics of the liquid medium and the adsorbed layer.[23] For the data reported here, two circuit components provide the most useful information on the properties of the SAMs; L_2 and R_2, the inductance and resistance associated with the mass loading of the crystal. Eqs. 3 and 4 show the relationship between each of these terms,[23]

$$L_2 = L_1 \frac{\omega_0}{N\pi}\left(\frac{2\rho\eta}{\omega \bar{c}_{66}\rho_q}\right)^{1/2} \tag{3}$$

$$R_2 = L_1 \frac{\omega_0}{N\pi}\left(\frac{2\omega\rho\eta}{\bar{c}_{66}\rho_q}\right)^{1/2} \tag{4}$$

Where ω_0 is the resonance frequency, L_1 is the inductance associated with the unperturbed QCM crystal, ρ_q is the density of the quartz comprising the QCM, ω is the resonance frequency of the QCM after SAM adsorption, and c_{66} is the piezoelectrically stiffened quartz constant.[23] Most of the quantities that describe the equivalent circuit components are constant properties of the materials used, and their values are known. The quantity ω_0 is measured and it is the terms ρ and η, the adlayer density and viscosity, respectively, which reflect the properties of the adsorbed SAM layer. It is these latter two quantities that are of primary interest in this work and, in particular, how these adlayer properties depend on the identity of the thiol aliphatic chain length and on the time allowed for SAM annealing after initial deposition.

Materials and Methods

Materials. 1-Hexanethiol (C_6-SH), 1-nonanethiol (C_9-SH), 1-dodecanethiol (C_{12}-SH), and 1-octadecanethiol (C_{18}-SH) were obtained from Sigma-Aldrich (Milwaukee, WI) and used as received. QCM crystals were obtained from McCoy Crystals/Corning Frequency Control (Mount Holly Springs, PA). The crystals were cleaned with Piranha solution, a 3:1 solution of sulfuric acid-hydrogen peroxide (*caution! Strong oxidizer*) for 30 seconds, rinsed with copious amounts of distilled water, and dried thoroughly with nitrogen prior to use.

Monolayer Deposition. SAMs were grown *in situ* on clean QCM crystals at 14°C, without stirring, from 1 mM ethanolic thiol solutions. The temperature was controlled using a circulating water bath and a jacketed 100 mL beaker. The beaker and oscillator were covered to minimize evaporative losses.

Impedance spectroscopy. Impedance spectra were collected using a QCM driven by an oscillator circuit (Maxtek, Inc, Cypress, CA). The phase angle and reflected signal from the oscillator-QCM circuit was measured as a function of frequency using a HP 4192A LF Impedance Analyzer (Hewlett Packard, Palo Alto, CA). The impedance analyzer was interfaced to a personal computer and controlled using LabView™ v. 7.0 code (National Instruments, Austin, TX). Impedance spectra were collected at 30 minute intervals. The frequency was scanned from 5.92 MHz to 5.95 MHz with 50 Hz resolution. Time zero for each experiment was established by immersion of the QCM crystal in the thiol solution.

Results and Discussion

The central goal of this work is to understand how the viscoelastic properties of the alkanethiol monolayer adsorbed on the QCM electrodes evolves over time. It is interesting to understnad how the viscoelastic evolution process of the SAM depends on the length of the thiol aliphatic chain and on the time the SAM is immersed in solution. The SAM properties measured in this work are related to alkane chain annealing; the initial mass deposition reaction, dominated by interactions between the thiol S and the Au electrode, is essentially complete within less than a minute after immersion of the QCM in solution. In order to gain information on the SAM viscoelastic properties, the impedance data is fit to the BVD model circuit and monitor how specific model circuit elements change with time. It is the changes in these model parameters that relate to the physical characteristics of the system through Eqs. 3 and 4. To extract the information of interest, we must first determine the appropriate values for the other circuit components in this model, and this matter is considered next.

Modeling Impedance Response. We note at the outset that the equivalent circuit model is not capable of distinguishing the individual circuit elements, and treats the inductive and resistive components as single elements. For these experiments, the interpretation hinges on understanding which of the experimental quantities is varying and thus which model circuit elements are changing and which are being held comparatively constant. The spectrum obtained for each impedance measurement was fit to a corresponding model system. A blank spectrum (Figure 4.2) and a spectrum for a QCM with an alkanethiol adlayer (Figure 4.3) were fit for each data point.

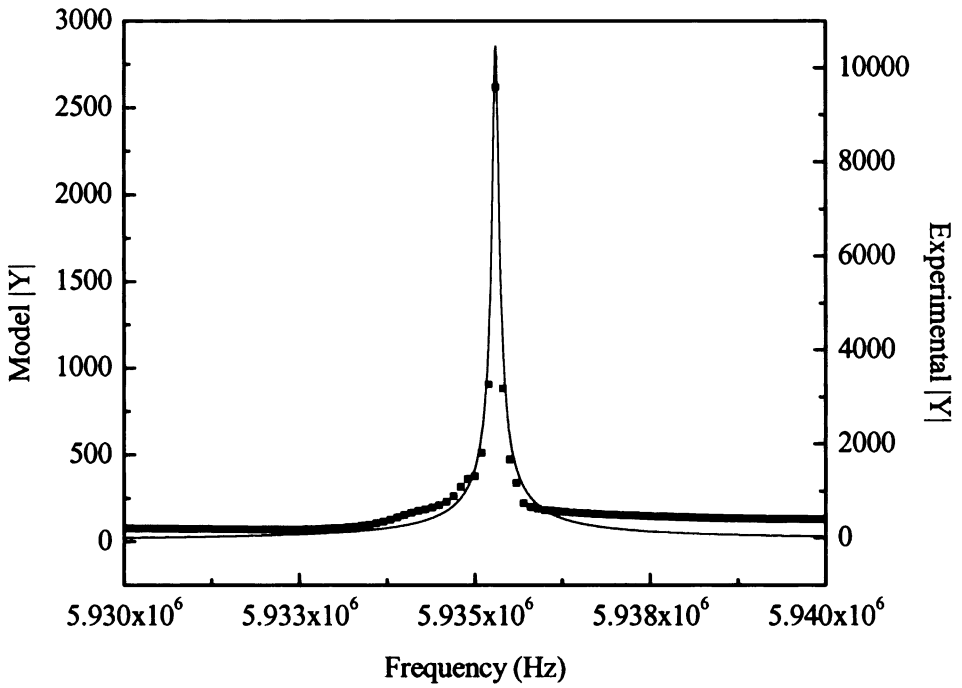

Figure 4.2. Comparison of experimental data (▪) and model fit (–) for a blank QCM crystal

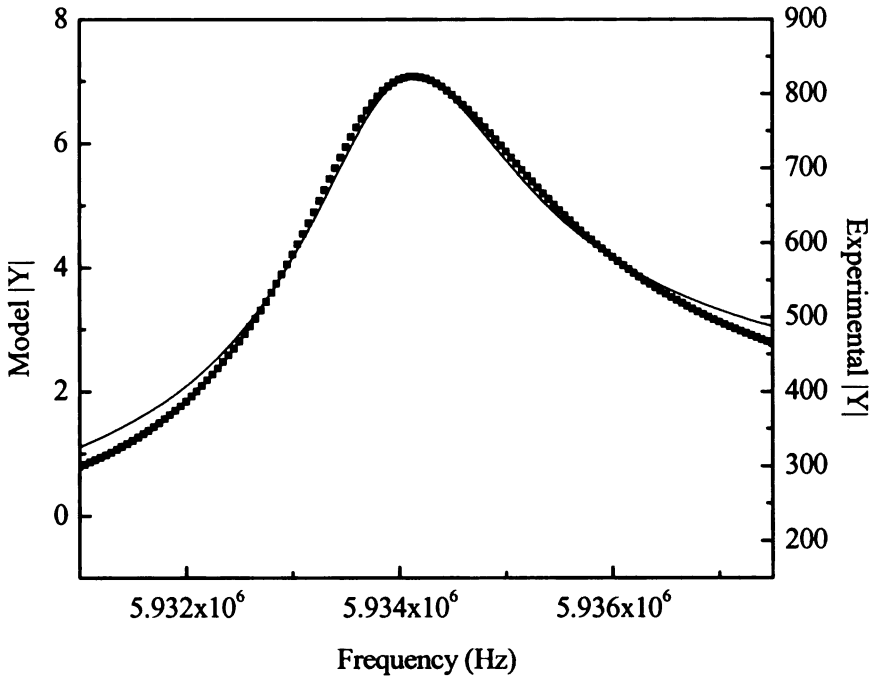

Figure 4.3. Comparison of experimental data (▪) and model fit (—) for a C_{16}-SH monolayer on QCM crystal

For a blank QCM, where there is no adlayer but only the solvent overlayer, the quantity L_3 (Figure 4.1b) is identically zero. The quantity C_p, the parasitic capacitance determined by the physical connection between the QCM and the oscillator circuit, and the quantity C_0, the intrinsic capacitance of the QCM, cannot be separated experimentally, and these quantities are treated as a single capacitance. The intrinsic device quantities C_1, L_1, and R_1 were determined by fitting the spectral lineshape of a bare QCM (Figure 4.2), and these values will remain constant throughout a measurement. There is no discernible information related to the viscoelastic properties of the adlayer in these terms. With the addition of a monolayer to the QCM, the quantities L_2, R_2 and L_3 can all change because the adlayer will add mass and alter the coupling between the QCM device and the

solution. The quantity L_3 will change by a fixed amount within the first minute after introduction of the thiol,[22] an amount which can be estimated based on the QCM surface area, but was seen experimentally to remain essentially unchanged throughout all experiments. It is the terms L_2 and R_2 that contain viscoelastic information on the SAM, and these quantities will vary most significantly with time. To fit the SAM spectra, C_1, L_1, R_1, and L_3 are held constant and R_2 and L_2 are used as the experimental variables (Figure 4.3).

Interestingly, we find the value of C_p plays a primary role in determining the dispersive nature of the observed lineshape. This parameter changes upon QCM immersion in solution, which is expected, and differs from C_p for the blank QCM, likely because of the presence of the SAM between the QCM electrode and the oscillator connections. The change in going from the QCM in air to the QCM in solution was similar for all samples, consistent with C_p being dominated by the contact between the QCM electrode and the oscillator circuitry. For all of the SAMs studied here, the spectra exhibited a time-dependent evolution that could be accounted for by changes in L_2 and R_2. The dominant effect of L_2 is to change the resonance center frequency in a manner consistent with the Sauerbrey equation, *i.e.* as the value of L_2 increases, the resonance center frequency decreases. This finding is expected based on Martin's treatment of the BVD model, where L_2 is related to the liquid mass loading of the QCM. Because the adlayer mass loading inductance term (L_3) is nominally constant over the 12 hour duration of the experiments, the observed changes can be attributed to inductive effects must be associated with changes in the evolution of the SAM viscoelastic properties. The effect of the quantity R_2, which depends on the viscoelastic properties of the adlayer in a

manner similar to L_2 (see Eqs. 3 and 4), is primarily on the resonance linewidth. Increasing R_2 results in a broadening of the resonance and a slight increase in the center frequency. This latter effect is expected based on the contribution of L_1 to R_2. The goal of the following discussion is to extract chemically useful information on SAMs from these QCM impedance data.

SAM viscoelastic properties. As noted above, the inductive impedance term L_2 in the BVD model has a similar functional form to R_2, and in terms of applying this model, we find that the term L_2 dominates the impedance resonance frequency while R_2 is related most closely to the linewidth of the resonance. We focus on the inductive term, but it should be noted that the temporal behavior of L_2 and R_2 are functionally the same (Figure 4.4).

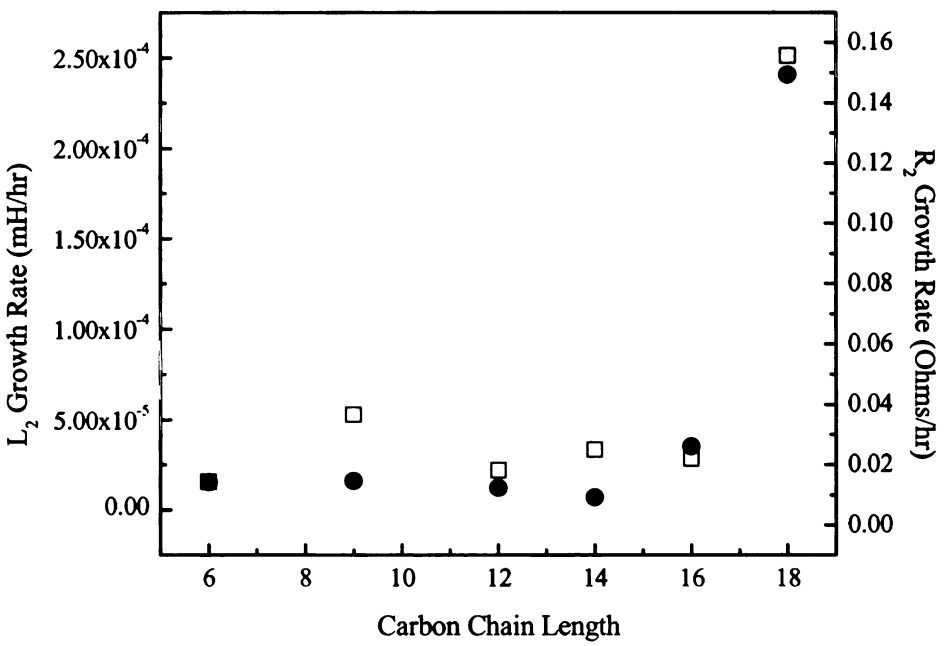

Figure 4.4. Comparison of growth behavior of L_2 (■) and R_2 (●).

Figures 4.5a and 4.5b show a series of impedance spectra taken over a period of 12 hours, to provide a sense of how these spectra evolve in time.

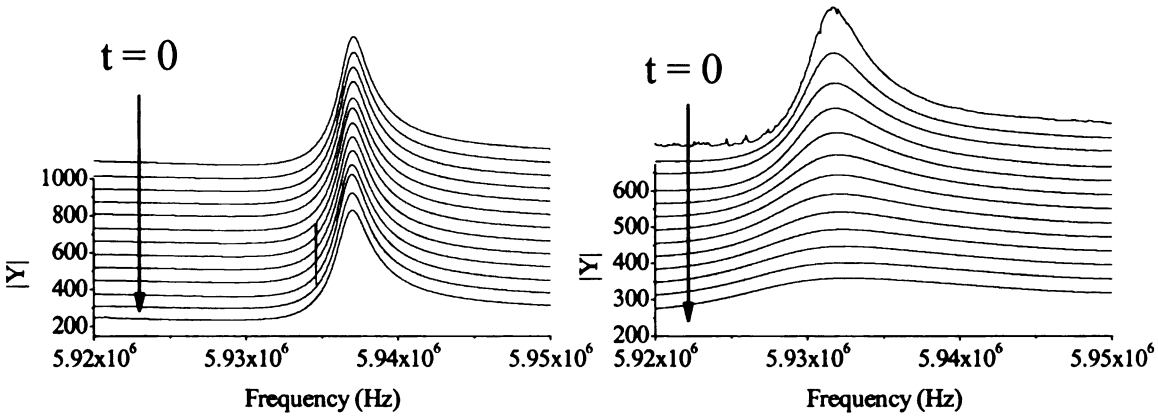

Figure 4.5. Time-dependent impedance responses of a) C_9–SH and b) C_{18}–SH SAMs on Au-coated QCM. Spectra were acquired starting at time zero, at 1 hour intervals for a period of 12 hours.

Because the adlayer mass loading (L_3) is constant, it must be changes in L_2 and R_2, specifically the terms ρ and η in Eqs. 3 and 4, account for the spectral evolution (Figure 4.5). Examining the term L_2, we see that this quantity varies in a nominally linear manner over the 12 hour observation time (Figure 4.6).

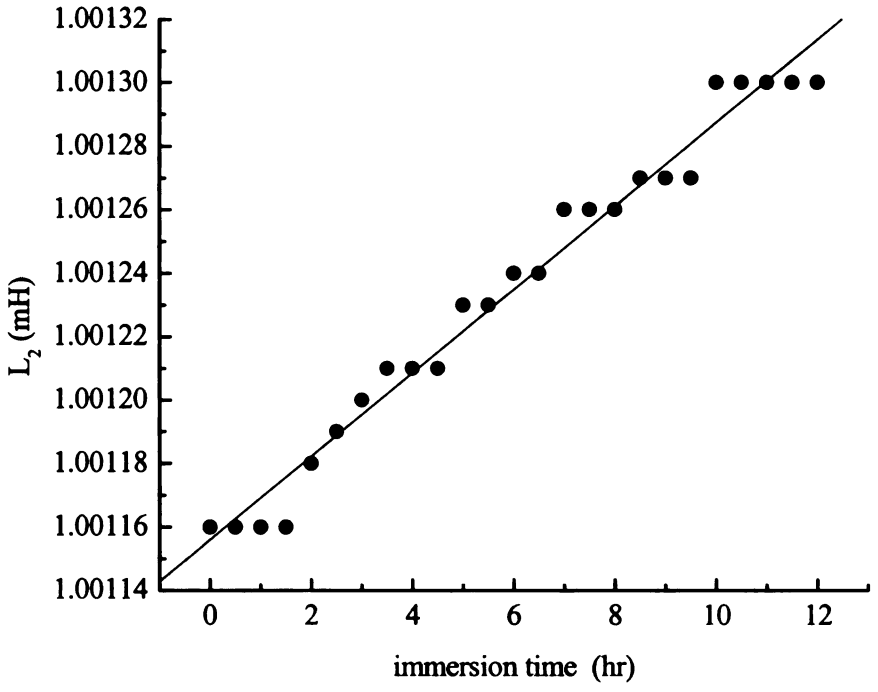

Figure 4.6. C_9 monolayer growth from ethanolic solution

There are several interesting features contained in the L_2 data. In Figure 4.6, it can be seen that the structural evolution of the SAM proceeds at a nominally constant rate. The slope of the temporal growth in inductance is the same, to within our experimental uncertainty, for all of the SAMs examined (Figure 4.7).

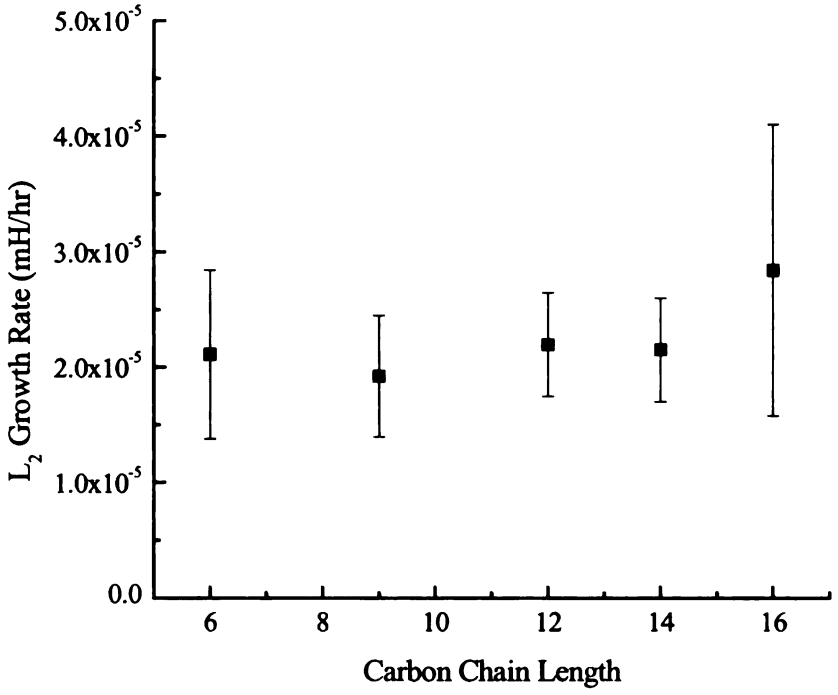

Figure 4.7. Initial growth rate of L_2 for alkanethiol SAMs of varying carbon chain length.

The growth rate is modest, on the order of a 2% change in L_2 per hour, and the nominal value of L_2 is 1 mH. The value of L_2 after 12 hours of annealing is nominally independent of SAM aliphatic chain length (Figure 4.8).

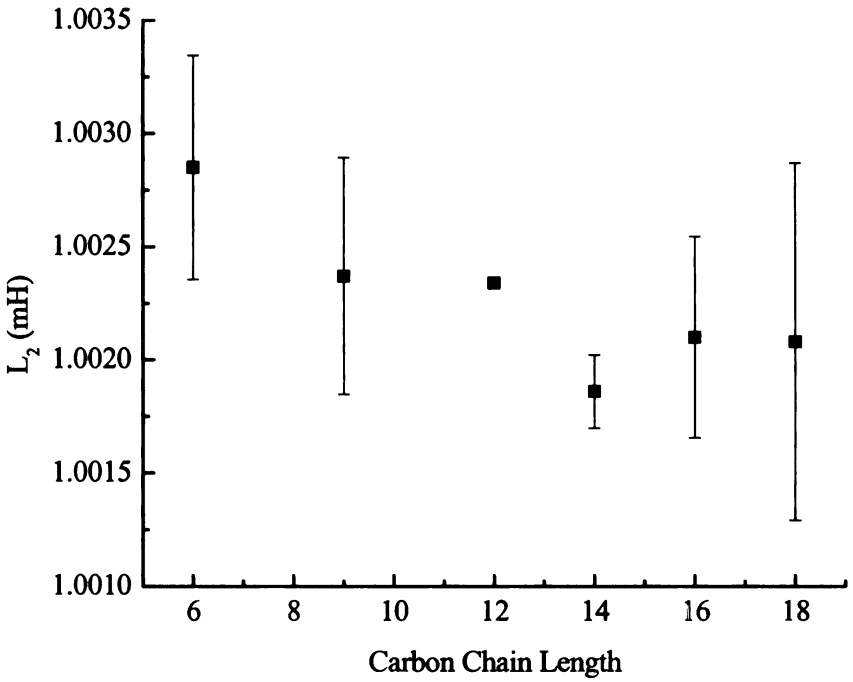

Figure 4.8. Inductance of alkanethiol SAMs of varying carbon chain length

These interesting findings provide some insight into the evolution of SAM viscoelastic properties. The data reported here indicate that the aliphatic chain length, at least in the range of $C_9 - C_{16}$, does not play a dominant role in determining the viscoelastic properties of alkanethiol SAMs. There are two possible contributions to the structural evolution of the SAMs; rearrangement or adsorption and desorption of the thiol head groups on the Au surface to form a well organized monolayer, and the evolution of the aliphatic chains. It is clear that these two processes cannot be separated cleanly because the formation of predominantly all-*trans* aliphatic chains is a cooperative effect, requiring the presence of neighboring chains. Our data appear to implicate head group mediated organization as the dominant process, consistent with what is known about SAMs. While the initial mass

deposition is fast for SAMs, the organization of the headgroups into a well-ordered array may take substantially longer, depending on the experimental conditions. For the interaction of aliphatic chains with one another, the characteristic energy of interaction is ca. 300 cal/mol-CH_2. For a C_{16} system, the energetic driving force for chain annealing will be ca. 4.8 kcal/mol. In contrast, the enthalpy of the Au-S bond formation has been measured to be on the order of 20 kcal/mol.[13] The relative energies of these processes indicate that the limiting factor in achieving an organized monolayer is the equilibrium adsorption and desorption of the thiol groups on the Au surface, consistent with our findings.

From the L_2 values, it is possible to extract the quantity $\rho\eta$ (Eq. 3), and the dependence of $\rho\eta$ on thiol aliphatic chain length is presented in Figure 4.9.

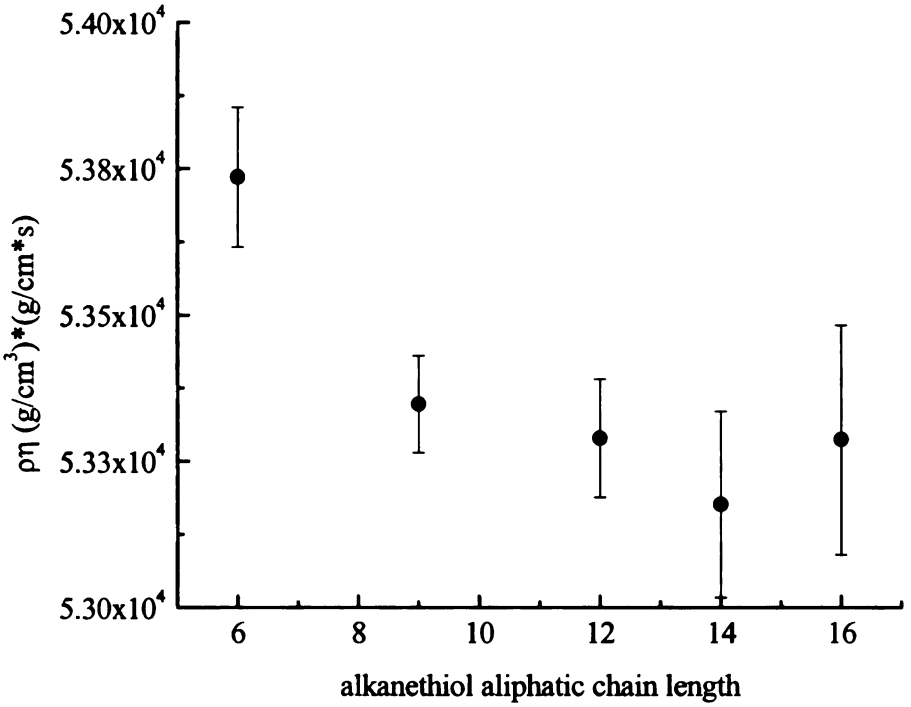

Figure 4.9. Viscoelastic response (ρη) for alkanethiol SAMs of varying carbon chain length

These data indicate that the shortest aliphatic chain examined, C_6-SH, exhibits a ρη value slightly higher than that of the other thiols, and for chain lengths C_9 – C_{16}, there is no discernible chain length dependence for ρη. This finding is interesting in that the higher the ρη value, the more "rigid" the adlayer appears to the QCM. For sufficiently short SAM aliphatic chains, there is limited opportunity for viscous interactions with the solvent. It is known that for the longer aliphatic chains examined, there is a break in the extent of SAM organization at C_9. Once the CH_2 attractive interactions become sufficiently strong, the SAM is capable of creating a predominantly all-*trans* aliphatic chain structure. For such an organized structure, it would appear that the chain length of the SAM would matter little, because in all cases the structure of the SAM in contact with

the solvent is the same. Our experimental data lend credence to this explanation, as the $\rho\eta$ values are approximately constant for chain lengths between C_9 and C_{16}. In the above discussion, the term $\rho\eta$ has been considered, without attempting to separate the density and viscosity contributions. The density of thiol head groups will be determined by the Au substrate, and should be the same for all of the SAMs. Changes in aliphatic chain length will not affect the density because the thickness of the film scales with number of carbons, so the primary experimental variable in the term $\rho\eta$ is the adlayer viscosity, η. Therefore, evaluation of the L_2 variable, as determined thorough model fitting of experimental data, can be used to investigate the relative viscosities of the SAMs as a function of aliphatic chain length.

C_{18} SAMs. In the discussion to this point, the focus has been on the results for alkanethiols C_6-SH through C_{16}-SH. The results of that work indicate that the viscoelastic properties of the SAMs in this aliphatic chain length range are remarkably similar. In contrast, the data recorded for C_{18}-SH is fundamentally different. These data are presented below and the uniqueness of C_{18}-SH may be attributed to the fact that the measurements are performed at 14°C, and the solubility of C_{18}-SH in ethanol at this temperature is limited. Figure 4.5b shows the time-dependent impedance response of QCMs exposed to a C_{18}-SH solution. These data stand in sharp contrast to the spectra shown in Figure 4.5a for C_9, (which are the same functional form for C_{16} and shorter aliphatic chains) and demonstrate that the deposition and structural evolution mechanism is fundamentally different for C_{18}-SH. Coincident with this spectral evolution, we observe bulk deposition of material on the QCM surface (Figure 4.10).

Figure 4.10. QCM crystal with a) C_{16}-SH monolayer and b) C_{18}-SH monolayer. Both SAMs were deposited from ethanolic solution.

The formation of physical deposits on the QCM electrodes perturbs the response of the device significantly, leading to values obtained for both growth rate and $\rho\eta$ which are significantly different from the C_6-C_{16} examples. The C_{18} growth rate is an order of magnitude faster than the corresponding growth rates for the other SAMs (growth rate = (3.0±2.0) x 10^{-4} mH/hr for C_{18} versus ~10^{-5} mH/hr for C_6-C_{16}). The observed $\rho\eta$ value for C_{18}-SH is 25% lower than those obtained for the C_9-C_{16} SAMs. Further examination of the C_{18}-SH monolayer deposition at elevated temperatures would be required to elucidate more information on the deposition kinetics and viscoelastic properties of SAMs with C_{18} and longer aliphatic chains.

Conclusions

The time evolution of the impedance spectra of QCM devices that have been modified by the presence of an alkanethiol SAM adlayer have been measured. This study addresses the issue of how the viscoelastic properties of the SAM vary with aliphatic chain length and time after initial formation. Impedance spectra can be interpreted in the context of an equivalent circuit model used by Martin to understand QCM response in liquids.[23] In the equivalent circuit, two components dominate the physical and chemical contributions of the adlayer to the QCM response. These quantities, L_2 and R_2 in Figure 4.1b, have similar time-courses for all of the alkanethiols examined in this study, and from these quantities information can be extracted about the quantity $\rho\eta$, which is related to the viscoelastic properties of the SAM adlayer. SAMs having between 9 and 16 carbons in their aliphatic chains are characterized by nominally the same value of $\rho\eta$ indicating similar solvent-monolayer interfacial environments. The C_6SH monolayer has a slightly higher $\rho\eta$ value, a finding which is ascribed to the absence of aliphatic chain organization and thus a stronger coupling to the solvent. In other words, the shorter aliphatic chain gives rise to a different adlayer-solvent coupling than is seen for the longer alkanethiols. This difference is coupling is manifested in this model by a higher viscosity term. We believe the viscosity term to dominate changes in $\rho\eta$ because both the monolayer density and bulk thiol density are constant for the systems reported here. It was found that deposition of C_{18}-SH differed from that of the shorter alkanethiols, likely a consequence of the limited solubility of this alkanethiol. The anomalous behavior of C_{18} SAMs can be attributed to the bulk deposition of the thiol on the QCM surface.

This study shows that simple measurements of the impedance spectrum of a QCM crystal during alkanethiol monolayer deposition can be used in conjunction with modeling of the response to provide information on the evolution of monolayer organization. Our findings indicate that the viscoelastic properties of alkanethiol SAMs change little with aliphatic chain length for systems where the aliphatic chains are long enough to exhibit organization due to attractive interchain interactions.

References

1. Allara, D. L.; Nuzzo, R. G., Spontaneously Organized Molecular Assemblies .1. Formation, Dynamics, and Physical-Properties of Normal-Alkanoic Acids Adsorbed from Solution on an Oxidized Aluminum Surface. *Langmuir* **1985,** 1, (1), 45-52.

2. Bain, C. D.; Troughton, E. B.; Tao, Y. T.; Evall, J.; Whitesides, G. M.; Nuzzo, R. G., Formation of Monolayer Films by the Spontaneous Assembly of Organic Thiols from Solution onto Gold. *Journal of the American Chemical Society* **1989,** 111, (1), 321-335.

3. Bain, C. D.; Evall, J.; Whitesides, G. M., Formation of Monolayers by the Coadsorption of Thiols on Gold - Variation in the Head Group, Tail Group, and Solvent. *Journal of the American Chemical Society* **1989,** 111, (18), 7155-7164.

4. Nuzzo, R. G.; Allara, D. L., Adsorption of Bifunctional Organic Disulfides on Gold Surfaces. *Journal of the American Chemical Society* **1983,** 105, (13), 4481-4483.

5. Bain, C. D.; Whitesides, G. M., Formation of Monolayers by the Coadsorption of Thiols on Gold - Variation in the Length of the Alkyl Chain. *Journal of the American Chemical Society* **1989,** 111, (18), 7164-7175.

6. Bain, C. D.; Biebuyck, H. A.; Whitesides, G. M., Comparison of Self-Assembled Monolayers on Gold - Coadsorption of Thiols and Disulfides. *Langmuir* **1989,** 5, (3), 723-727.

7. Nuzzo, R. G.; Fusco, F. A.; Allara, D. L., Spontaneously Organized Molecular Assemblies .3. Preparation and Properties of Solution Adsorbed Monolayers of Organic Disulfides on Gold Surfaces. *Journal of the American Chemical Society* **1987,** 109, (8), 2358-2368.

8. Nuzzo, R. G.; Zegarski, B. R.; Dubois, L. H., Fundamental-Studies of the Chemisorption of Organosulfur Compounds on Au(111) - Implications for Molecular Self-Assembly on Gold Surfaces. *Journal of the American Chemical Society* **1987,** 109, (3), 733-740.

9. Bain, C. D.; Whitesides, G. M., Modeling Organic-Surfaces with Self-Assembled Monolayers. *Angewandte Chemie-International Edition in English* **1989,** 28, (4), 506-512.

10. Dubois, L. H.; Nuzzo, R. G., Synthesis, Structure, and Properties of Model Organic-Surfaces. *Annual Review of Physical Chemistry* **1992,** 43, 437-463.

11. Folkers, J. P.; Zerkowski, J. A.; Laibinis, P. E.; Seto, C. T.; Whitesides, G. M., Designing Ordered Molecular Arrays in 2 and 3 Dimensions. *Acs Symposium Series* **1992,** 499, 10-23.

12. Lee, T. R.; Laibinis, P. E.; Folkers, J. P.; Whitesides, G. M., Heterogeneous Catalysis on Platinum and Self-Assembled Monolayers on Metal and Metal-Oxide Surfaces. *Pure and Applied Chemistry* **1991,** 63, (6), 821-828.

13. Schessler, H. M.; Karpovich, D. S.; Blanchard, G. J., Quantitating the balance between enthalpic and entropic forces in alkanethiol/gold monolayer self-assembly. *Journal of the American Chemical Society* **1996,** 118, 9645-9651.

14. Brust, M.; Walker, M.; Bethell, D.; Schiffrin, D. J.; Whyman, R., Synthesis of Thiol-Derivatized Gold Nanoparticles in a 2-Phase Liquid-Liquid System. *Journal of the Chemical Society-Chemical Communications* **1994,** (7), 801-802.

15. Chailapakul, O.; Sun, L.; Xu, C. J.; Crooks, R. M., Interactions between Organized, Surface-Confined Monolayers and Vapor-Phase Probe Molecules .7. Comparison of Self-Assembling N-Alkanethiol Monolayers Deposited on Gold from Liquid and Vapor-Phases. *Journal of the American Chemical Society* **1993,** 115, (26), 12459-12467.

16. Thomas, R. C.; Sun, L.; Crooks, R. M.; Ricco, A. J., Real-Time Measurements of the Gas-Phase Adsorption of Normal-Alkylthiol Monolayers and Multilayers on Gold. *Langmuir* **1991,** 7, (4), 620-622.

17. Schlenoff, J. B.; Li, M.; Ly, H., Stability and self-exchange in alkanethiol monolayers. *Journal of the American Chemical Society* **1995,** 117, (50), 12528-12536.

18. McCarley, R. L.; Dunaway, D. J.; Willicut, R. J., Mobility of the alkanethiol-gold (111) interface studied by scanning probe microscopy. *Langmuir* **1993,** 9, (11), 2775-2777.

19. Ulman, A., Formation and structure of self-assembled monolayers. *Chemical Reviews* **1996,** 96, (4), 1533-1554.

20. Poirier, G. E.; Tarlov, M. J.; Rushmeier, H. E., 2-Dimensional Liquid-Phase and the Px-Root-3-Phase of Alkanethiol Self-Assembled Monolayers on Au(111). *Langmuir* **1994,** 10, (10), 3383-3386.

21. Sauerbrey, G., Verwendung Von Schwingquarzen Zur Wagung Dunner Schichten Und Zur Mikrowagung. *Zeitschrift Fur Physik* **1959,** 155, (2), 206-222.

22. Karpovich, D. S.; Blanchard, G. J., Direct Measurement of the Adsorption-Kinetics of Alkanethiolate Self-Assembled Monolayers on a Microcrystalline Gold Surface. *Langmuir* **1994,** 10, (9), 3315-3322.

23. Martin, S. J.; Granstaff, V. E.; Frye, G. C., Characterization of a quartz crystal microbalance with simultaneous mass and liquid loading. *Analytical Chemistry* **1991,** 63, (20), 2272-81.

24. Martin, S. J.; Bandey, H. L.; Cernosek, R. W.; Hillman, A. R.; Brown, M. J., Equivalent-Circuit Model for the Thickness-Shear Mode Resonator with a Viscoelastic Film Near Film Resonance. *Analytical Chemistry* **2000,** 72, (1), 141-149.

25. Bandey, H. L.; Martin, S. J.; Cernosek, R. W.; Hillman, A. R., Modeling the Responses of Thickness-Shear Mode Resonators under Various Loading Conditions. *Analytical Chemistry* **1999,** 71, (11), 2205-2214.

26. Shen, D.; Kang, Q.; Huang, M.; Zhang, H.; Yang, M., Equivalent circuit model and impedance analysis for the fine response characteristics to liquid viscodensity for a piezoelectric quartz crystal sensor with longitudinal wave effect. *Analytica Chimica Acta* **2005,** 551, (1-2), 15-22.

27. Muramatsu, H.; Tamiya, E.; Karube, I., Computation of equivalent circuit parameters of quartz crystals in contact with liquids and study of liquid properties. *Analytical Chemistry* **1988,** 60, (19), 2142-6.

28. Noel, M. A. M.; Topart, P. A., High-Frequency Impedance Analysis of Quartz-Crystal Microbalances .1. General-Considerations. *Analytical Chemistry* **1994,** 66, (4), 484-491.

29. Beck, R.; Pittermann, U.; Weil, K. G., Impedance analysis of quartz oscillators, contacted on one side with a liquid. *Berichte der Bunsen-Gesellschaft* **1988,** 92, (11), 1363-8.

30. Kipling, A. L.; Thompson, M., Network analysis method applied to liquid-phase acoustic wave sensors. *Analytical Chemistry* **1990,** 62, (14), 1514-19.

Chapter 5

Optical Organophosphate Sensor Based upon Gold Nanoparticle Functionalized Fumed Silica Gel

Introduction

Over the past several years, organophosphates and phosphonates (OPPs) have become increasingly important as analytes for several reasons. Many nerve agents and pesticides are organophosphates or organophosphonates, so detecting small quantities and/or low concentrations of these compounds critically important for human health and safety. In certain cases, sequestration is desirable owing to the toxicity of the analyte. Ratification of the Chemical Warfare Convention (CWC) has underscored the need to develop rapid, sensitive, and selective detectors for chemical warfare agents and other organophosphate/phosphonate compounds in order to verify compliance with the provisions of the treaty.[1] Contamination of groundwater and agricultural products entering the human food chain by organophosphate/phosphonate pesticides has also led to the need for sensitive detection and sequestration methods.[2-9] We report here on the development of a high-surface area material based upon silica microparticles. The use of covalently attached gold nanoparticles (AuNPs) as a surface area enhancing scaffold and a foundation for surface modification chemistry allows for the creation of a high affinity material that is selective primarily for OPP compounds.[10-13] Once the analyte(s) have

been sorbed onto this novel material, the coated silica particles can be suspended in a solvent and the AuNP plasmon resonance can be monitored with relatively high signal to noise ratio, depending on the choice of solvent. While there are technical challenges associated with this approach, we have chosen to use fumed silica in conjunction with AuNPs because the fumed silica can be suspended in aqueous and other solutions without aggregation for extended periods of time, unlike AuNPs, because silica microparticles are more amenable to physical separation methodologies, such as filtering, than AuNPs, and because this structural motif provides a relatively high surface-to-volume ratio to enhance the adsorption and sequestration of OPP species.

Current methods for detection of OPP compounds include chromatographic techniques,[14-19] mass spectrometric methods,[15, 17] electrochemical detection,[3, 6, 7, 20, 21] biosensors,[3, 7-9, 20, 21] and fluorescent beads.[22] While these techniques have many advantages, including sensitivity and selectivity, they are often time consuming and labor intensive. The ideal OPP sensor would possess the sensitivity and selectivity of the already-established methods and would reduce the dependence on expensive instrumentation. Robustness, simplicity, the ability to sequester the analyte of interest, and possible incorporation into existing air filtration schemes would be beneficial, and there are several recent examples of OPP sensors based on nanoparticles which begin to satisfy these requirements.[3, 6, 8, 22] Both AuNPs and zirconium oxide (ZrO_2) nanoparticles have shown promise in the detection of OPPs. Pavlov, Xiao and Willner have demonstrated the utility of AuNP plasmon resonance measurements for the optical determination of OPPs[23] and Liu and coworkers[6] have demonstrated an OPP sensor based on the affinity of the analyte for ZrO_2 nanoparticles. In that work, the binding of the

OPPs to the nanoparticles was determined electrochemically. In this work, we combine the chemical advantages of Liu's sensor with the simple detection scheme of Pavlov's sensor to create a high-surface area optical sensor and sequestration medium for OPPs. The sensor / dosimeter methodology we report here utilizes several well established chemical reactions to achieve relatively low level detection and OPP sequestration simultaneously.

The material and measurement methodology is based on a series of well established silica and gold surface modification reactions. First, the silica gel is functionalized with a mercaptosilane[24-27] followed by attachment of AuNPs by stirring the functionalized silica gel in an aqueous citrate-stabilized AuNP colloidal solution.[11, 28-30] Following the attachment of AuNPs, the citrate stabilizer is displaced by exposing the silica-bound AuNPs to an ethanolic solution of an ω-hydroxythiol.[31] The hydroxyl termini on the AuNPs are then reacted with $POCl_3$, H_2O and Zr^{4+} to form a zirconium-phosphate (ZP) terminated surface. This chemistry was pioneered by the Mallouk, Thompson and Katz groups,[13, 25, 32, 33] and the Blanchard group has made extensive use of ZP chemistry to grow robust interfacial films efficiently.[34-37] Because the ZP chemistry operates by using Zr^{4+} to link phosphate and/or phosphonate groups, the terminal Zr^{4+} ions on our modified AuNPs have a high affinity for OPPs.[6, 35] The ZP chemistry could be used directly on the silica gel to produce a surface with high affinity for OPPs, and it is possible that the chemistry applied to the AuNPs could also react with any residual surface silanol groups on the silica gel. Here the AuNPs are used as optical reporting agents, where the plasmon resonance band of the AuNP is sensitive to the condition of the ZP linkage bound to its surface.

Both the material and the associated plasmon resonance detection methodology reported on here are useful in several regards. First, the covalent nature of the attachment chemistry makes it robust and able to be stored under ambient conditions. Second, the incorporation of AuNPs provides access to the plasmon resonance, a band that is remarkably sensitive to changes in the local dielectric environment of the AuNPs. The plasmon resonance band is observed to blue-shift when OPPs bind to the ZP-modified particles, and this data may be interpreted in the context of two spectrally overlapped bands, rendering an apparent blue-shift. The magnitude of the observed spectral shift is independent of OPP concentration after its initial appearance at a threshold OPP concentration in the microgram/liter range, and we understand this behavior through a simple complexation model.

Materials and Methods

Materials. Silica gel (Grade 633, 200-425 mesh, average surface area 480 m^2/g, with an average particle diameter of 63.6 μm, as determined by scanning electron microscopy) was purchased from Spectrum and used as received. Sodium citrate, hydrogen tetrachloroaurate ($HAuCl_4 \cdot 3H_2O$, 99.9+%), methylphosphonic acid (MPA) (Figure 5.1a), diethylchlorophosphate (DECP) (Figure 5.1b), and 3-mercaptopropyltrimethoxysilane (MPTMS) were purchased from Sigma-Aldrich and used as received.

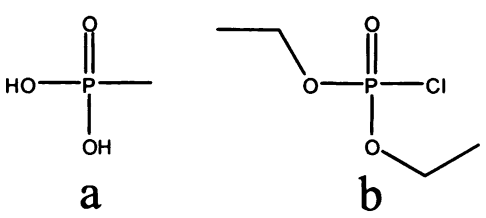

Figure 5.1. OPP analytes a) methylphosphonic acid and b) diethylchlorophosphate

6-Mercapto-1-hexanol and phosphorous oxychloride ($POCl_3$) were purchased from Fluka and used as received. Collidine was purchased from Spectrum and used as received. Zirconium(IV) oxychloride octahydrate ($ZrOCl_2 \cdot 8H_2O$) was purchased from Allied and used as received.

Preparation of AuNP Colloid. AuNPs were synthesized by reduction and stabilization with sodium citrate according to a modification of a published procedure.[38] A 1% (w/w) solution of $HAuCl_4 \cdot 3H_2O$ was added to a vigorously stirred aqueous solution of sodium citrate. The solutions were combined for an overall molar ratio of 3:1 sodium citrate:$HAuCl_4 \cdot 3H_2O$. The plasmon resonance band of the resulting colloid was centered at ca. 530 nm. SEM images of particles made using this method indicate an average particle size of 20 nm (Figure 5.2).

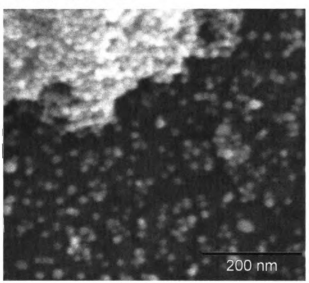

Figure 5.2. SEM image of AuNPs prepared by the citrate reduction method. Average particle size is 20 nm.

Silica Gel Functionalization. Silica gel (0.5 g) was placed into a round bottom flask with an oval stir bar. A 5% (v/v) solution of MPTMS in toluene (10 mL) was added to the

round bottom flask and stirred at room temperature for 24 hours. The silica gel was filtered, rinsed with copious amounts of toluene and ethanol, and returned to a dry round bottom flask. The aqueous solution of AuNPs (50 mL) was added to this round bottom flask and stirred for 24 hours at room temperature, filtered, then rinsed with water and ethanol. These reaction conditions provide a AuNP:Silica particle ratio of ca. 10^9. The silica gel coated with AuNPs was returned to a round bottom flask and a 10 mM ethanolic solution of 6-mercapto-1-hexanol (10 mL) was added. The slurry was stirred at room temperature overnight. The product was filtered, rinsed with ethanol and ethyl acetate and dried under vacuum in a round bottom flask for a minimum of two hours. The flask was purged with argon, then placed under vacuum again. To this round bottom flask was added a solution of 3.5% (v/v) $POCl_3$/5% (v/v) collidine in anhydrous acetonitrile. The resulting slurry was kept under an argon atmosphere and stirred overnight. The silica gel slurry was filtered, rinsed with acetonitrile, then acetone, and distilled water. The silica gel was returned to a dry round bottom flask. To this flask was added a solution of 5 mM $ZrOCl_2$ in 60:40 ethanol-water and the slurry was stirred at room temperature overnight. The functionalized silica gel was filtered, rinsed with ethanol and dried under vacuum for a minimum of 24 hours prior to use. For measures of model analytes, the analytes were introduced as ethanolic solutions and the resulting slurry stirred at room temperature overnight prior to spectroscopic analysis.

UV-visible spectroscopy. UV-visible spectroscopy was performed in transmission mode using a Cary model 300 UV-visible spectrometer (Varian), with 1 nm resolution. Spectra over the range of 400 nm to 800 nm were acquired at a scan rate of 600 nm/min. Measurements were made using 3 mL of ethanolic solution (0.50 g silica gel/5 mL

ethanol) for each measurement. The maximum absorbance for the PR was determined by integration of the spectrum.

Scanning Electron Microscopy (SEM). The samples were imaged using a JEOL JSM-6300F Scanning Electron Microscope at 25kV accelerating voltage. The sample was placed on a SEM stub and was sputter coated with 3 nm of gold prior to analysis.

Results and Discussion

Four central issues are considered in this work. These are the chemical selectivity of the AuNP-coated silica gel, the morphology of this system, the mechanism by which the interaction of OPPs with the AuNP-coated silica gel are observed, and the sensitivity of this material to the presence of OPPs. These issues will be considered separately.

Chemical selectivity. The chemistry used to achieve selective adsorption of the OPPs onto the AuNPs is, as noted above, zirconium bisphosphonate (ZP) chemistry. This chemistry has been studied extensively by the Clearfield group[39-41] in the solid state and by the Mallouk, Thompson and Katz groups[11, 13, 25, 32, 33, 42-45] for binding at surfaces. It is difficult in many instances to determine the strength of the ZP bond because the equilibrium for bond formation lies far to the right, but indirect estimates of the strength of the ZP bond indicate that it is ca. 60 kcal/mol or larger, under favorable conditions.[37] The issue is thus what other compounds can complex with Zr^{4+} and whether or not Zr^{4+}, once in place can be displaced by other metal ions. Bakiamoh and Blanchard have found that $Zr(RPO_3)^{2+}$ can form complexes with RSO_3^- and RCO_2^-, but these complexes are not as strong as the $Zr(RPO_3)_2$ system.[46] While not quantitative, the formation constant for OPPs with the $Zr(RPO_3)^{2+}$ functionalized surface should be sufficiently more favorable

than for complexation with sulfonates and carboxylates and that OPPs will displace these compounds in a competitive system. It is also important to note that while there may be slight differences in binding efficiency for the different OPPs, in all cases the binding to Zr^{4+} is sufficiently strong that preferential binding phenomena are not expected. These AuNP-coated silica particles are thus selective for the entire class of OPP compounds rather than for a specific OPP.

Also of concern in the design of this sensor is the use of Zr^{4+} as opposed to other metal ions. There is a body of literature on the use of other metals in bisphosphonate structures and the conclusion of that work is that most other metal ions, especially with a formal charge lower than that of Zr^{4+}, will not bind as strongly to phosphates or phosphonates.[47] The only other metal ion that is known to bind to phosphates or phosphonates as strongly is Hf^{4+}.[48-50]

Morphology. We show in Figure 5.3 a scanning electron microscope (SEM) image of silica gel particles prior to their reaction with the AuNP-containing solution.

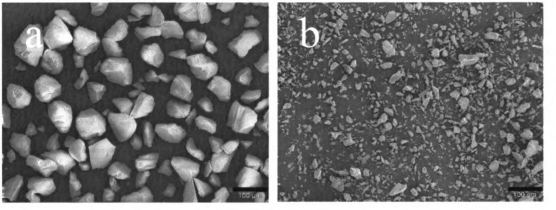

Figure 5.3. SEM image of a) unfunctionalized silica gel beads with average particle size of approximately 63.6 μm and b) AuNP-functionalized silica gel beads with average particle size of approximately 10 μm. Measurement bar indicates 100 μm.

The silica particles are not regular in shape and are characterized experimentally as having an average diameter of 63.6 μm (Figure 5.3a). The treatment to which the silica particles are subjected appears to have a significant influence on their morphology. As can be seen in Figures 5.3a and 5.3b, the average particle size is substantially smaller following reaction of the silica particles with silane and AuNPs. While this may be due in part to the harsh nature of the functionalization chemistry, it is more likely a result of milling caused by the rigorous physical agitation required for the functionalization of the silica gel. This size reduction is advantageous as the resulting slurrys remain suspended longer than the non-functionalized silica gel particles. The SEM images reveal an apparent spatially heterogeneous distribution of AuNPs, implying that the surface AuNP coverage is not characterized by a homogeneous monolayer. Despite the limited resolution of our images, it is clear that the functionalized surface (Figure 5.4b) exhibits more roughness than the non-functionalized surface (Figure 5.4a).

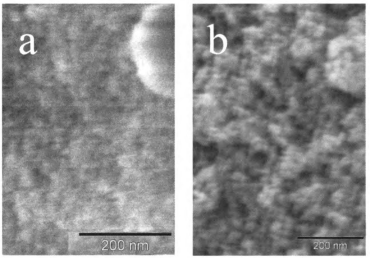

Figure 5.4. SEM image of the surface of a) unfunctionalized silica gel beads (as seen in Figure 5.3a) and b) AuNP-functionalized silica gel beads (as seen in Figure 5.3b). The measurement bar represents 200 nm in each image.

This rougher surface, combined with the macroscopic observation of the purple color of the silica gel, is indicative of the binding of AuNPs to the silica gel. Further attempts to characterize this apparent roughness using atomic force microscopy were unsuccessful due to the large difference in the size domains of the silica gel and AuNPs. A significant issue lies in understanding the reaction efficiency and resulting optical properties of the AuNPs that are bound to the silica particles, and this issue is considered next.

Characterization of the AuNP-coated silica. Because the optical properties of AuNPs are comparatively well understood, we use absorption spectroscopy as the basis for understanding AuNP surface coverage of the silica particles. We use absorption spectroscopy to determine the amount of AuNP present and estimate the silica particle concentration and surface area based on particle size and mass used. Because of the change in silica particle size seen upon deposition of AuNPs, we provide a AuNP surface coverage range.

Using a 0.5 g sample of modified silica particles in 10 mL of ethanol, we observe the plasmon resonance band with a peak centered near 528 nm, and a background-corrected absorbance of 3.27 (Figure 5.5, black trace).

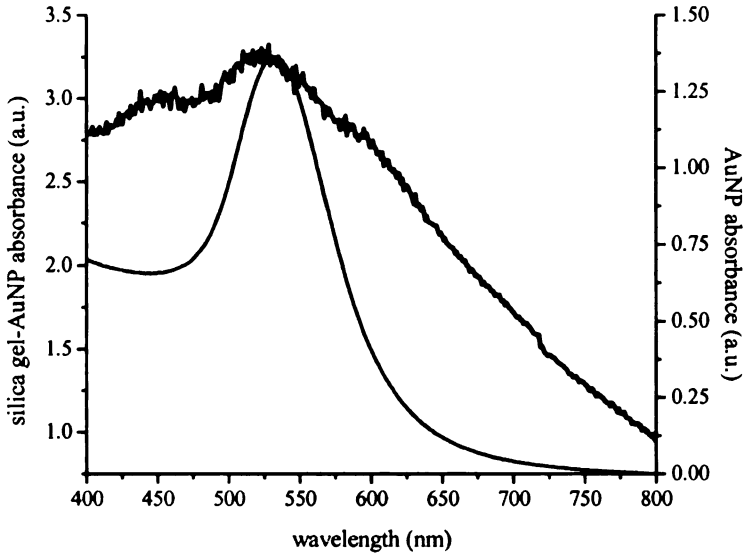

Figure 5.5. UV-visible spectrum of AuNP-functionalized silica gel beads with the spectrum of unfunctionalized silica gel beads subtracted in ethanol (black line) and citrate stabilized AuNPs (gray line).

Despite the adsorption of the AuNPs onto the silica gel substrate, there was not a significant plasmon band shift compared to the citrate stabilized AuNPs in the same solvent (Figure 5.5, gray trace). The active surface of the bound AuNPs apparently experiences an environment similar to that of the unbound AuNPs. There are clearly some differences, however, as can be seen in the different band profiles for the free and surface bound AuNPs. The added width of the bound AuNP plasmon band could be due to a range of binding sites on the silica particles. It should also be noted here that despite the high absorbance of 3.27, we remain well within the linear response range of the instrument used in these measurements, which has an upper limit of 5 absorbance units. The literature value for the extinction coefficient for 30 nm AuNPs is 4.7×10^9 L/mol-cm,[51-53] and this value is used for the nanoparticles in this study. Using a 1 cm pathlength cuvette, a concentration of 6.96×10^{-10} M is calculated. This corresponds to a density of

4.19×10^{11} AuNP/cm^3. With this AuNP loading density, we consider next the number of silica particles present, and their surface area.

There are subtle features in the plasmon resonance spectrum for the surface bound AuNPs at ca. 450 nm and ca. 580 nm (Figure 5.5). While the limited S/N ratio of the data and the breadth of the plasmon resonance make any detailed assignment difficult, we can speculate that there are several types of coupling of the AuNP to the silica, and the 580 nm band reflects a subgroup of AuNPs bound in a different manner. This band (Figure 5.6) does not exhibit a positional-dependence on OPP concentration.

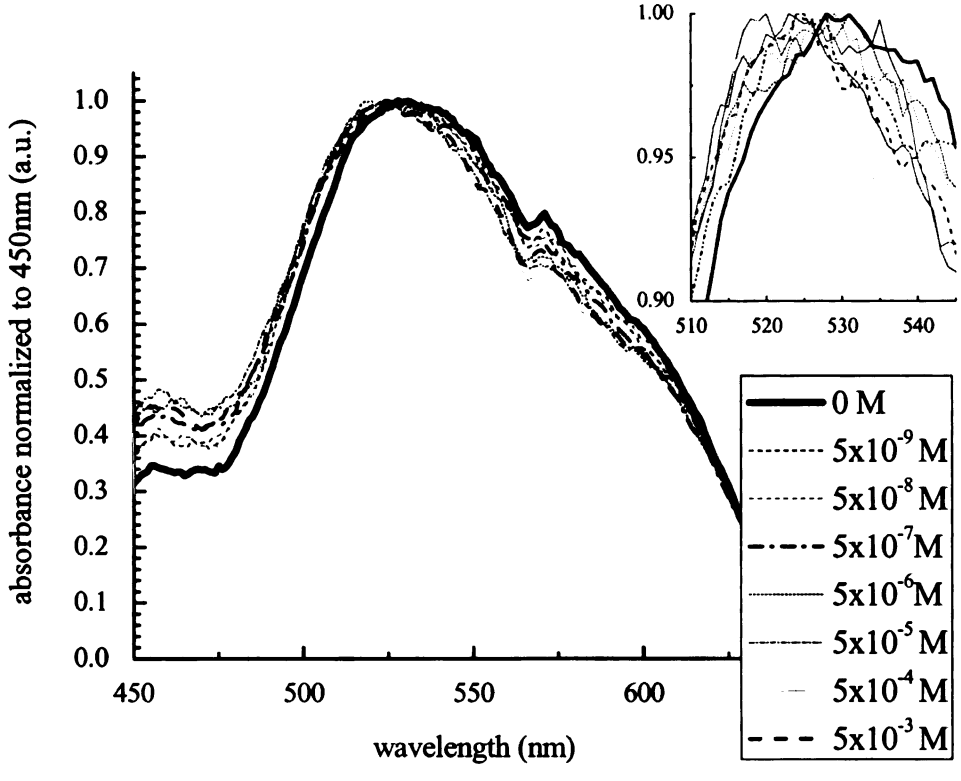

Figure 5.6. UV-visible spectra of silica gel sensor exposed to varying concentrations of DECP. Absorbance has been normalized to 450 nm absorbance.

Further, more detailed spectroscopic studies could perhaps shed some light on the origin of the 580 nm band.

Several assumptions are made for the purposes of simplicity in calculations. First an upper bound of 63.6 μm was placed on silica particle size (from the experimental diameter). Also, spherical particles are assumed as well. While this is clearly not a highly accurate estimate, the concern here is the establishment of a range of surface coverage rather than determining a precise value. The volume of a 63.6 μm diameter spherical particle is 1.35×10^{-7} cm^3. A density for the silica particle of 2.0 g/cm^3 is assumed, recognizing that this is somewhat less than that of fused silica (2.2 g/cm^3). This estimate is made under the assumption that the porosity of the silica gel likely reduces its density compared to the corresponding solid material. Using a value of $\rho = 2.0$ g/cm^3, the mass of a silica particle is estimated to be 2.69×10^{-7} g. In a 0.5 g sample, there are thus 1.86×10^6 particles in a 10 mL sample volume. From this estimate of 4.19×10^{11} AuNP/cm^3 and 1.86×10^5 silica particles/cm^3, we obtain 2.25×10^6 AuNP/silica particle. The size of the AuNPs used in this work is ca. 10 nm radius, so the corresponding "footprint" of an AuNP is 3.14×10^{-12} cm^2/AuNP. If the silica particle were covered with a uniform monolayer of AuNPs, 4.04×10^7 AuNP would be on each silica particle. Comparing the absorbance-based estimate of 2.25×10^6 AuNP/particle to a maximum coverage of 4.04×10^7 AuNP/silica particle yields a surface coverage of 5.6 % of a monolayer. If we make the same estimate as above, but using 10 μm diameter silica particles, to more accurately reflect the reacted particle size distribution shown in Figure 5.3b, a silica particle density in solution of 4.77×10^7 particles/cm^3 is assumed, and a surface area of 3.14×10^{-6} cm^2/particle is calculated. For these smaller silica particles, the absorbance data indicate the presence of 8784 AuNP per silica particle and a theoretical maximum coverage of 1.00×10^6 AuNP per silica particle, corresponding to a

0.8% AuNP surface coverage. From these two silica particle size limits, we see that the surface coverage ranges from 0.8% to 5.6%, depending on particle size. While it may be tempting to make a closer estimate of AuNP coverage, we believe that this would not be a useful exercise given the particle size distribution present in the samples. This range of coverage probably provides a realistic estimate of the coverage range that exists within a given sample. With this coverage range in hand, we now turn to understanding the mechanism for the AuNP plasmon band shift that is seen upon exposure to OPPs.

A spectral blue-shift is observed on complexation of the surface-modified AuNPs with OPPs. The plasmon resonance is well understood and generally the band position and linewidth are expected to vary with particle size and dielectric constant of the local environment (Eq. 1).[54]

$$\sigma(\omega)_{abs} = 9\frac{\omega}{c}\varepsilon_m^{3/2}V_0\frac{\varepsilon_2(\omega)}{[\varepsilon_1(\omega)+\varepsilon_m]^2+\varepsilon_2(\omega)^2} \quad (1)$$

where ε_m is the dielectric constant of the medium surrounding the nanoparticle, V_0 is the particle volume, and ε_1 and ε_2 are the real and imaginary components, respectively, of the frequency-dependent dielectric response of metallic gold.[55] For the experimental conditions described here, neither the particle volume nor the dielectric response of the metal are influenced to any significant extent by the binding of the OPP to the particle surface. The plasmon resonance frequency changes observed here are influenced most significantly by the dielectric constant of the AuNP immediate environment. The blue-shift indicates OPP binding causes a decrease in the dielectric response of AuNP immediate environment. While the position of the pre-exposure band is influenced by the size of the nanoparticles and the degree of nanoparticle binding it is likely that the AuNP surface coverage would influence the absorbance but not the magnitude of the spectral

blue-shift. Based on this information, the blue band in the overlapped band model presented below is used to represent the complexed form of the ZP-coated AuNP.

Interpreting the band shift. The measured plasmon resonance band can be treated as two spectrally overlapped bands, one associated with the free form of the AuNP and one associated with an OPP complexed to an AuNP through a ZP linkage. In this model, the spectral shift associated with complexation is due to the modulation of the dielectric response of the environment immediately surrounding the AuNP. Within the framework of this model, we begin by assuming that only one complexation event per AuNP is required to produce the observed spectral shift. If multiple complexation events were required to produce the observed band shift, the OPP concentration dependence of this effect would have a different functional form than is seen experimentally (*vide infra*). The complexation reaction can be described by

$$\text{OPP} + \text{ZP-AuNP} \rightarrow \text{OPP-ZP-AuNP} \quad (2)$$

$$K = [\text{OPP-ZP-AuNP}]/[\text{ZP-AuNP}][\text{OPP}] \quad (3)$$

Where OPP-ZP-AuNP is the complex between the OPP analyte and the ZP-functionalized AuNP. The extinction coefficients of the free and complexed AuNPs are taken to be the same owing to the slight perturbation that the complexation event causes to the AuNP electronic transitions. Under this condition, the ratio of the free and complexed absorption bands is proportional to [ZP-AuNP]/[OPP-ZP-AuNP]. In this model, when [ZP-AuNP]/[OPP-ZP-AuNP] ≤ 0.1 or ≥ 10, the AuNP plasmon band will appear to be either that of the fully complexed form (blue band) or the free form (red band), respectively. For spectrally overlapped bands, the apparent center wavelength will correspond to the weighted average of the band maxima for the free and complexed

forms. When [ZP-AuNP]/[OPP-ZP-AuNP] = 1, giving rise to a plasmon band intermediate between the free and complexed forms, $K = [OPP]^{-1}$, and this point is observed experimentally for [DECP] = 5×10^{-7} M. With the value of K in hand, [ZP-AuNP]/[OPP-ZP-AuNP] can be calculated as a function of [OPP], and thus estimate the experimental plasmon band center wavelength.

Sensor response to OPP Compounds. To determine the response of the silica gel to OPPs, we prepared 2 mM solutions of MPA and DECP in ethanol. Ten mL of either MPA or DECP solution was added to a clean 20 mL scintillation vial containing approximately 0.5 g of functionalized silica gel and a stir bar. Ten mL ethanol with no analyte was added to separate vials containing 0.5g functionalized silica gel as a blank. For all of these measurements, the portions of functionalized silica gel used came from the same batch. The resulting slurries were stirred overnight prior to analysis to ensure completion of the ZP complexation reaction. In practice, the kinetics of ZP complex formation are fast, with Mallouk previously reporting indistinguishable results from incubation times of one hour and 24 hours.[32] The sample containing no analyte demonstrated a plasmon resonance maximum at 519 nm ± 3 nm (1σ) (Figure 5.7, trace a, Table 5.1).

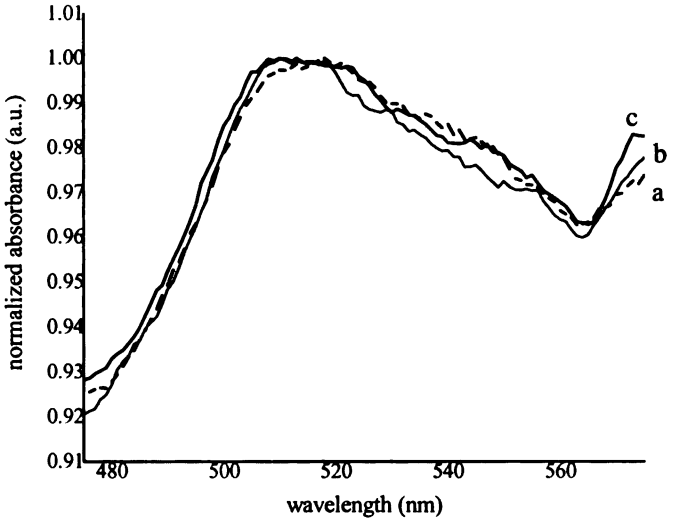

Figure 5.7. Response of MPTMS functionalized silica gel sensor to 24 hour exposure to a) ethanol, b) 2 mM MPA, and c) 2 mM DECP

Analyte	PR (nm)	Blue Shift (nm)
2mM MPA	516 ± 6	3
2mM DECP	514 ± 4	4
EtOH (blank)	519 ± 2	

Table 5.1. Response of sensor to OPP compounds compared to the ethanol control sample

Both samples containing OPPs exhibited a plasmon resonance blue-shift relative to the reference samples. The silica gel slurry with MPA analyte exhibited a plasmon resonance at 514 nm ± 4 nm (Figure 5.7, trace b) and the silica gel slurry with DECP analyte exhibited a plasmon resonance at 516 nm ± 7 nm (Figure 5.7, trace c), corresponding to blue-shifts of 5 nm and 3 nm, respectively. The uncertainties, as determined through multiple measurements of the same sample, appear relatively large,

owing to the width of the plasmon resonance bands and the limited S/N available with these data due to background scattering.

The sensitivity of our coated silica particles to OPPs was evaluated using DECP as a model OPP for concentrations ranging from $5x10^{-9}$ M to $5x10^{-3}$ M (Figure 5.6). The plasmon resonance band maximum of the analyte-exposed silica gel was compared to that of non-exposed silica gel to determine presence and magnitude of the plasmon resonance band shift. At DECP concentrations lower than $5x10^{-7}$ M, the plasmon resonance band does not manifest a spectral shift outside the spectral resolution of the measurement (± 1 nm) (Table 5.2).

DECP Concentration (M)	PR (nm)	Blue Shift from 0 mM (nm)
0	528	--
5×10^{-9}	531	--
5×10^{-8}	529	--
5×10^{-7}	525	3
5×10^{-6}	520	8
5×10^{-5}	523	5
5×10^{-4}	518	10
1×10^{-3}	526	2
5×10^{-3}	524	4

Table 5.2. Sensitivity of sensor to DECP

For DECP concentrations higher than $5x10^{-7}$ M (86.3μg/L) the modified AuNP plasmon resonance exhibits a blue-shift relative to the unexposed AuNP-modified silica particles. The errors associated with these measurements was < 1 nm for replicate measurements

and further analysis was conducted using a larger ± 3 nm error associated with experimental error due to expected scattering due to the silica gel. It should be noted that the blue-shift does not appear to reach a plateau for high OPP concentration extremes, despite the expectation of sensor saturation. The reason for this finding is likely due to the uncertainty attributed to the measurement, resulting from the background scattering from the silica particles in ethanol solution. The sensor response can be viewed as a digital response, with there being either a shift or not, making it most useful as a presumptive test for the presence or absence of OPP compounds.

We show the comparison of the experimental data to the model in Figure 5.8, where the solid lines are the model calculations for 1:1 OPP:AuNP (black trace) 2:1 OPP:AuNP (dark gray trace) and 3:1 OPP:AuNP (light gray trace), and the individual data points are the experimental band positions as a function of [OPP].

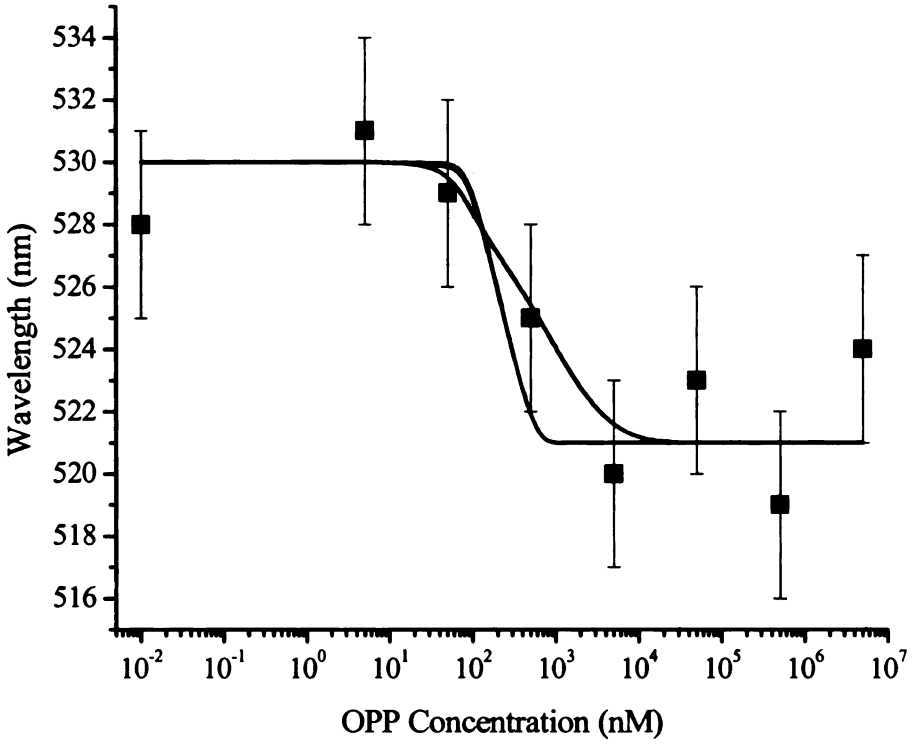

Figure 5.8. Comparison of observed PR bands to 1:1 free-complexed AuNP model (black trace), 2:1 free-complexed AuNP model (dark gray trace) and 3:1 model (light gray trace).

While there may be some contribution of 2:1 and 3:1 complexation the correspondence between the 1:1 OPP:AuNP model and the experimental data in the most variable range follows the functional form of the data more closely, especially in terms of the concentration-dependence. This correspondence between model and experimental data suggests that the assumption of a 1:1 OPP:AuNP complexation stoichiometry is valid. It should be noted that there is little distinction between 2:1 and 3:1 complexation, a finding that supports the assertion that the most noticeable change in the AuNP optical response occurs for the first complexation event. While further complexation may occur between the AuNPs and the OPP, it appears that it will not have a significant effect on the data.

We also believe that this approach to studying complexation processes holds significant promise for a number of other systems that are adaptable to surface-modification chemistry on AuNPs.

S/N Enhancement. The observed signal-to-noise ratio (S/N) for the plasmon resonance spectra of the silica gel-AuNP suspensions in ethanol prior to their exposure to an OPP was 5.8, and, significantly, there was a background signal of ca. 2.5 absorbance units. The attenuation of the transmitted light due to scattering loss gives rise to the large background. One way to reduce the scattering background is to use a solvent system that is better matched to the refractive index of the silica particles. The refractive index of silica gel is approximately 1.46.[56] By approaching the refractive index of the immersion solvent to that of the silica gel, the S/N was enhanced because of a decrease in the observed background absorbance (Table 5.3).

Solvent	Solvent Refractive Index	S/N	Background Abs (a.u.)
EtOH	1.3614	5.8	2.5
DMF	1.4305	23.1	1.75
$CHCl_3$	1.4458	36.2	1.75
DMSO	1.4783	42.0	0.37

Table 5.3. Influence of solvent refractive index on S/N ratio and background absorbance

We found that by using DMSO as the solvent, (n = 1.48), we could produce a seven-fold increase in S/N compared to ethanol (n = 1.36). This increase in S/N is associated with

the decreased background scattering observed from the DMSO solution to a level of 0.37 absorbance units (Table 5.3, Figure 5.9).

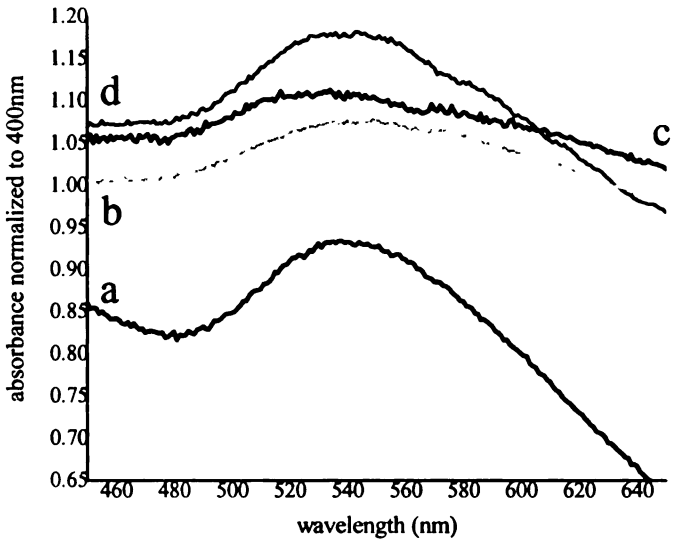

Figure 5.9. S/N of sensor in a) DMSO (S/N = 42), b) DMF (S/N = 23.1), c) ethanol (S/N= 5.8), and d) chloroform (S/N = 36.2)

We expect that this sort of increase in S/N and reduction in background signal will be especially beneficial in studies that focus on small concentrations of OPPs.

Conclusion

The detection of OPPs has become increasingly important due to concerns about organophosphate/phosphonate based chemical warfare agents and pesticides. While sensitive and class-selective detection is vital, the construction of such detection systems using simple and robust detection methodology is also of importance. The material presented here, hybrid silica gel-AuNP-ZP particles, is robust and the plasmon optical response is capable of detecting comparatively low levels of OPPs complexed to the ZP termini of the particles. These materials are synthesized simply and can be made on a

large scale, if required. The AuNP plasmon resonance shift observed is independent of OPP concentration beyond a threshold concentration of ca. $5x10^{-7}$ M for DECP, corresponding to a $K \sim 2 \times 10^6$ M^{-1}. From the functional form of the plasmon resonance maximum concentration-dependence, that the stoichiometry on the AuNP-ZP-OPP complex is estimated to be 1:1, consistent with the estimated silica gel surface loading of 1.00×10^6 to 4.04×10^7 AuNPs per silica gel particle. The sensitivity of this methodology may be improved by using a solvent system where its refractive index matches more closely the refractive index of the silica. The S/N ratio of the AuNP plasmon resonance band is improved seven-fold from 5.8 in ethanol to 42 in DMSO.

This composite material is simple to synthesize construct and utilize, and its use in the detection and sequestration of OPPs makes it useful for a host of applications in chemical warfare and pesticide analysis and remediation. The simple optical detection method is amenable to the incorporation of these materials in field-portable instruments. Continued improvements in the sensitivity and chemical selectivity of this novel material will afford its use as a sensor for presumptive testing for OPPs.

References

1. Convention on the Prohibition of the Development, Production, Stockpiling and Use of Chemical Weapons and on Their Destruction. **Organisation for the Prohibition of Chemical Weapons 2005.**

2. Halamek, J.; Pribyl, J.; Makower, A.; Skladal, P.; Scheller, F. W., Sensitive detection of organophosphates in river water by means of a piezoelectric biosensor. *Analytical and Bioanalytical Chemistry* **2005,** 382, (8), 1904-1911.

3. Hu, S.-Q.; Xie, J.-W.; Xu, Q.-H.; Rong, K.-T.; Shen, G.-L.; Yu, R.-Q., A label-free electrochemical immunosensor based on gold nanoparticles for detection of paraoxon. *Talanta* **2003,** 61, (6), 769-777.

4. Janotta, M.; Karlowatz, M.; Vogt, F.; Mizaikoff, B., Sol-gel based mid-infrared evanescent wave sensors for detection of organophosphate pesticides in aqueous solution. *Analytica Chimica Acta* **2003,** 496, (1-2), 339-348.

5. Kunz, R. R.; Leibowitz, F. L.; Downs, D. K., Ultraviolet photolytic vapor generation from particulate ensembles for detection of malathion residues in aerosols. *Analytica Chimica Acta* **2005,** 531, (2), 267-277.

6. Liu, G.; Lin, Y., Electrochemical sensor for organophosphate pesticides and nerve agents using zirconia nanoparticles as selective sorbents. *Analytical Chemistry* **2005,** 77, (18), 5894-5901.

7. Liu, G.; Lin, Y., Biosensor Based on Self-Assembling Acetylcholinesterase on Carbon Nanotubes for Flow Injection/Amperometric Detection of Organophosphate Pesticides and Nerve Agents. *Analytical Chemistry* **2006,** 78, (3), 835-843.

8. Simonian, A. L.; Good, T. A.; Wang, S. S.; Wild, J. R., Nanoparticle-based optical biosensors for the direct detection of organophosphate chemical warfare agents and pesticides. *Analytica Chimica Acta* **2005,** 534, (1), 69-77.

9. Wang, C.; Li, C.; Ji, X.; Orbulescu, J.; Xu, J.; Leblanc, R. M., Peptidolipid as Binding Site of Acetylcholinesterase: Molecular Recognition of Paraoxon in Langmuir Films. *Langmuir* **2006,** 22, (5), 2200-2204.

10. Chen, M. M. Y.; Katz, A., Synthesis and Characterization of Gold-Silica Nanoparticles Incorporating a Mercaptosilane Core-Shell Interface. *Langmuir* **2002,** 18, (22), 8566-8572.

11. Doron, A.; Katz, E.; Willner, I., Organization of Au Colloids as Monolayer Films onto ITO Glass Surfaces: Application of the Metal Colloid Films as Base

Interfaces To Construct Redox-Active Monolayers. *Langmuir* **1995,** 11, (4), 1313-17.

12. Shipway, A. N.; Katz, E.; Willner, I., Nanoparticle arrays on surfaces for electronic, optical, and sensor applications. *ChemPhysChem* **2000,** 1, (1), 18-52.

13. Schilling, M. L.; Katz, H. E.; Stein, S. M.; Shane, S. F.; Wilson, W. L.; Buratto, S.; Ungashe, S. B.; Taylor, G. N.; Putvinski, T. M.; Chidsey, C. E. D., Structural Studies of Zirconium Alkylphosphonate Monolayers and Multilayer Assemblies. *Langmuir* **1993,** 9, (8), 2156-2160.

14. Black, R. M.; Muir, B., Derivatisation reactions in the chromatographic analysis of chemical warfare agents and their degradation products. *Journal of Chromatography, A* **2003,** 1000, (1-2), 253-281.

15. Hooijschuur, E. W. J.; Kientz, C. E.; Brinkman, U. A. T., Analytical separation techniques for the determination of chemical warfare agents. *Journal of Chromatography, A* **2002,** 982, (2), 177-200.

16. Isetun, S.; Nilsson, U.; Colmsjoe, A.; Johansson, R., Air sampling of organophosphate triesters using SPME under non-equilibrium conditions. *Analytical and Bioanalytical Chemistry* **2004,** 378, (7), 1847-1853.

17. Kientz, C. E., Chromatography and mass spectrometry of chemical warfare agents, toxins and related compounds: state of the art and future prospects. *Journal of Chromatography, A* **1998,** 814, (1 + 2), 1-23.

18. Marx, S.; Zaltsman, A.; Turyan, I.; Mandler, D., Parathion Sensor Based on Molecularly Imprinted Sol-Gel Films. *Analytical Chemistry* **2004,** 76, (1), 120-126.

19. Sega, G. A.; Tomkins, B. A.; Griest, W. H., Analysis of methylphosphonic acid, ethyl methylphosphonic acid and isopropyl methylphosphonic acid at low microgram per liter levels in groundwater. *Journal of Chromatography, A* **1997,** 790, (1 + 2), 143-152.

20. Joshi, K. A.; Tang, J.; Haddon, R.; Wang, J.; Chen, W.; Mulchandani, A., A disposable biosensor for organophosphorus nerve agents based on carbon nanotubes modified thick film strip electrode. *Electroanalysis* **2005,** 17, (1), 54-58.

21. Wang, J.; Chen, G.; Muck, A.; Chatrathi, M. P.; Mulchandani, A.; Chen, W., Microchip enzymatic assay of organophosphate nerve agents. *Analytica Chimica Acta* **2004,** 505, (2), 183-187.

22. Bencic-Nagale, S.; Sternfeld, T.; Walt, D. R., Microbead Chemical Switches: An Approach to Detection of Reactive Organophosphate Chemical Warfare Agent Vapors. *Journal of the American Chemical Society* **2006,** 128, (15), 5041-5048.

23. Pavlov, V.; Xiao, Y.; Willner, I., Inhibition of the Acetylcholine Esterase-Stimulated Growth of Au Nanoparticles: Nanotechnology-Based Sensing of Nerve Gases. *Nano Letters* **2005,** 5, (4), 649-653.

24. Goss, C. A.; Charych, D. H.; Majda, M., Application of (3-mercaptopropyl)trimethoxysilane as a molecular adhesive in the fabrication of vapor-deposited gold electrodes on glass substrates. *Analytical Chemistry* **1991,** 63, (1), 85-8.

25. Kallury, K. M. R.; Macdonald, P. M.; Thompson, M., Effect of Surface Water and Base Catalysis on the Silanization of Silica by (Aminopropyl)alkoxysilanes Studied by X-ray Photoelectron Spectroscopy and 13C Cross-Polarization/Magic Angle Spinning Nuclear Magnetic Resonance. *Langmuir* **1994,** 10, (2), 492-9.

26. Moon, J. H.; Shin, J. W.; Kim, S. Y.; Park, J. W., Formation of Uniform Aminosilane Thin Layers: An Imine Formation To Measure Relative Surface Density of the Amine Group. *Langmuir* **1996,** 12, (20), 4621-4624.

27. Pihl, J.; Kabir, M. S.; Persson, S. H. M., Preferential adhesion of gold nanoparticles using lithographically patterned substrates. *Materials Research Society Symposium Proceedings* **2002,** 705, (Nanopatterning: From Ultralarge-Scale Integration to Biotechnology), 199-203.

28. Freeman, R. G.; Grabar, K. C.; Allison, K. J.; Bright, R. M.; Davis, J. A.; Guthrie, A. P.; Hommer, M. B.; Jackson, M. A.; Smith, P. C.; et al., Self-assembled metal colloid monolayers: an approach to SERS substrates. *Science (Washington, D. C.)* **1995,** 267, (5204), 1629-31.

29. He, H. X.; Zhang, H.; Li, Q. G.; Zhu, T.; Li, S. F. Y.; Liu, Z. F., Fabrication of Designed Architectures of Au Nanoparticles on Solid Substrate with Printed Self-Assembled Monolayers as Templates. *Langmuir* **2000,** 16, (8), 3846-3851.

30. Zheng, J.; Zhu, Z.; Chen, H.; Liu, Z., Nanopatterned assembling of colloidal gold nanoparticles on silicon. *Langmuir* **2000,** 16, (10), 4409-4412.

31. Lin, S.-Y.; Tsai, Y.-T.; Chen, C.-C.; Lin, C.-M.; Chen, C.-h., Two-Step Functionalization of Neutral and Positively Charged Thiols onto Citrate-Stabilized Au Nanoparticles. *Journal of Physical Chemistry B* **2004,** 108, (7), 2134-2139.

32. Lee, H.; Kepley, L. J.; Hong, H. G.; Mallouk, T. E., Inorganic Analogs of Langmuir-Blodgett Films - Adsorption of Ordered Zirconium 1,10-

Decanebisphosphonate Multilayers On Silicon Surfaces. *Journal of the American Chemical Society* **1988,** 110, (2), 618-620.

33. Guang, C.; Hong, H. G.; Mallouk, T. E., Layered Metal Phosphates and Phosphonates - From Crystals to Monolayers. *Accounts of Chemical Research* **1992,** 25, (9), 420-427.

34. Major, J. S.; Blanchard, G. J., Covalently Bound Polymer Multilayers for Efficient Metal Ion Sorption. *Langmuir* **2001,** 17, (4), 1163-1168.

35. Kohli, P.; Blanchard, G. J., Design and Demonstration of Hybrid Multilayer Structures: Layer-by-Layer Mixed Covalent and Ionic Interlayer Linking Chemistry. *Langmuir* **2000,** 16, (22), 8518-8524.

36. Kohli, P.; Blanchard, G. J., Probing Interfaces and Surface Reactions of Zirconium Phosphate/Phosphonate Multilayers Using 31P NMR Spectrometry. *Langmuir* **2000,** 16, (2), 695-701.

37. Kohli, P.; Rini, M. C.; Major, J. S.; Blanchard, G. J., Elucidating the balance between metal ion complexation and polymer conformation in maleimide vinyl ether polymer multilayer structures. *Journal of Materials Chemistry* **2001,** 11, (12), 2996-3001.

38. Turkevich, J.; Stevenson, P. C.; Hillier, J., The nucleation and growth processes in the synthesis of colloidal gold. *Discussions of the Faraday Society* **1951,** No. 11, 55-75.

39. Wang, Z.; Heising, J. M.; Clearfield, A., Sulfonated Microporous Organic-Inorganic Hybrids as Strong Bronsted Acids. *Journal of the American Chemical Society* **2003,** 125, (34), 10375-10383.

40. Yang, C. Y.; Clearfield, A., The preparation and ion-exchange properties of zirconium sulfophosphonates. *Reactive Polymers, Ion Exchangers, Sorbents* **1987,** 5, (1), 13-21.

41. Ruvarac, A.; Milonjic, S.; Clearfield, A.; Garces, J. M., On the mechanism of ion exchange in zirconium phosphates. XVIII. Effect of crystallinity upon the K+-H+ exchange of a-zirconium phosphate. *Journal of Inorganic and Nuclear Chemistry* **1978,** 40, (1), 79-85.

42. Hong, H. G.; Sackett, D. D.; Mallouk, T. E., Adsorption of Well-Ordered Zirconium Phosphonate Multilayer Films on High Surface-Area Silica. *Chemistry of Materials* **1991,** 3, (3), 521-527.

43. Cao, G.; Hong, H. G.; Mallouk, T. E., Layered metal phosphates and phosphonates: from crystals to monolayers. *Accounts of Chemical Research* **1992,** 25, (9), 420-7.

44. Fang, M.; Kaschak, D. M.; Sutorik, A. C.; Mallouk, T. E., A \"Mix and Match\" Ionic-Covalent Strategy for Self-Assembly of Inorganic Multilayer Films. *Journal of the American Chemical Society* **1997,** 119, (50), 12184-12191.

45. Katz, H. E., Multilayer Deposition of Novel Organophosphonates with Zirconium(IV). *Chemistry of Materials* **1994,** 6, (12), 2227-32.

46. Bakiamoh, S. B.; Blanchard, G. J., Demonstration of Oriented Multilayers through Asymmetric Metal Coordination Chemistry. *Langmuir* **1999,** 15, (19), 6379-6385.

47. Yang, H. C.; Aoki, K.; Hong, H. G.; Sackett, D. D.; Arendt, M. F.; Yau, S. L.; Bell, C. M.; Mallouk, T. E., Growth and Characterization of Metal(Ii) Alkanebisphosphonate Multilayer Thin-Films On Gold Surfaces. *Journal of the American Chemical Society* **1993,** 115, (25), 11855-11862.

48. Ansell, M. A.; Cogan, E. B.; Neff, G. A.; von Roeschlaub, R.; Page, C. J., Self-assembly of thin film superstructures based on alternating metal-bisphosphonate and cobalt diisocyanide layers. *Supramolecular Science* **1997, 4,** (1-2), 21-26.

49. Obrien, J. T.; Zeppenfeld, A. C.; Richmond, G. L.; Page, C. J., Fourier-Transform Infrared-Spectroscopy Studies of Hafnium Alkylbis(Phosphonate) Multilayers On Gold - Effects of Alkylbis(Phosphonate) Chain-Length, Substrate Roughness, and Surface Functionalization On Film Structure and Order. *Langmuir* **1994,** 10, (12), 4657-4663.

50. Zeppenfeld, A. C.; Fiddler, S. L.; Ham, W. K.; Klopfenstein, B. J.; Page, C. J., Variation of Layer Spacing in Self-Assembled Hafnium-1,10-Decanediylbis(Phosphonate) Multilayers As Determined By Ellipsometry and Grazing Angle X-Ray-Diffraction. *Journal of the American Chemical Society* **1994,** 116, (20), 9158-9165.

51. Koplin, E.; Niemeyer, C. M.; Simon, U., Formation of electrically conducting DNA-assembled gold nanoparticle monolayers. *Journal of Materials Chemistry* **2006,** 16, (14), 1338-1344.

52. Link, S.; Wang, Z. L.; El-Sayed, M. A., Alloy Formation of Gold-Silver Nanoparticles and the Dependence of the Plasmon Absorption on Their Composition. *Journal of Physical Chemistry B* **1999,** 103, (18), 3529-3533.

53. Maye, M. M.; Han, L.; Kariuki, N. N.; Ly, N. K.; Chan, W.-B.; Luo, J.; Zhong, C.-J., Gold and alloy nanoparticles in solution and thin film assembly:

spectrophotometric determination of molar absorptivity. *Analytica Chimica Acta* **2003,** 496, (1-2), 17-27.

54. Leff, D. V.; Ohara, P. C.; Heath, J. R.; Gelbart, W. M., Thermodynamic Control of Gold Nanocrystal Size: Experiment and Theory. *Journal of Physical Chemistry* **1995,** 99, (18), 7036-41.

55. Hoevel, H.; Fritz, S.; Hilger, A.; Kreibig, U.; Vollmer, M., Width of cluster plasmon resonances: bulk dielectric functions and chemical interface damping. *Physical Review B: Condensed Matter and Materials Physics* **1993,** 48, (24), 18178-88.

56. Refractive Index and Transmittance of Representative Glasses. In *CRC Handbook of Chemistry and Physics*, 77 ed.; Lide, D. R., Ed. CRC Press: Boca Raton, FL, 1996; pp 10-263.

Chapter 6

Optical Organophosphate/Phosphonate Sensor Based upon Gold Nanoparticle Functionalized Quartz

Introduction

As discussed in the previous chapter, concerns about release and disposal of chemical warfare agents (CWAs) and environmental contamination from pesticides has lead to an increased need to detect organophosphorous compounds sensitively and selectively. Organophosphate/phosphonate compounds (OPPs) can have devastating physical effects including muscular paralysis leading to death.[1] The Chemical Warfare Convention (CWC), ratified in 1997, cited an urgent need to develop detectors for CWAs and other OPP compounds in order to verify compliance with the provisions of the treaty that prohibits the use of chemical warfare agents as well as the continued development, production and storage thereof.[2] Additionally, concerns surrounding the impact of organophosphorous pesticides on the environment and on the food chain has lead to the need for rapid detection these compounds as well.[3-10] This chapter discusses an OPP sensor based on monitoring the plamson resonance (PR) of gold nanoparticles (AuNPs) covalently attached to a planar solid substrate. This device can be used to qualitatively detect the presence of OPP compounds using simple optical spectroscopic measurements

as an inexpensive, robust, presumptive test for the presence of these compounds in a variety of matrices.

There are a number of techniques currently in use for the detection of CWAs, CWA metabolites, and other OPP compounds including chromatography,[11-19] mass spectrometry,[12, 14] electrochemistry,[4, 7, 8, 20-22] biosensors,[4, 8-10, 20, 21] and others.[23] Recent work in the field has focused on the use of nanoparticles of various compositions and their use in the detection of OPPs[4, 7, 9, 23]. Both AuNPs and zirconium oxide (ZrO_2) nanoparticles have shown promise for use in the detection of OPP compounds. In the case of AuNPs, Pavlov and coworkers[24] have demonstrated that in the absence of thiocholine, a product of the decomposition of acetylthiocholine by acetocholine esterase (AChE), AuNPs do not form. Therefore, if AChE is inhibited and cannot break down acetylthiocholine, a decrease in the plasmon resonance intensity will occur. Additionally, they bound 2-3 nm diameter AuNP "seeds" to a planar surface using an aminopropylsilane film and created a solid-phase sensing platform based on the same chemistry which was also analyzed by UV-visible spectroscopy. Liu and coworkers[7] also demonstrated a planar solid-phase sensing platform for OPPs based upon the affinity of OPP compounds for zirconium. In this case, they electrochemically deposited ZrO_2 nanoparticles on a gold electrode and probed for the OPP methyl parathion electrochemically. Both these instances demonstrate the potential of a planar substrate format for chemical sensing. Ideally, however, the chemical specificity of the zirconium based sensor could be combined with the simple design of the bound AuNP sensor to create a robust sensor that is simple to construct and utilize with optical rather than electrochemical detection. It is this type of sensor we describe here.

The sensing platform we have developed is based on a series of well established surface chemistries. First, quartz surfaces are functionalized with either amino- or mercaptosilane compounds.[25-28] The AuNPs are attached through simple deposition from the solution phase by soaking in an AuNP colloid.[29-32] The AuNPs are necessary for optical sensing due to the characteristic PR in the visible spectrum associated with these particles. Finally the AuNPs are functionalized through displacement of the citrate stabilizers by a ω-hydroxythiol compound.[33] The sensing platform is completed using zirconium-phosphate/phosphonate (ZP) chemistry previously described by our group.[34-37] Many CWAs and OPP pesticides contain phosphoesters. Because of this, such analytes demonstrate good affinity for ZP-functionalized surfaces.[7, 35]

While these sensors are less sensitive than some other techniques, including one demonstrated by our research group for OPP detection,[38] they provide a very simple use platform. These sensors are robust and their analysis is inexpensive and simple and shows promise for use as a presumptive sensor of OPP compounds in a variety of matrices including liquids, liquid extracts of solid matrices, and perhaps biological tissues.

Materials and Methods

Materials. Sodium citrate, hydrogen tetrachloroaurate ($HAuCl_4 \cdot 3H_2O$, 99.9+%), methylphosphonic acid (MPA), diethylchlorophosphate (DECP), 3-aminopropyl-triethoxysilane (APTES), and 3-mercaptopropyltrimethoxysilane (MPTMS) were purchased from Sigma-Aldrich and used as received. 3-Aminopropyldimethylethoxy-silane (APDMES) was purchased from Gelest and used as received. 6-Mercapto-1-

hexanol and phosphorous oxychloride ($POCl_3$) were purchased from Fluka and used as received. Collidine was purchased from Spectrum and used as received. Zirconium(IV) oxychloride octahydrate ($ZrOCl_2 \cdot 8H_2O$) was purchased from Allied and used as received.

Preparation of AuNP Colloid. AuNPs were synthesized from $HAuCl_4$ by reduction and stabilization with sodium citrate according to a modified published procedure.[39] Briefly, an aqueous solution of sodium citrate was brought to a boil. While stirring vigorously, an aqueous solution of $HAuCl_4 \cdot 3H_2O$ was added. For these procedures a 1% (w/w) solution of $HAuCl_4 \cdot 3H_2O$ was used. The solutions were combined for an overall molar ratio of 3:1 sodium citrate:$HAuCl_4 \cdot 3H_2O$. The plasmon resonance band of the resulting colloid in water was approximately 530 nm.

Preparation of sensor. Quartz substrates were soaked in piranha solution (3:1 sulfuric acid:hydrogen peroxide) for at least 30 minutes. The substrates were then rinsed with copious amounts of distilled water and ethyl acetate, and dried with N_2. For surface activation with an amine terminus, a 5% solution of 3-aminopropyltriethoxysilane or 3-aminopropyldimethylethoxysilane in toluene was used. For surface activation with a thiol terminus a 5% solution in toluene of 3-mercaptopropyltrimethoxysilane was used. This step will be referred to hereafter as the linking step and the compound used as the linker. The substrates were soaked overnight at room temperature, then rinsed with ethyl acetate and dried with N_2. The substrates were then immersed in the AuNP colloid overnight at room temperature, then rinsed with ethyl acetate and dried with N_2. Following attachment of AuNPs to the quartz surface, the citrate stabilizer was displaced by soaking the sample in a 10 mM 6-mercapto-1-hexanol solution in ethanol overnight at room temperature, then rinsed with ethyl acetate and dried with N_2. After this step the

sample was dried in an oven for five minutes. The sample was then placed into a round bottom flask, put under vacuum, then purged with Ar for at least 2 hours. To the round bottom flask under vacuum was added a 5% collidine/3.5% $POCl_3$ solution in anhydrous acetonitrile. The sample was soaked for a minimum of two hours, and then rinsed with anhydrous acetonitrile, acetone and water. The sample was then rinsed with ethyl acetate and dried with N_2. To the phosphorylated sample was added a 5 mM $ZrOCl_2$ solution in 60:40 ethanol-water. The sample was soaked overnight at room temperature, then rinsed with ethyl acetate and dried with N_2. A representation of the AuNP functionalized quartz sensor can be seen in Figure 6.1.

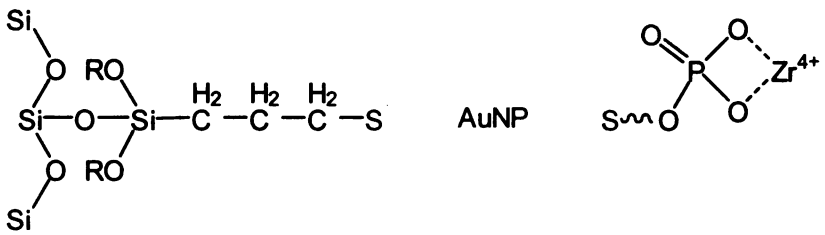

Figure 6.1. Representation of the AuNP-functionalized quartz sensor

Following this step, a baseline UV-visible spectrum was taken to obtain the blank PR for the sensor substrate. The analytes were introduced as ethanolic solutions of MPA or DECP and soaked overnight. Additionally, ethanol was used as a control analyte for all analyses. The samples were thoroughly rinsed with ethanol and dried with N_2 prior to spectroscopic analysis.

SEM Imaging. Substrates for SEM imaging were prepared on indium tin oxide (ITO) substrates under conditions identical to those discussed for the quartz substrates up to the attachment of AuNPs. This was the final step for the ITO samples. The samples were

imaged using a JEOL JSM-6300F Scanning Electron Microscope at 25kV accelerating voltage.

UV-visible Spectroscopy. The samples were examined prior to and following exposure to analytes. The sensors were analyzed in air. The spectra were acquired in transmission mode from 300 to 800 nm using a Cary model 300 UV-visible spectrometer (Varian) and acquisition time was ca. 1 minute per spectrum.

Sensitivity Studies. Ethanolic solutions of the DECP analyte were prepared to concentrations of 5mM to 5nM. Blank UV-visible spectra were acquired for the sensor substrates in air prior to immersion in the analyte. The sensors were immersed in analyte solution for 24 hours, rinsed with ethyl acetate, and dried with N_2. The after-immersion UV-visible spectra were again acquired in air.

Results and Discussion

SEM Imaging. APTES was explored first as the quartz-AuNP linker. Despite efforts to make the surface visually homogeneous, the sensors retained an uneven distribution of AuNPs on the surface (6. 2a). AuNPs on the surface (6. 2a).

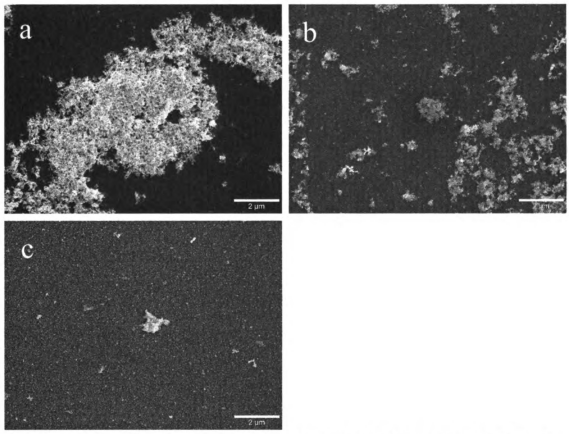

Figure 6.2. SEM images of AuNPs on ITO substrates at 10,000 times magnification A) APTES linker, B) APDMES linker C) MPTMS. Measurement bar indicates 2 µm.

It has been suggested that the cause of this visual surface heterogeneity is polymerization of the linker on the surface leading to local areas of increased concentration of both linker and subsequently AuNPs.[26, 27, 29] Multilayer coverage of the linker would in turn lead to a greater degree of heterogeneity in the AuNP coverage. SEM images at 10,000 X magnification verified that the sensors prepared with APTES did have a greater degree of aggregation on the surface than either of the other two sensors (Figure 6.2). In an effort to make the surface more uniform, APDMES was used as the quartz AuNP linker. Literature precedent suggests that the presence of a single ethoxy in APDMES leads to a monolayer coverage of the silane on quartz surfaces.[26, 27] Monolayer coverage should, in

turn, lead to better uniformity of AuNP coverage on the surface. In this case, the substrates were more visually homogeneous, although with lower apparent AuNP density (Figure 6.2b). To achieve a more robust sensor, MPTMS was used as the linker. This linker takes advantage of the strong S-Au bond that has been exploited in self-assembled monolayer chemistry[40, 41] as well as methods to attach various forms of gold to silicon substrates of various geometries.[38, 42, 43] Despite the presence of a trimethoxy species in MPTMS, which was implicated in the case of APTES to create multilayer coverage, the resulting sensors had a macroscopically visually regular surface (Figure 6.2c).

The SEM images showed aggregates in the approximately 10μm size regime in the case of APTES, while aggregates in the 1μm range were observed in the cases of APDMES and MPTMS. Additionally, there were a greater number of aggregates observed in the APTES sensors. At 100,000 X magnification, both amine terminated linkers showed the majority of AuNPs on the surface present in the form of aggregates (Figure 6.3 panels a and b).

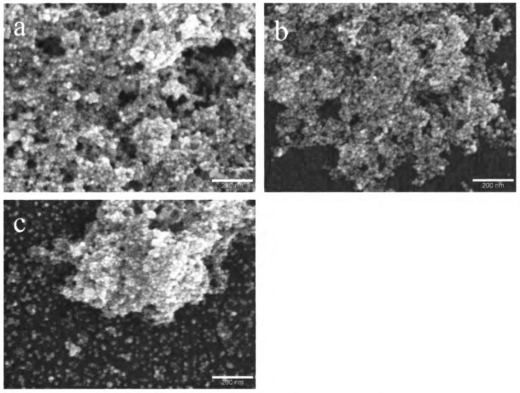

Figure 6.3. SEM images of AuNPs on ITO substrates at 100,000 times magnification A) APTES linker, B) APDMES linker C) MPTMS. Measurement bar indicates 200 nm.

In some places on these substrates, there were no observable non-aggregated AuNPs. On the substrate prepared with MPTMS, the AuNPs were much more evenly dispersed on the surface. While some aggregates were present (Figure 6.3, panel c), there was a large population of either isolated AuNPs or aggregates of a very small number of particles.

UV-Visible Spectroscopy. Sensors were prepared using all three quartz-AuNP linkers to explore the effect of the three linkers on the spectroscopic response. When APTES was used as the linker, a blue shift of 4 nm was observed in the spectrum following exposure to MPA (Figure 6.4).

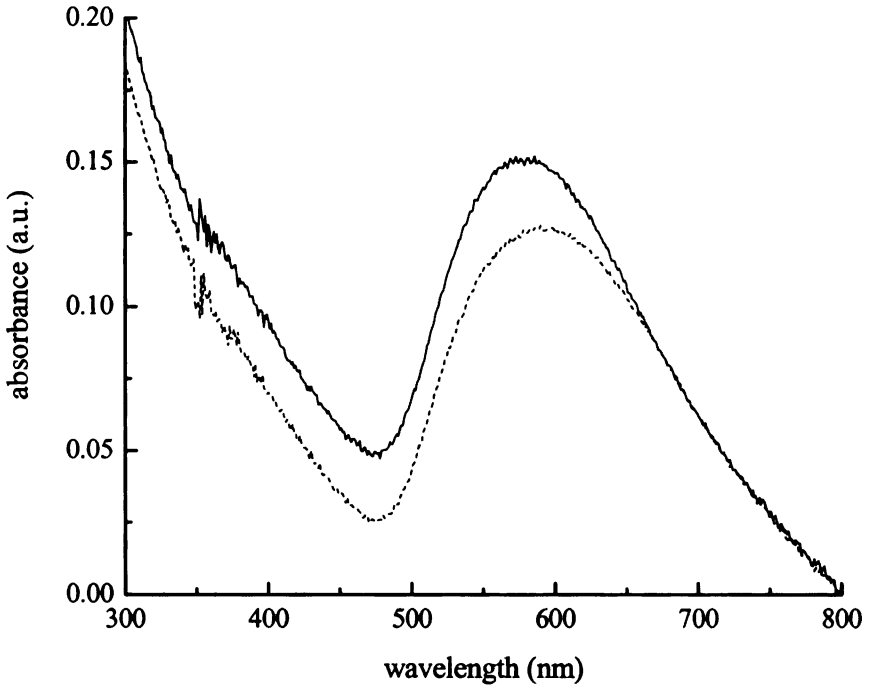

Figure 6.4. APTES linker PR before (dashed line) and after (solid line) exposure to 2 mM MPA (~200ppm). PR blue shifted 4 nm upon exposure.

While this result was consistent with the results discussed in the previous chapter for AuNPs on a silica gel substrate, the other linkers were explored to determine if similar or better results could be seen while achieving a more homogenous sensor surface.

As seen in the imaging study, APDMES produced a similar, though slightly more homogenous, substrate to APTES. The spectra obtained for the substrates before and after exposure to MPA, DECP demonstrated blue shifted plasmon resonance bands of 17 nm and 5 nm, respectively (Table 6.1).

Analyte	Before/After Exposure	PR (nm)	ΔPR (nm)
Methylphosphonic acid	before	593	-17
	after	576	
Triethylchlorophosphate	before	555	-5
	after	550	
Ethanol (blank)	before	568	8
	after	576	

Table 6.1. Plasmon resonance band shifts for APDMES sensor exposed to analytes.

Additionally, when exposed to ethanol the sensor demonstrated a red shifted plasmon resonance of 8 nm (Table 6.1), allowing for differentiation of the response in the presence of the solvent. This response showed the same trend as observed with the APTES linker but was greater in magnitude indicating the more uniform surface served to better elucidate the diagnostic blue shift.

While the attachment chemistry is efficient and the sensor effective when an amine group is used in the linker, MPTMS was explored as an alternative as the MPTMS substrates appeared to be more homogeneous when viewed microscopically. The behavior of the sensors, however, was consistent with the observations made for the APTES sensors demonstrating blue shifted plasmon resonances of 13 nm and 10 nm for MPA and DECP, respectively (Figure 6.5 panels a and b, Table 6.2).

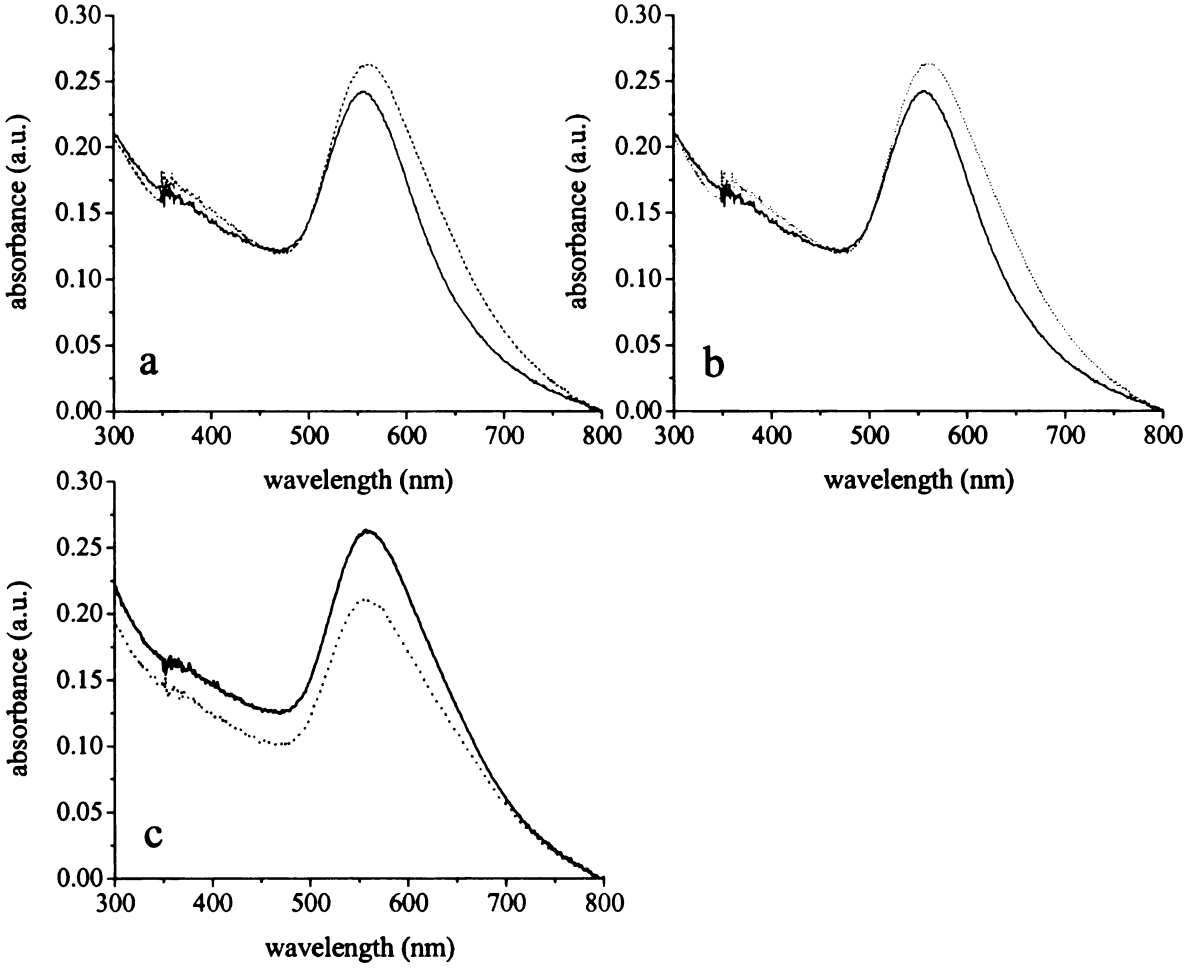

Figure 6.5. a) MPTMS PR before (dashed line) and after (solid line) exposure to 2 mM MPA. PR blue shifted 13 nm upon exposure.
b) MPTMS PR before (dashed line) and after (solid line) exposure to 2 mM DECP. PR blue shifted 10 nm upon exposure.
c) MPTMS PR before (dashed line) and after (solid line) exposure to ethanol. No blue shift observed.

Analyte	Before/After Exposure	PR (nm)	ΔPR (nm)
Methylphosphonic acid	before	570	-13
	after	557	
Triethylchlorophosphate	before	564	-10
	after	554	
Ethanol	before	554	3
	after	557	

Table 6.2. Plasmon resonance band shifts for MPTMS sensor exposed to analytes.

Ethanol was again seen to red shift the plasmon resonance position, by 3 nm in this instance (Figure 6.5c, Table 6.2).

The major influence on the absorbance of AuNPs comes from the dependence of the absorption cross section and the PR wavelength on the dielectric response of the nanoparticle and the medium (Eq. 1)[44]

$$\sigma(\omega)_{abs} = \left(\frac{24\pi^2 R^3 \varepsilon_m^{3/2}}{\lambda}\right)\left(\frac{\varepsilon''(\omega)}{\left(\varepsilon'(\omega)+2\varepsilon_m\right)^2+\left(\varepsilon''(\omega)\right)^2}\right) \quad (1)$$

where ε_m is the dielectric constant of the medium surrounding the nanoparticle, R is the particle radius, and $\varepsilon'(\omega)$ and $\varepsilon''(\omega)$ are the real and imaginary components, respectively, of the frequency-dependent dielectric response of metallic gold. Under the condition that $\varepsilon''(\omega)$ is small, the resonance occurs where $\varepsilon'(\omega) = -2\varepsilon_m$, and the primary contribution to the PR is in the first term of equation 1. Thus, the major influences on changes in the position of the plamson resonance can be attributed to the size of the AuNP and the local dielectric environment it experiences (ε_m). Typically, the plasmon resonance wavelength

of AuNPs is most greatly affected by changes in AuNP size of the AuNPs.[44, 45] When increases in the size of the AuNPs are the greatest influence, red shifts and broadening of the plasmon resonance peak are observed. This is due to quantum size effects as well as the particle size distribution. Because increasing the size of the particles is expected to produce a red shift in the position of the plasmon resonance band, it is unlikely that the small size change caused by OPP binding has an influence on the plasmon resonance position in this case. Therefore, the plasmon resonance blue shift in the presence of OPP compounds is due to the influence of the local dielectric change when OPP compounds have been chemisorbed to the sensor substrate. This dielectric change is not seen when the sensor is soaked in ethanol. The slight red shift observed when the sensor is exposed to ethanol is likely due to either minor aggregation effects arising from the mobility of the AuNPs on the surface or residual ethanol causing a dielectric change, relative to air, near the AuNP surface. Because the analytes were prepared in ethanol solution, it is most likely that the effect of the ethanol is incorporated into the effect observed with the OPP analytes and the blue shift observed in these cases is actually great enough to overcome the influence of the solvent. Additionally, the blue-shift is believed to be the consequence of the change in the local dielectric environment associated with OPP binding. Because binding of the OPP analytes to the AuNP surface would be expected to slightly enlarge the particles, if the effect was due to size changes, a red-shift would be expected. The most significant other parameter associated with PR position is the medium dielectric constant. As seen in equation 1, under resonance conditions the PR wavelength is proportional to $\varepsilon_m^{3/2}$. Therefore, a decrease in ε_m would result in a blue-shift. We believe that this is the case for this sensor.

Sensitivity. It is important to note here that this sensor is class-specific and not able to differentiate between individual OPP compounds. As this sensor design is intended to be a presumptive test for the presence of OPP compounds, we do not view this as a limitation of the sensor. The sensitivity of the sensor was explored using concentrations of DECP ranging from 5×10^{-3} to 5×10^{-9} M (Table 6.3).

Concentration (M)	**Average Blue Shift (nm)**
5×10^{-03}	16.00 ± 5.66
5×10^{-04}	15.00 ± 5.67
5×10^{-05}	4.00 ± 1.00
5×10^{-06}	2.00 ± 0
5×10^{-07}	5.00 ± 2.65
5×10^{-08}	2.00 ± 0
5×10^{-09}	2.00 ± 6.78

Table 6.3. Sensitivity to DECP

A blue shift of 2 nm was considered a negative result because the spectral resolution of the instrument was 1 nm and the experimental data are characterized by a modest signal-to-noise ratio. At concentrations greater than or equal to 5×10^{-5} M, a blue shift in the plasmon resonance band of the sensor was observed, characteristic of the presence of OPP compounds. The magnitude of the blue-shift was in the range of 4 - 16 nm (Figure 6.6), well outside the uncertainty of the measurement. The level of uncertainty associated

with these measurements suggest they are useful only as a qualitative determinant of OPP presence and are not, in their present form, capable of quantitative analysis.

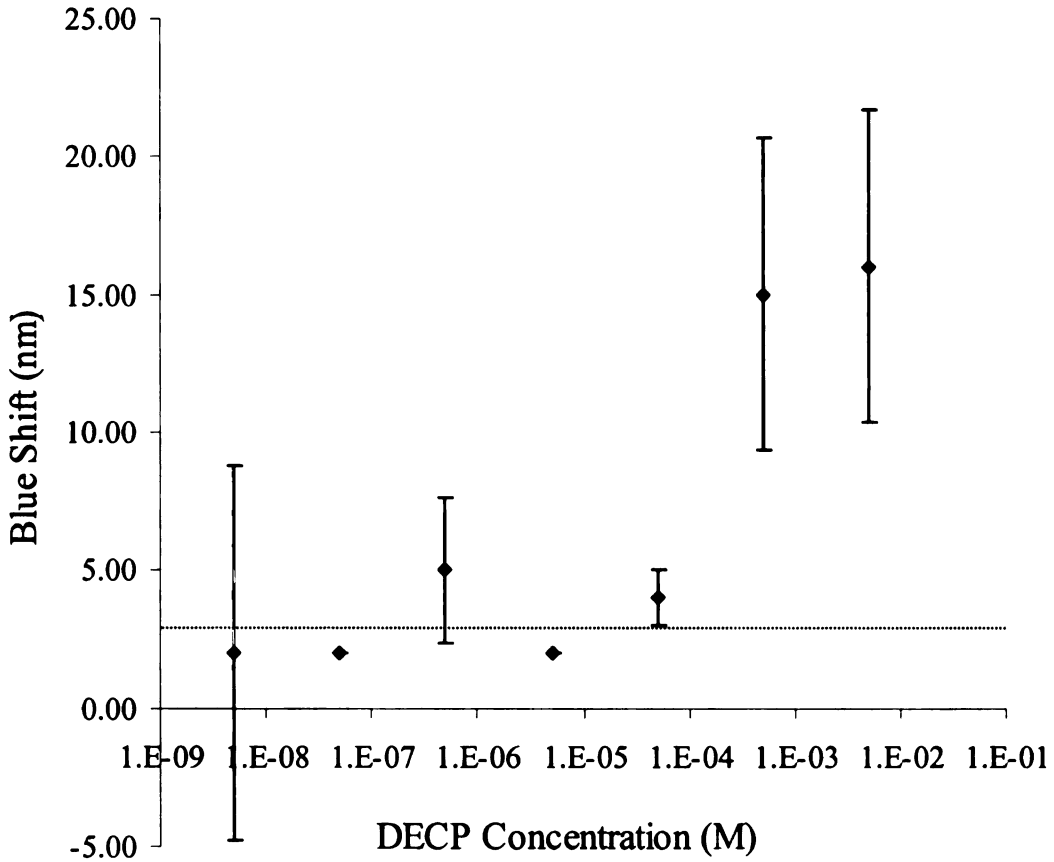

Figure 6.6. Observed PR response of the sensor to variations in DECP concentration.

The relatively large variation in band shift is due to the degree of scattering imparted by the sensor itself. While not as sensitive as methods based on mass spectrometric detection or our previously reported silica gel-based sensor,[38] this limit of detection is on the same order of magnitude as reported for other methods based on UV-visible detection.[46-49]

At high analyte concentrations, the magnitude of the blue shift is seen to be independent of DECP concentration due to rapid saturation of binding sites. Due to this

rapid saturation, there is limited dynamic range associated with this sensor and it exhibits a digital response associated with DECP binding.

The sensor response can be explained by considering that there are two spectrally overlapped bands, with one band attributed to AuNPs terminated with uncomplexed Zr^{4+} and the other attributed to Zr^{4+} complexed to an analyte OPP compound. In chapter 5, the ability to model this spectral response was demonstrated. In this case, the response has been attributed to the dominance of a 1:1 OPP:ZP-AuNP binding event.[38] There may be contributions from 2:1 and 3:1 OPP:ZP-AuNP binding, but these contributions are minor. In the case of these sensors the position of the plasmon resonance changes with variations in the degree of AuNP surface coverage achieved during sensor construction. The blanks had plasmon resonance bands ranging from 519 nm to 577 nm. Therefore, the same rigorous mathematical interpretation could not be made. However, the sensor behavior is consistent with the previous study. The blue shift obtained OPP attachment was independent of the blank plasmon resonance band position for the sensor and the magnitude of the blue shift is more important as a diagnostic tool than the absolute position of the band after exposure in the case of these planar OPP sensors.

Conclusions

Concerns about the impact of organophosphate/phosphonate compounds, used as pesticides or chemical warfare agents, have made the detection of these compounds increasingly a priority. When developing sensors for these compounds, it is important to consider the simplicity of construction and durability of the sensors in addition to the vital standards being sensitivity and selectivity for OPP compounds in a variety of

matrices. We have presented an OPP sensor based on optical detection of ZP modified AuNPs bound covalently to a planar quartz substrate. These sensors are simple to construct, rugged, and utilize simple detection with a UV-visible spectrometer. We have shown through SEM imaging that while APTES and APDMES both serve to bind large numbers of AuNPs to the quartz surface, using MPTMS as the quartz-AuNP linker results in the sensor substrate with the most uniform surface coverage. After displacement of citrate stabilizing agents on the AuNP surface with a mercaptoalcohol and subsequent ZP chemistry, the completed sensors were tested for their ability to bind OPP compounds. These sensors demonstrate a blue shift in the plasmon resonance band when exposed to the OPP compounds MPA and DECP, but display a more typical red shift in the presence of ethanol.

Sensitivity studies conducted using DECP as the OPP analyte show that the sensor is able to detect OPP analytes at concentrations $> 5 \times 10^{-5}$ M. Below this level, the response of the sensor does not produce a band shift in excess of the instrumental uncertainty. At DECP concentrations of $\geq 5 \times 10^{-5}$ M, the sensor response is independent of the analyte concentration and a characteristic blue-shift is observed in the spectrum. This can be explained by the spectrum of the sensor being dominated by the bands associated with the complexed AuNP-ZP-OPP species. While further improvements are necessary to decrease the detection limit of this type of optical OPP sensor, the current sensor provides a simple and robust qualitative method of detecting OPPs above the limit of detection and has potential for use as a presumptive test for OPP presence.

References

1. Koelle GB. Anticholinesterase Agents. *The Phamacological Casis of Therapeutics*. Fourth ed. New York: Macmillan Company; 1970:442-465.

2. Weapons OftPoC. Convention on the Prohibition of the Development, Production, Stockpiling and Use of Chemical Weapons and on Their Destruction. 2005.

3. Halamek J, Pribyl J, Makower A, Skladal P, Scheller FW. Sensitive detection of organophosphates in river water by means of a piezoelectric biosensor. *Analytical and Bioanalytical Chemistry.* 2005;382(8):1904-1911.

4. Hu S-Q, Xie J-W, Xu Q-H, Rong K-T, Shen G-L, Yu R-Q. A label-free electrochemical immunosensor based on gold nanoparticles for detection of paraoxon. *Talanta.* 2003;61(6):769-777.

5. Janotta M, Karlowatz M, Vogt F, Mizaikoff B. Sol-gel based mid-infrared evanescent wave sensors for detection of organophosphate pesticides in aqueous solution. *Analytica Chimica Acta.* 2003;496(1-2):339-348.

6. Kunz RR, Leibowitz FL, Downs DK. Ultraviolet photolytic vapor generation from particulate ensembles for detection of malathion residues in aerosols. *Analytica Chimica Acta.* 2005;531(2):267-277.

7. Liu G, Lin Y. Electrochemical sensor for organophosphate pesticides and nerve agents using zirconia nanoparticles as selective sorbents. *Analytical Chemistry.* 2005;77(18):5894-5901.

8. Liu G, Lin Y. Biosensor Based on Self-Assembling Acetylcholinesterase on Carbon Nanotubes for Flow Injection/Amperometric Detection of Organophosphate Pesticides and Nerve Agents. *Analytical Chemistry.* 2006;78(3):835-843.

9. Simonian AL, Good TA, Wang SS, Wild JR. Nanoparticle-based optical biosensors for the direct detection of organophosphate chemical warfare agents and pesticides. *Analytica Chimica Acta.* 2005;534(1):69-77.

10. Wang C, Li C, Ji X, Orbulescu J, Xu J, Leblanc RM. Peptidolipid as Binding Site of Acetylcholinesterase: Molecular Recognition of Paraoxon in Langmuir Films. *Langmuir.* 2006;22(5):2200-2204.

11. Black RM, Muir B. Derivatisation reactions in the chromatographic analysis of chemical warfare agents and their degradation products. *Journal of Chromatography, A.* 2003;1000(1-2):253-281.

12. Hooijschuur EWJ, Kientz CE, Brinkman UAT. Analytical separation techniques for the determination of chemical warfare agents. *Journal of Chromatography, A.* 2002;982(2):177-200.

13. Isetun S, Nilsson U, Colmsjoe A, Johansson R. Air sampling of organophosphate triesters using SPME under non-equilibrium conditions. *Analytical and Bioanalytical Chemistry.* 2004;378(7):1847-1853.

14. Kientz CE. Chromatography and mass spectrometry of chemical warfare agents, toxins and related compounds: state of the art and future prospects. *Journal of Chromatography, A.* 1998;814(1 + 2):1-23.

15. Marx S, Zaltsman A, Turyan I, Mandler D. Parathion Sensor Based on Molecularly Imprinted Sol-Gel Films. *Analytical Chemistry.* 2004;76(1):120-126.

16. Sega GA, Tomkins BA, Griest WH. Analysis of methylphosphonic acid, ethyl methylphosphonic acid and isopropyl methylphosphonic acid at low microgram per liter levels in groundwater. *Journal of Chromatography, A.* 1997;790(1 + 2):143-152.

17. Lacassie E, Marquet P, Gaulier JM, Dreyfuss MF, Lachatre G. Sensitive and specific multiresidue methods for the determination of pesticides of various classes in clinical and forensic toxicology. *Forensic Science International.* Sep 2001;121(1-2):116-125.

18. Namera A, Watanabe T, Yashiki M, Iwasaki Y, Kojima T. Simple analysis of arylamide herbicides in serum using headspace-solid phase microextraction and GC/MS. *Forensic Science International.* Sep 1999;103(3):217-226.

19. Tarbah FA, Mahler H, Temme O, Daldrup T. An analytical method for the rapid screening of organophosphate pesticides in human biological samples and foodstuffs. *Forensic Science International.* Sep 2001;121(1-2):126-133.

20. Joshi KA, Tang J, Haddon R, Wang J, Chen W, Mulchandani A. A disposable biosensor for organophosphorus nerve agents based on carbon nanotubes modified thick film strip electrode. *Electroanalysis.* 2005;17(1):54-58.

21. Wang J, Chen G, Muck A, Chatrathi MP, Mulchandani A, Chen W. Microchip enzymatic assay of organophosphate nerve agents. *Analytica Chimica Acta.* 2004;505(2):183-187.

22. Wang J, Pumera M, Chatrathi MP, et al. Single-channel microchip for fast screening and detailed identification of nitroaromatic explosives or organophosphate nerve agents. *Analytical Chemistry.* Mar 2002;74(5):1187-1191.

23. Bencic-Nagale S, Sternfeld T, Walt DR. Microbead Chemical Switches: An Approach to Detection of Reactive Organophosphate Chemical Warfare Agent Vapors. *Journal of the American Chemical Society.* 2006;128(15):5041-5048.

24. Pavlov V, Xiao Y, Willner I. Inhibition of the Acetylcholine Esterase-Stimulated Growth of Au Nanoparticles: Nanotechnology-Based Sensing of Nerve Gases. *Nano Letters.* 2005;5(4):649-653.

25. Goss CA, Charych DH, Majda M. Application of (3-mercaptopropyl)trimethoxysilane as a molecular adhesive in the fabrication of vapor-deposited gold electrodes on glass substrates. *Analytical Chemistry.* 1991;63(1):85-88.

26. Kallury KMR, Macdonald PM, Thompson M. Effect of Surface Water and Base Catalysis on the Silanization of Silica by (Aminopropyl)alkoxysilanes Studied by X-ray Photoelectron Spectroscopy and 13C Cross-Polarization/Magic Angle Spinning Nuclear Magnetic Resonance. *Langmuir.* 1994;10(2):492-499.

27. Moon JH, Shin JW, Kim SY, Park JW. Formation of Uniform Aminosilane Thin Layers: An Imine Formation To Measure Relative Surface Density of the Amine Group. *Langmuir.* 1996;12(20):4621-4624.

28. Pihl J, Kabir MS, Persson SHM. Preferential adhesion of gold nanoparticles using lithographically patterned substrates. *Materials Research Society Symposium Proceedings.* 2002;705(Nanopatterning: From Ultralarge-Scale Integration to Biotechnology):199-203.

29. Doron A, Katz E, Willner I. Organization of Au Colloids as Monolayer Films onto ITO Glass Surfaces: Application of the Metal Colloid Films as Base Interfaces To Construct Redox-Active Monolayers. *Langmuir.* 1995;11(4):1313-1317.

30. Freeman RG, Grabar KC, Allison KJ, et al. Self-assembled metal colloid monolayers: an approach to SERS substrates. *Science (Washington, D. C.).* 1995;267(5204):1629-1631.

31. He HX, Zhang H, Li QG, Zhu T, Li SFY, Liu ZF. Fabrication of Designed Architectures of Au Nanoparticles on Solid Substrate with Printed Self-Assembled Monolayers as Templates. *Langmuir.* 2000;16(8):3846-3851.

32. Zheng J, Zhu Z, Chen H, Liu Z. Nanopatterned assembling of colloidal gold nanoparticles on silicon. *Langmuir.* 2000;16(10):4409-4412.

33. Lin S-Y, Tsai Y-T, Chen C-C, Lin C-M, Chen C-h. Two-Step Functionalization of Neutral and Positively Charged Thiols onto Citrate-Stabilized Au Nanoparticles. *Journal of Physical Chemistry B.* 2004;108(7):2134-2139.

34. Major JS, Blanchard GJ. Covalently Bound Polymer Multilayers for Efficient Metal Ion Sorption. *Langmuir.* 2001;17(4):1163-1168.

35. Kohli P, Blanchard GJ. Design and Demonstration of Hybrid Multilayer Structures: Layer-by-Layer Mixed Covalent and Ionic Interlayer Linking Chemistry. *Langmuir.* 2000;16(22):8518-8524.

36. Kohli P, Blanchard GJ. Probing Interfaces and Surface Reactions of Zirconium Phosphate/Phosphonate Multilayers Using 31P NMR Spectrometry. *Langmuir.* 2000;16(2):695-701.

37. Kohli P, Rini MC, Major JS, Blanchard GJ. Elucidating the balance between metal ion complexation and polymer conformation in maleimide vinyl ether polymer multilayer structures. *Journal of Materials Chemistry.* 2001;11(12):2996-3001.

38. Newman J.D.S; Roberts JMB, G.J. Optical Organophosphate Sensor Based upon Gold Nanoparticle Functionalized Fumed Silica Gel. *Anal. Chem.* 2007;in press.

39. Turkevich J, Stevenson PC, Hillier J. The nucleation and growth processes in the synthesis of colloidal gold. *Discussions of the Faraday Society.* 1951;No. 11:55-75.

40. Nuzzo RG, Allara DL. Adsorption of bifunctional organic disulfides on gold surfaces. *Journal of the American Chemical Society.* 1983;105(13):4481-4483.

41. Nuzzo RG, Fusco FA, Allara DL. Spontaneously organized molecular assemblies. 3. Preparation and properties of solution adsorbed monolayers of organic disulfides on gold surfaces. *Journal of the American Chemical Society.* 1987;109(8):2358-2368.

42. Chen MMY, Katz A. Synthesis and Characterization of Gold-Silica Nanoparticles Incorporating a Mercaptosilane Core-Shell Interface. *Langmuir.* 2002;18(22):8566-8572.

43. Maya L, Stevenson KA, Muralidharan G, Thundat TG, Kenik EA. Assembly of Gold Nanoclusters on Silicon Surfaces. *Langmuir.* 2002;18(6):2392-2397.

44. Hoevel H, Fritz S, Hilger A, Kreibig U, Vollmer M. Width of cluster plasmon resonances: bulk dielectric functions and chemical interface damping. *Physical Review B: Condensed Matter and Materials Physics.* 1993;48(24):18178-18188.

45. Haes AJ, Zou S, Schatz GC, Van Duyne RP. A Nanoscale Optical Biosensor: The Long Range Distance Dependence of the Localized Surface Plasmon Resonance

of Noble Metal Nanoparticles. *Journal of Physical Chemistry B.* 2004;108(1):109-116.

46. Cheicante RL, Stuff JR, Durst HD. Separation of Sulfur-Containing Chemical Warfare Related-Compounds in Aqueous Samples by Micellar Electrokinetic Chromatography. *Journal of Chromatography A.* Sep 1995;711(2):347-352.

47. Melanson JE, Wong BLY, Boulet CA, Lucy CA. High-sensitivity determination of the degradation products of chemical warfare agents by capillary electrophoresis-indirect UV absorbance detection. *Journal of Chromatography A.* Jun 2001;920(1-2):359-365.

48. Cheicante RL, Stuff JR, Durst HD. Analysis of Chemical Weapons Degradation Products by Capillary Electrophoresis with Uv Detection. *Journal of Capillary Electrophoresis.* Jul-Aug 1995;2(4):157-163.

49. Oehrle SA, Bossle PC. Analysis of Nerve Agent Degradation Products Using Capillary Ion Electrophoresis. *Journal of Chromatography A.* Feb 1995;692(1-2):247-252.

Chapter 7

Conclusions and Future Work

Due to their unique properties gold nanoparticles (AuNPs) have become a widely studied area in many areas of chemistry. AuNPs are finely divided particles of gold which have properties which fall between those observed for atomic and bulk gold. These properties, both optical and electronic, have been studied with the goal of utilizing AuNPs in areas ranging from signal-enhancing substrates, to sensing technologies, to medical technologies. This thesis has covered three areas which are useful in the study of AuNPs; formation, characterization, and application of AuNPs and surface-modified gold.

Formation. The thermodynamic potential for formation of AuNPs using amines as the reducing and stabilizing agent can be predicted though electrochemical interrogation of $HAuCl_4$ and the potential reducing agent using cyclic voltammetry. Comparison of the oxidation potential of an amine to the reduction and oxidation potentials of the $HAuCl_4$ in a given solvent system can be the first line of predictability for the potential of a given $HAuCl_4$-amine system to result in the formation of a gold colloid. If the oxidation potential of the amine lies between the reduction potential of $HAuCl_4$ to Au^0 and the oxidation potential of Au^0 to Au^{1+}, the amine can be considered a viable reducing agent.

This initial screening of the reducing agent is useful for both monomeric and polymeric amines and may help to determine which systems bear further investigation.

In addition to the thermodynamic considerations, the kinetics of the redox reaction also plays a role in the formation of AuNPs. The kinetics of AuNP formation was probed using time-resolved ultra-violet-visible spectrometry. It was found that amines which were thermodynamically predicted not to function as reducing agents did not show any evidence of AuNP formation as determined through a lack of PR in the visible spectrum. When thermodynamically predicted amines did successfully reduce Au^{3+} to AuNPs, it was found that, among reducing agents with the same number of amines per mole, an increase in the oxidation potential resulted in a decrease in the rate of PR evolution. This indicated that the system was operating in the Marcus inverted region, as explained by Marcus electron transfer theory.

Several amines which were predicted on thermodynamic grounds to function as reducing agents either showed limited evidence of AuNP formation, as determined by the presence of a small PR band, or no PR band at all. These exceptions were understood in terms of competitive polymerization events which kinetically precluded AuNP formation. In the case of aniline and 3-aminophenol, the polymerization of the reducing agents takes place faster than the formation of AuNPs and therefore no AuNPs are observed spectroscopically. In the case of 4-aminophenol, the kinetics of the reduction of $HAuCl_4$ to AuNPs and the polymerization of the amine are similar and both AuNPs and poly(4-aminophenol) are observed in the time-resolved spectrum.

Poly(allylamine hydrochloride) (PAH) was investigated in further detail as a potential polymeric reducing and stabilizing agent. It was predicted to function as a

reducing agent under the thermodynamic considerations and it was found that the kinetics of the system are first order in $HAuCl_4$ at constant PAH concentration. When the PAH concentration is varied, the system kinetics vary to the third power. This validates the postulated reduction mechanism where one Au^{3+} ion is reduced by three amine groups. Knowledge of the concentration dependence helps provide information which can help to optimize the formation of AuNP-PAH composites. This information could also be applied to other polymeric reducing agents as well.

While the kinetics of the system at room temperature can be readily predicted, the reaction rate is also quite slow. In order to speed up the reaction it is possible to add heat energy into the system and maintain a degree of control over the optical behavior of the resulting colloid. With sufficiently small molar ratios of PAH:$HAuCl_4$, the position of the PR band can be both controlled and roughly correlated to AuNP size. A linear relationship exists between the position of the PR band and the ratio of the reactants in solution. Additionally, a general increase is seen in the size of non-aggregated particles in the composite material with an increase in the reactant ratio. This data can be considered together to conclude that the increase in particle size is responsible for the red-shift in the PR band maximum.

Taken together the electrochemical and spectroscopic investigations of these $HAuCl_4$-amine systems can provide predictive information about their potential to result in AuNP colloids. The thermodynamic and kinetic information gained is important to understanding the degree of control achievable in a given system in terms not only of final outcome but also of growth rate. Predictive knowledge about the formation of AuNPs using amines as the reducing and stabilizing agent has a great deal of potential.

The ubiquitous nature of amines in biological systems indicates this knowledge could be of great use when designing polymer films for sensing applications and biomedical applications. It could also be important for understanding potential *in situ* AuNP formation for use as therapeutic agents. Interrogation of poly-peptides, for example poly-tryptophan, would be quite useful for these types of investigations. In initial studies of poly-tryptophan as a reducing agent, solubility was found to be a limitation in both electrochemical and kinetic studies. Other poly-amino acids or poly-peptides may not have the same limited solubility and could therefore be more useful.

Characterization. Impedance spectroscopy conducted on QCM crystals is a characterization method for surface-modified gold which can be useful in probing the viscoelastic properties of adlayers in addition to the more typical mass uptake studies. The study discussed here addressed the issue of how the viscoelastic properties of alkanethiol SAMs vary with aliphatic chain length and time after initial formation. The collected impedance spectra were interpreted in the context of an equivalent circuit model used to understand QCM response in liquids. It was found that the quantities L_2 and R_2 in the equivalent circuit to denote the inductance and resistance of liquid loading, respectively, dominate the physical and chemical contributions of the adlayer in the QCM response. Both have similar temporal behavior for all of the alkanethiols examined in this study. The quantity L_2 was used to extract information about the value of $\rho\eta$, which is related to the viscoelastic properties of the SAM adlayer. The $\rho\eta$ value for the C_6SH monolayer was found to have a higher value than that observed for SAMs having between 9 and 16 carbons in the aliphatic chain. This is indicative of the C_6SH monolayer having a different solvent-monolayer interface than the SAMS formed longer

carbon chain alkanethiol. This is likely due to the lack of organization in short chain alkanethiol SAMs. Monolayers formed from C_9-C_{16}SH had similar values of $\rho\eta$, indicating the similarity of the interfaces between these alkanethiol SAMs and the solvent. The viscosity is believed to dominate changes in $\rho\eta$ because both the monolayer density and bulk thiol density are constant for the systems reported here. The deposition of C_{18}-SH was also studied and differed from that of the shorter alkanethiols, likely a consequence of its limited solubility. The anomalous behavior of C_{18} SAMs can be attributed to the bulk deposition of the thiol on the QCM surface. These studies were conducted at 14°C and it would be useful to expand this work to higher temperatures. This would serve the purpose of both examining the changes which occur in the behavior of the SAMs at elevated temperature along with increasing the aliphatic chain lengths able to be probed by increasing the range of soluble alkanethiols. Also interesting to study would be the physical behavior of other surface modifications to the Au electrodes on the QCM crystal. These may include the chemisorption of polymers and polymer multi-layers or the behavior of a composite material such as the PAH-AuNP discussed in chapter 3.

Application. Due to environmental and health concerns surrounding the use of organophosphate/phosphonate (OPP) based compounds, their detection has become increasingly important. While sensitive and class-selective detection is fundamental, it is also important to develop sensors which are simple and robust. The sensors described here are based on zirconium phosphonate (ZP)-functionalized AuNPs which are immobilized on a silica platform. These sensors are capable of detecting relatively low

levels of OPPs which complex irreversibly to the ZP termini of the AuNPs. The detection is based on simple UV-visible detection of shifts in the PR position.

First, a hybrid silica gel-AuNP-ZP sensor was developed which was simple to synthesize and could be produced on a large scale if required. These silica-gel based sensors were found to exhibit a characteristic blue-shift in the presence of OPP compounds. Additionally they have a limit of detection of ca. $5x10^{-7}$ M for diethylchlorophosphate (DECP). This corresponds to a $K \sim 2 \times 10^6$ M^{-1}. The functional form of the PR maximum concentration-dependence can be used to model the stoichiometry of the AuNP-ZP-OPP complex, which is estimated to be 1:1. This is consistent with the calculated silica gel surface loading of 1.00×10^6 to 4.04×10^7 AuNPs per silica gel particle. Additionally, because sensing is conducted in a solvent system for this type of sensing platform, the sensitivity can be further improved from a signal-to-noise (S/N) ratio of 5.8 in ethanol by selecting a solvent with a refractive index closer to that of silica in order to reduce scattering. A S/N of 42 was achieved in DMSO.

Another sensor was created based on the same detection chemistry but where the ZP-modified AuNPs were covalently bound to a planar quartz substrate. The detection methodology for these also utilized optical detection based on UV-visible spectrometry. For this sensor platform, the influence of different quartz-AuNP linkers was explored and it was found through scanning electron microscopy that 3-mercaptopropyltrimethoxysilane (MPTMS) was the quartz modifier which created the surface most uniformly covered with AuNPs when compared to 3-aminopropyltriethoxysilane and 3-aminoproplydimethylethoxysilane. Sensors created with all three linkers demonstrated the characteristic blue-shift associated with OPP

binding to the ZP-modified nanoparticles, but MPTMS was used due to the relative visual and microscopic uniformity of the sensors. Sensitivity studies conducted on this sensor geometry, again using DECP as the analyte, show that the sensor is capable of detection of DECP at concentrations $\geq 5 \times 10^{-5}$ M. Below this concentration, no characteristic band shift if observed which occurs at a level greater than the uncertainty provided by the instrument. The behavior of this system is consistent with the behavior observed in the case of the silica gel based sensor. While the current sensor provides a simple and robust qualitative method of detecting OPPs above the limit of detection, and has potential for use as a presumptive test for OPP presence, improvements are still needed to decrease the limit of detection. This may be achieved by improving the surface coverage of AuNPs on the quartz surface or by immersion of the substrate in an index of refraction matching solvent in order to decrease scattering associated with the quartz substrate. Also, it would be important to further study the response of these sensors to DECP more complex matrices such as water or soil extracts. It would also be important to determine the sensor response to other analytes including structurally similar but non-OPP compounds to determine any possible interferences which may also result in a spectral blue-shift.

The three areas of study presented here encompass three areas of interest in AuNP research; formation, characterization, and application. The formation and stabilization of AuNPs thorough reduction of $HAuCl_4$ by amines has the potential to be useful in the preparation of bio-compatible AuNP materials. This could have significant impact in the use of AuNPs in therapeutics. The preparation of polymeric-amine-AuNP composites, such as the PAH-AuNP described, could be important in the development of stable AuNP preparations. The technique of impedance spectroscopy was described and the

information gained from comparison to the equivalent circuit model was utilized to provide information about the viscoelastic properties of SAMs adsorbed onto a QCM with Au electrodes. While applied in this instance to simple adlayers adsorbed on the QCM, the information gained from using this technique could also be applied to the study of AuNP composite materials to elucidate their mechanical properties. Finally, the application of AuNPs in a sensory device was described. This sensor was based on the surface-modification of AuNPs using ZP chemistry to create a class-selective presumptive sensor for OPP compounds. This variety of studies indicates the breadth of potential in the area of AuNP research.